Scuola Internazionale Superiore di Studi Avanzati - Trieste

Accretion discs in Active Galactic Nuclei: observations versus theory

Thesis submitted for the degree of

"Magister Philosophiae"

Astrophysics Sector

Candidate:

Paola Marziani

Supervisors:

Prof. Massimo Calvani,
Prof. Pietro Rafanelli

Academic Year 1988/89

SISSA – Via Beirut 2-4 – 34014 TRIESTE – ITALY

Foreword

The discovery of quasars by Marteen Schmidt in 1963 opened a new horizon in extragalactic astronomy. Quasars were characterized by an enormous luminosity output, considering the cosmological distances suggested by their redshifts. It became soon clear that the energy production of quasars could not be explained by any conventional mechanism. Rees, in 1969, proposed what is now the most widely accepted explanation: the luminosity of quasars is due to the release of gravitational energy trough accretion of matter constrained in a disc onto a supermassive black hole. In the meantime, it was recognized that the same mechanism should be at work also in other more nearby and less powerful objects, like Seyfert galaxies, and Broad Line Radio Galaxies. Together with quasars, they were grouped in the unique class of Active Galactic Nuclei (AGN). The presence of accreting matter constrained in an accretion disc around the supermassive black hole became subject of observational test with the discovery of a broad feature in quasars ultraviolet continuum, the Big Bump *by Malkan and Sargent in 1982. Since then, the increasing effort for gaining indirect evidence on the accretion disc did not basically change our knowledge: the* Big Bump *remains the* sole *indirect probe in favour of the accretion disc.*

At the same time, also the physical and kinematical conditions of the regions producing the strong emission line spectrum (called the Broad line Region, BLR) observed in quasars and Seyfert galaxies were unclear.

The estimations of the distance of the BLR to the central object changed, at least for low luminosity AGN, as the data on spectral variability grew: the computed distances reduced to values at which the outer regions of the accretion disc are expected to be present. As a consequence, it is becoming a proper question to ask whether the accretion disc contributes to the BLR, leaving perhaps an unmistakable signature of its presence.

In this work we will be mainly concerned with this problem. The problem can be stated in the following way: is there a support for the idea that a keplerian disc emits at least part of the Broad Lines, or, alternatively, is the kinematics of the BLR rotational?

In Chapter 1, the most basic facts about AGN are recalled, with particular reference to the theory of line formation, and to the problems which are relevant for the discussion in the following Chapters. In Chapter 2 we review the evidence that supports the presence of the accretion disc. In particular, we analyze the physical meaning of the Big Bump. *Next, assuming that the disc is indeed present, we study whether the outer regions are able to emit the low ionization lines of the AGN spectra. Since we find this possibility likely, we consider the possibility of a kinematical signature due to the disc in the emission line profiles. In Chapter 3, the observations of line profiles are reviewed, and it is stressed*

that no current model based on an ensamble of gaseous clouds in radial motion is entirely satisfactory. We find that some hints in favour of a disc geometry are present. In chapter 4 we thus reanalyze the data, and extensively discuss whether the accretion disc is responsible for the emission of the Balmer lines. A last paragraph is devoted to the conclusion and to the further work that remains to be done.

Acknowledgments

I'm greatly indebted to my supervisors, M. Calvani and P. Rafanelli for encouragement and support.

I have benefitted of many stimulating discussions on topics related to the subject of this work with C.M. Urry, J.W. Sulentic, J.Acosta. I wish to thank especially W.G. Mathews, for having held a cycle of lectures on the *Broad Line Region* at the Padova Department of Astronomy, from which I learned so much.

Contents

Chapter 1

Introduction

Active Galactic Nuclei (AGN) share the following basic properties:

- a great bolometric luminosity ($L_{bol} \sim 10^{42}-10^{47} erg\ s^{-1}$) due to the presence of a strong, non-thermal continuum, which ranges from the radio to the hard-X ray domain and is emitted in a region of very small size ($d \ll 0.1pc$);
- the presence of strong emission lines ($L_{H}\alpha \sim 10^{39} - 10^{44} erg\ s^{-1}$), coming from a wide range of ionization states, with the exception of BL Lac objects.

The small size of the continuum emitting region implies that an extremely efficient mechanism is responsible for the luminosity output of AGN. The upper limit of the non-thermal luminosity of AGN, $10^{47}\ erg\ s^{-1}$, corresponds to a complete conversion of 1.7 $M_{\odot}\ yr^{-1}$into radiative energy. At the efficiencies of nuclear burning $\eta \approx 0.01$, this would mean that a mass of 250 $M_{\odot}\ yr^{-1}$is burned. In the hypothesis that the energy output is sustained by hot, young stars, the presence of $\sim 10^{7}$ O stars in a volume of $10^{-6}\ pc^{3}$ is required! The segregation of such amount of mass in this volume would lead to its collapse onto a massive, compact object. The conversion of gravitational potential energy into thermal and nonthermal energy is on the contrary more efficient ($\eta \sim 10$ %, and may reach 40 % in case of a rotating black hole), if the gas is constrained in an accretion disc and is accreting onto a compact massive object. The formation of an accretion disc is a likely event, provided that the angular momentum per unit mass exceeds a small critical value (see Appendix A). The presence of massive black holes at the center of galactic nuclei seems to be a common phenomenon also in non–active or weakly active galaxies. The main observational evidences are a central surface brightness too high to be described in terms of standard King models (*e.g.* Binney and Tremaine (1987)), and a *hump* in the stellar velocity dispersion, indicating that a large central condensation of mass is indeed present in some of the nearest galaxies, like M31, M32 and M81 (see the reviews by Kormendy (1988), Filippenko (1988) and Dressler (1989); and Filippenko and Sargent (1988) for M81). Masses of the order of $10^{6} - 10^{9}\ M_{\odot}$are required in

AGN for having a bolometric luminosity smaller than the Eddington luminosity, and are indirectly indicated by the observed line width ($\sim 10^5$ km s^{-1}) of the broad permitted emission lines (e.g. Woltjer, 1959), under the assumption that the lines are predominantly produced by the bulk motions of gas gravitationally bound to the central objects.

1.1 AGN classification

Various AGN classes are defined according mainly to the values of the following parameters (*e.g.* Lawrence, 1987):

- the bolometric luminosity L_{bol};
- the emission line width, from optical and uv spectroscopy;
- the ratio between the optical luminosity and the radio power;
- the polarization degree of the nonthermal continuum.

Seyfert galaxies are AGN of bolometric luminosity $L_{bol} \sim 10^{42} - 10^{44}\ erg\ s^{-1}$. They are divided in two subgroups according to the width of the permitted lines (Khachikyan and Weedman, 1974):

1. Seyfert 1 (hereafter Sey–1) galaxies have very broad permitted lines in the optical and ultraviolet spectrum, and narrower forbidden lines. Typical Full Width Half Maximum (FWHM) of the HI, HeI, HeII, CIII, CIV, MgII, and FeII lines are $\sim 2000 - 5000\ km/s$, and typical Full Width Zero Intensity (FWZI) values are $\sim 1 \cdot 10^4\ km/s \approx 0.03\ c$, with extreme cases ranging up to $3 \cdot 10^4\ km/s \approx 0.1\ c$. In this class the forbidden lines have FWHM $\sim 500\ km/s$, much less than that of the permitted lines. The optical spectrum of a typical Sey–1 galaxy is shown in Fig. (1.1).

2. Seyfert 2 (hereafter Sey–2) galaxies have permitted and forbidden lines with similar widths $\sim 400 km/s$. Extreme values are reached at $\sim 200\ km/s$ [1] and $\sim 1200\ km/s$ for NGC 1068.

Forbidden lines originating in ionization stages ranging from O^0, N^{+1} to Fe^{+6}, Fe^{+9} and in some cases to Fe^{+13} are observed in Sey–1 and Sey–2 galaxies.

[1] It is worth noting that this value of the FWHM cannot be considered *broad* in comparison with the value found for the absorption lines in normal galaxies. This value is common among objects which are otherwise indistinguishable from *classical* Sey–2 (Stauffer, 1982; Phillips *et al.*, 1983), for which the FWHM was generally $\geq 300\ km/s$. Hence, a criterion requiring that a Sey–2 galaxy should have emission lines FWHM greater than 300 km/s, that was widely applied in the past is no longer valid.

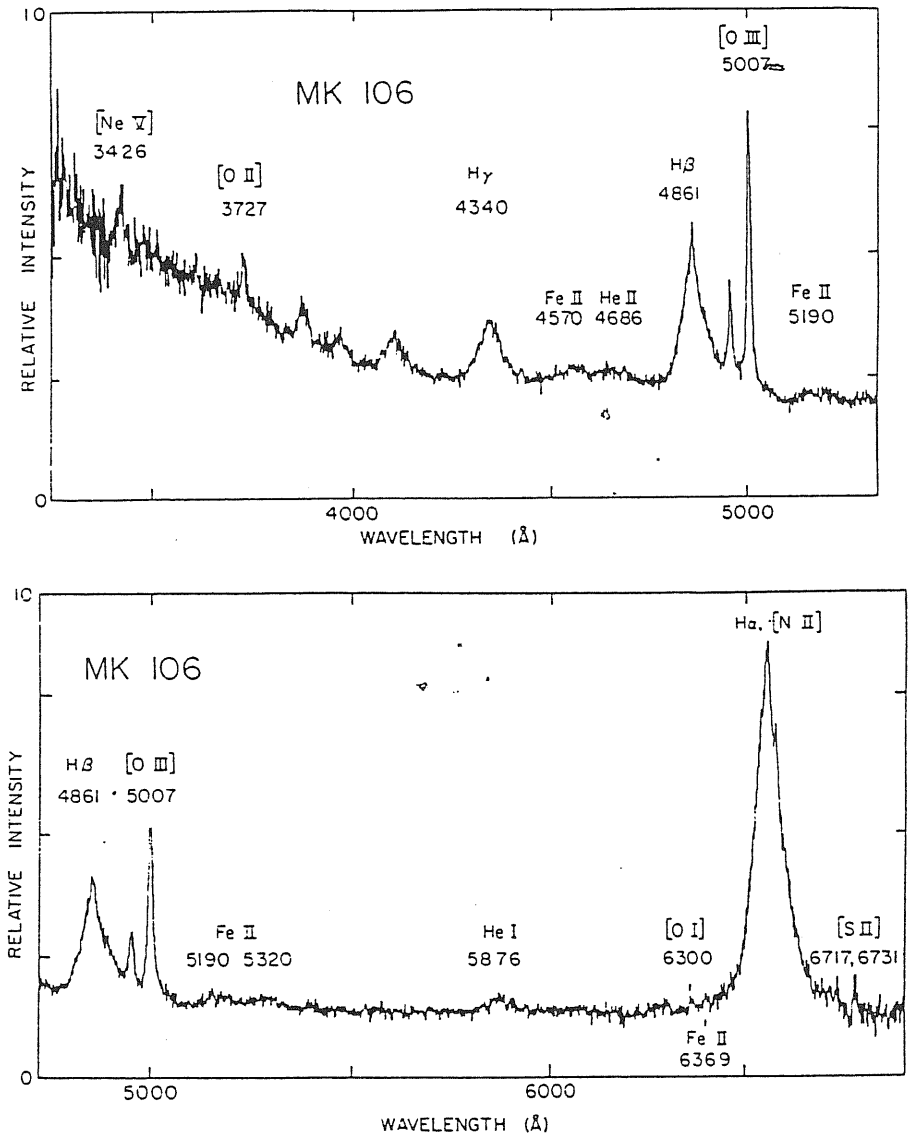

Figure 1.1: The optical spectrum of a Seyfert–1 galaxy. From: Osterbrock (1977)

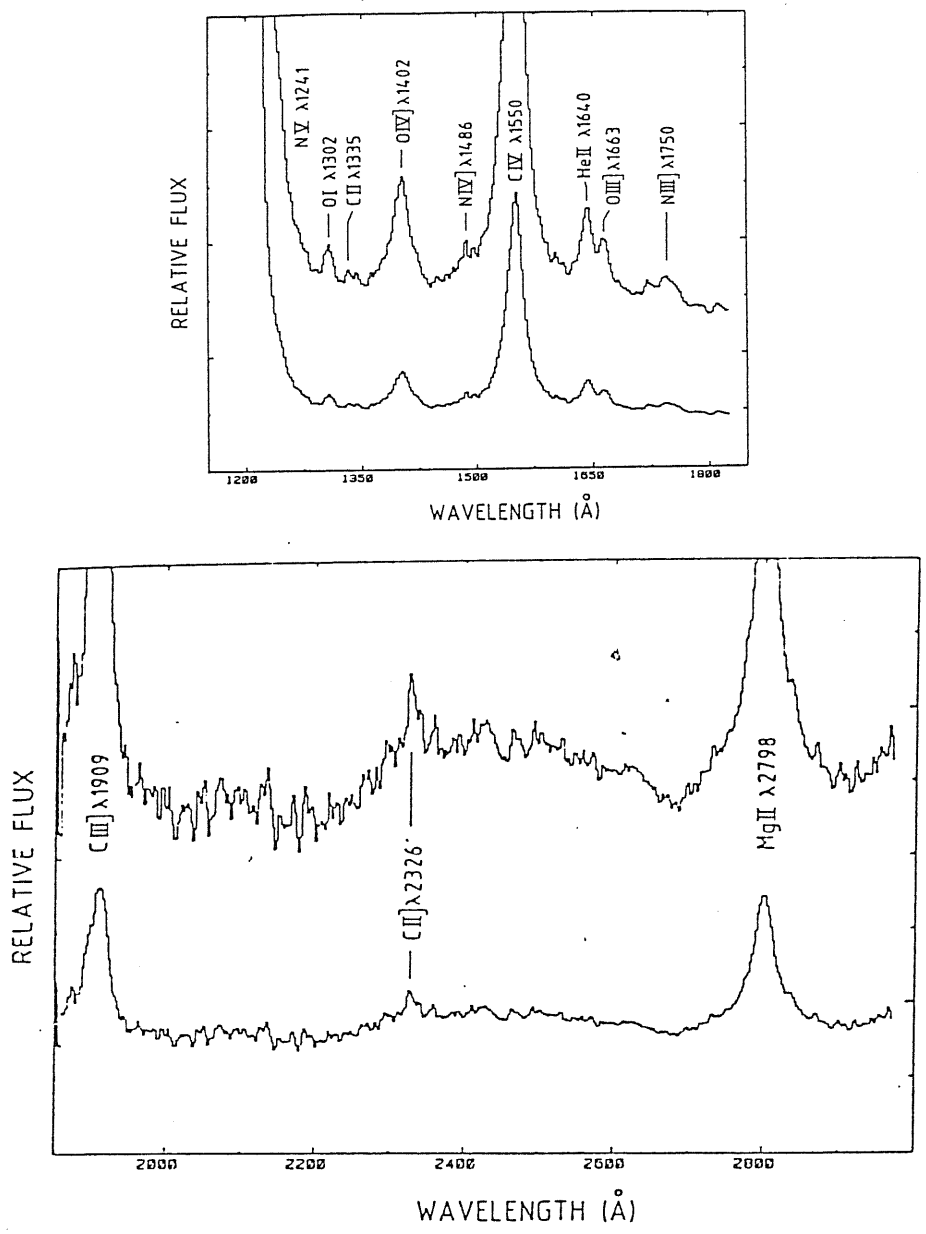

Figure 1.2: The average UV spectrum of Sey–1 galaxies. From: Veron–Cetty, Veron, and Tarenghi (1983)

Many Seyfert galaxies show a composite profile with a *narrow* permitted component superimposed over the broad profile of the permitted lines. A finer classification therefore involves the definition of *intermediate* Seyfert galaxies, according to the ratio of the Narrow to the Broad Component of the permitted Lines. Extrapolating this classification, Sey–2 galaxies can be regarded as intermediate objects that completely lack the Broad Component of the permitted lines. The ratio Narrow over Broad Component in *intermediate* types (Sey–1.5, Sey–1.8, Sey–1.9) correlates with the fraction of non thermal continuum f_{nth} (decreasing from 1 – 0.9 of Sey–1) (Osterbrock, 1981; Cohen, 1983) to the total observed continuum (i.e. nonthermal plus the underlying galaxian continuum). Intermediate objects are often strongly variable, but the fraction of *observed* nonthermal continuum at minimum, when sometimes the BC disappears, tends also to zero (Cohen *et al.*, 1988), and is inconsistent with the properties of Sey–2 galaxies, that have $f_{nth} \approx 0.4$. This suggests that *intermediate* objects should be regarded as Sey–1 subclasses rather than as objects in an evolutionary state between Sey–1 and Sey–2 objects (Miller 1988).

Seyfert galaxies are weak radio emitters: the radio power L_{radio} is $\sim 10^{-2} L_{opt}$, the optical luminosity. The radio–loud ($L_{radio} \geq L_{opt}$) counterparts of Sey–1 and Sey–2 galaxies are called respectively Broad Line Radio Galaxies (BLRG) and Narrow Line Radio Galaxies (NLRG), and are, morphologically, elliptical galaxies.

The emission line spectra of BLRG are similar to those of Sey–1, but some typical differences can be pointed out:

1. the spectra of lobe dominated BLRG, in contrast to Sey–1 galaxies, do not show detectable FeII emission blends or if present it is very weak (Osterbrock, Koski and Phillips, 1976; Osterbrock, 1977; Boroson and Oke, 1984);

2. the Balmer decrement is generally steeper in BLRG than in Sey–1 galaxies (Osterbrock, 1977; 1978; Grandi and Osterbrock, 1978);

3. the $[OIII]\lambda 5007/(H\beta)_{NC}$ ratio is greater in BLRG than in Sey–1 galaxies (Osterbrock, 1978). This may be due to an aperture effect: it is known that BLRG show extended, *Extranuclear Emission Line Regions (EELRs)*, whose spectrum is characterized by very high excitation degree ($[OIII]\lambda 5007/H\beta \gg 1$)(see, e.g. Robinson *et al.*, 1987, and below), and which are less common in Sey–1 galaxies (Rafanelli, 1989). Since most data were collected with large aperture, the EELRs contribution could have enhanced the $[OIII]\lambda 5007/H\beta$ ratio for the BLRG. This should however be checked through two-dimensional spectroscopy of a large sample of Sey–1 and BLRG.

All of the different properties between Sey–1 and BLRG listed above must however be considered as strong correlation, but not as absolute distinctions: for

example the Sey–1 galaxy IV Zw 29 has an optical spectrum identical to that of a BLRG. Conversely, the optical spectra of NLRG are indistinguishible from those of Sey–2 galaxies (Koski, 1978; Cohen and Osterbrock, 1981).

Quasi Stellar Objects (QSOs) and Quasi Stellar Radio Sources (quasars) are the analogues of Sey–1 galaxies and BLRG respectively, except that the features due to the underlying galaxy are not easily detectable in their optical image or spectrum.

They seem to represent the most luminous ($L_{bol} \geq 10^{45}\ erg\ s^{-1}$) examples of the same general phenomenon. This is supported by several hints:

1. the surrounding envelope due to the underlying galaxy has been detected in many nearby QSOs (Hutchings, 1983);

2. the optical and UV spectra of QSOs are very similar to those of Seyfert galaxies (*e.g.* Veron–Cetty, Veron and Tarenghi, 1983; Wampler *et al.*, 1984; Chen and Fang, 1987);

3. the luminosity function of Seyfert galaxies joins smoothly that of optically selected QSOs (*e.g.* Weedman, 1985).

High polarization objects (*blazars*) are only $\sim 1\%$ of quasars. They are grouped in two subclasses: BL Lac objects and Optically Violent Variable (OVV) QSOs. Among them, BL Lac objects are the most enigmatic. They have many extreme properties, as rapid variability, core dominated radio fluxes, high polarization and a continuum dominated by a featureless continuum, with little or no contribution due to the *Big Bump* (see Chapter 2). Emission lines are weak or absent, making difficult even the redshift determination. OVV QSOs have emission lines which remain almost constant while the continuum can vary up to a factor 100 (Angel and Stockman, 1980). These properties can be explained qualitatively by assuming that most of the observed flux is relativistically beamed toward us. Hence the continuum we observe is not the same that the BLR see. These objects are therefore not suited for the determination of the velocity field producing the line broadening, and will not be further considered in this work.

It seems therefore justified to refer to Seyfert galaxies, radio galaxies and Quasars as a unique class of objects, although some *second order* differences in the optical and ultraviolet spectrum seem to be present. The differences concerning the emission line profiles will be extensively discussed in Chapter 2. In this work, we will be mainly concerned with AGN which show a Broad Component in the permitted lines. It may be useful to call these objects *Broad Line Objects* or *type 1 objects*, (BLO), and *Narrow Line Objects* (NLO) or *type 2 objects* the Sey–2 galaxies and NLRG.

BLO and NLO differ markedly in bolometric luminosity (L_{bol} of Sey–1 and BLRG is typically a factor $\sim 10^2$ larger than that of Sey–2 and NLRG), and in their statistical properties: Seyfert galaxies and Radio Galaxies show more

frequently *type 2* spectra than *type 1*, with a ratio $\sim 2:1$ (Stauffer, 1982; Baldwin *et al.*, 1983), while only few QSO [2] show an emission spectrum of *type 2*. This may be due to a selection effect, since *type 2* AGN are generally a factor ~ 100 less luminous than *type 1*. The difficulty of finding optically selected type 2 AGN increases with distance. When a critical distance is reached, only the more luminous type 1 AGN are sampled.

1.2 A heuristic model of the BLR

The basic features of the emission line spectrum have led to single out two distinct emitting regions:

1. the *Narrow Line Region* (NLR), where the Narrow Components of the Balmer lines and the forbidden lines arise. The electron density n_e and the electron temperature T_e can be measured on the basis of several diagnostic line ratios (*e.g.* Aller, 1984). The line ratios most commonly used are [SII]λ6717/λ6731 and [OIII] $\lambda\lambda$5007+4959/λ4363. They give the following mean values: $T_e \simeq 10^4\ ^\circ K$ and $n_e \sim 500 - 1000\ cm^{-3}$. The emitting gas is located at $\sim 100 - 1000\ pc$ from the central source.

2. the *Broad Line Region (BLR)*, which emits the Broad Component of the permitted lines; for the BLR we lack any spectral diagnostic both for electron temperature T_e and density n_e. T_e is $\approx$ a few $10^4\ ^\circ K$, otherwise the iron should be two times ionized. The lack of any strong broad component in the forbidden lines implies that the value of n_e is larger than $10^7 cm^{-3}$ (the critical density of [OIII]λ5007), while the presence of the broad semi–forbidden CIIIλ]1909 line implies that n_e is less than $10^{9.5} cm^{-3}$

Yee (1980) and Shuder (1981) found that the luminosity of the Balmer Lines is proportional to the optical continuum luminosity at $\lambda \approx 4800$ Å, over eight order of magnitude of the continuum luminosity (see Fig. 1.3). This suggests that photoionization by the non–thermal continuum and recombination are the processes which produce the permitted lines.

Restricting our discussion to the BLO, the presence of the MgII λ2800 line moreover implies that the emitting gas is optically thick to the Lyman continuum. Under these assumptions, each Lyman continuum photon absorbed by the gas is transformed in radiation of lower energy and in a Lyα photon (see, *e.g.* Osterbrock, 1974).

The covering factor, defined as the fractional area of the sky subtended by the gas as viewed from the center, will be given by the ratio of the total Lyα photons

[2] A currently underway survey by Baldwin and collaborators has enhanced the number of known quasars with Sey–2 type spectrum, but their results have not been yet published.

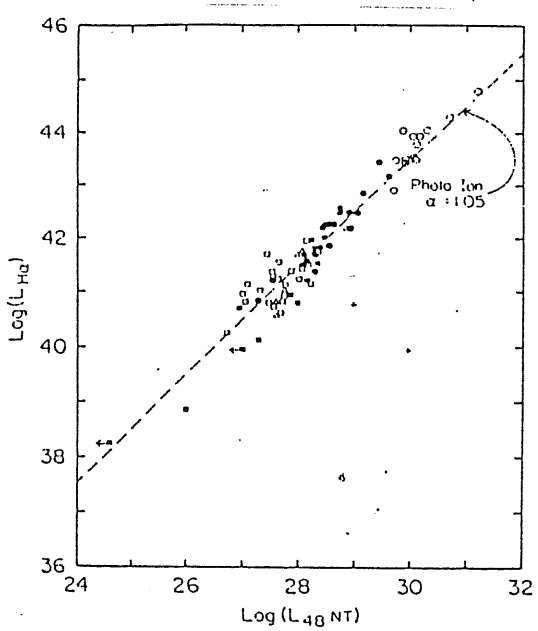

Figure 1.3: log Hα luminosity ($erg\ s^{-1}$) versus logarithm of the continuum luminosity at λ 4800 ($erg\ s^{-1}Hz^{-1}$). Open circles: QSOs, Filled circles: Sey–1 galaxies. The correlation expected if the ionizing source is provided by a power-law continuum with spectral index $\alpha = 1.05$ is shown by the dashed line. From: Shuder (1981)

to the number of photons emitted in the Lyman continuum:

$$f_c = \frac{Number\ of\ Ly\alpha\ photons}{Number\ of\ Ly\ continuum\ photons\ +\ Number\ of\ Ly\alpha\ photons} \tag{1.1}$$

The value of f_c obtained with this method is ≈ 0.1. Moreover early observations of high redshift quasars showed that the fraction of the continuum absorbed shortwards of the Lyman limit was around 10 %, confirming the previous estimate of f_c.

The ionization parameter Γ is defined as:

$$\Gamma = \frac{\int_{\nu_0}^{\infty} L_\nu d\nu}{4\pi R^2 c n_e} = \frac{density\ of\ ionizing\ photons}{electron\ density} \tag{1.2}$$

where ν_0 is the Rydberg frequency, L_ν is the luminosity at frequency $\nu > \nu_0$ and R is the distance between the BLR gas and the central source of ionizing photons. The observed ratio CIII]/CIV is explained for $\Gamma \approx 0.01$. The knowledge of Γ allows to employ the previous relation for deriving a first estimate of the BLR distance from the central source: $R \simeq 3 \cdot 10^{18}(L/(10^{46} erg\ s^{-1})^{1/2})$, for $\Gamma \approx 0.01$ and $n_e \approx 10^{10}\ cm^{-3}$.

Moreover detailed photoionization calculations (discussed in the next section) suggest that the column density is $N_c \sim 10^{22} - 10^{23} cm^{-2}$.

The value od N_c, coupled with the electron density deduced above, implies that the size of the emitting element is $r_e \approx 10^{12} cm$, much less than the distance R of the emitting regions from the central source.

The ratio of the emitting volume to the total volume (the *filling factor*) is given by:

$$f_f = \frac{f_c N_c}{n_e R} \sim 10^{-6} \ll 1 \tag{1.3}$$

Due to the estimate of a small filling factor and the size of the emitting element r_e smaller than R, the Broad Line flux is often regarded as *the collective emission from a large number of small clouds that fill only a small fraction of the total volume* (Mathews and Capriotti, 1985).

The thermal width of a line emitted by a single cloud is $\approx 4\ km\ s^{-1}$; hence at least 10^4 clouds are needed for explaining the observed width of the broad lines. The total number of clouds is probably much larger, since the profiles are generally smooth and do not show any irregularity for time scales of years.

This view of the emitting regions is a useful framework, but it is very simplified, and does not account for many observed features. The physical conditions of the BLR will be discussed more thoroughly in the next section, while Chapter 3 is devoted to an analysis of the BLR kinematics.

1.3 Theory of line formation

The observational and theoretical knowledge led to the *heuristic* model described earlier, in which a roughly spherical ensamble of many, small optically thick gas clouds undergoing rapid motion under (for now) unspecified acceleration mechanism, is photoionized by a powerful, non–thermal continuum source. The proportionality between line and continuum emission (Yee, 1980; Shuder, 1981) strongly suggests that photoionization followed by recombination is the main excitation mechanism for the BLR gas. Photoionization explains also why we see high ionization species such as C^{+3} and N^{+4}, while the temperature is not larger than $\approx 2 \cdot 10^4\ ^\circ K$ (*e.g.* Davidson and Netzer, 1979).

In this framework, the *standard model* (Kwan and Krolik, 1981, hereafter KK; Kwan, 1984) computes the line emergent flux from a single cloud of given chemical composition under the assumption of plane–parallel geometry.

Starting from the illuminated surface of the slab, the ionization, thermal and pressure equilibria are solved at each point. Simultaneously, the excited state population is also self–consistently computed for the HI, OI, HeI and FeII atoms. The continuum and line radiation transfer is treated computing at each optical depth a mean local escape probability (averaged on the line profile), which measures the probability that in a semi–infinite plane–parallel medium a line photon emitted toward the surface at a point of optical depth τ_0 escapes without undergoing subsequent scatterings.

The main physical processes entering the ionization balance are ionization both by radiative and collisional processes. Radiative processes include ionization from the ground state end excited states of HI atoms by incident and diffuse

Lyman continuum photons, spontaneous and induced recombination, ionization by incident hard UV and X radiation. Collisional processes involve collisional ionization from HI excited states by thermal electrons, and ionization from the ground state by non–thermal electrons, dielectronic and three body recombination and charge exchange processes (the last four processes were not included in the original KK work). Five main inputs are necessary: the ionization parameter Γ, the electron density n_e at the illuminated surface of the cloud, the shape of the photoionizing spectrum, the column density and the chemical composition. The final results are reached by fixing the column density at which a set of reliable line fluxes is obtained.

Near the illuminated surface of the cloud, the ionizing continuum creates a regions where the hydrogen is completely ionized (HII zone). The ionization structure at larger optical depths of the slab is of basilar importance for understanding the emitted fluxes: proceeding further in the cloud, after the Lyman continuum is exhausted, X–rays ionization of He, H and heavy element becomes the main source of heating. At high energy photoionization of heavy ions can dominate the opacity. X–rays will produce high energy electrons, which loose their energy via the following processes:

1. Coulomb collisions, directly heating the gas,

2. collisional ionization, yielding secondary electrons,

3. excitation of bound levels, especially of H^0, leading to line radiation.

If these effects are considered, a *Partially Ionized Zone* (PIZ) develops, with $H^+/H^0 \approx 0.1$ and $T \approx 8000\ ^\circ K$. This zone emits a strong contribution in the Balmer lines, the Mg II $\lambda 2800$ and the FeII lines and the Balmer continuum (Halpern and Grindlay, 1980; KK) (see Fig. 1.4)

Photoionization calculations are able to explain the observed line ratios within a factor of 2. Particularly the wide range of ionization species observed in the AGN spectrum are readily accounted for: the HII region emits the bulk of the high ionization lines, like CIV $\lambda 1549$, Lyα, NV, OIV, whether the PIZ allows to have simultaneously the presence of the MgII, FeII.

Despite this success, several problems remain to be solved in order to get a satisfactory agreement with the observations. The most important ones are:

- the Lyα problem. It is known that the expected value of the ratio Lyα/Hβ, under case B conditions and for density higher than $1.6 \cdot 10^4 cm^{-3}$, where $2s \longleftrightarrow 2p$ levels are collisionally exchanged in spite of the 2–photon continuum (*e.g.* Osterbrock, 1974; Netzer, 1982), is ≈ 34 and decreases at a minimum value ~ 23 to $T \sim 10^4\ ^\circ\ K$ as $n_e \rightarrow 0$.

  At sufficiently large optical depth Lyα is thermalized and a significant amount of hydrogen is sustained in excited states. If the heating rate

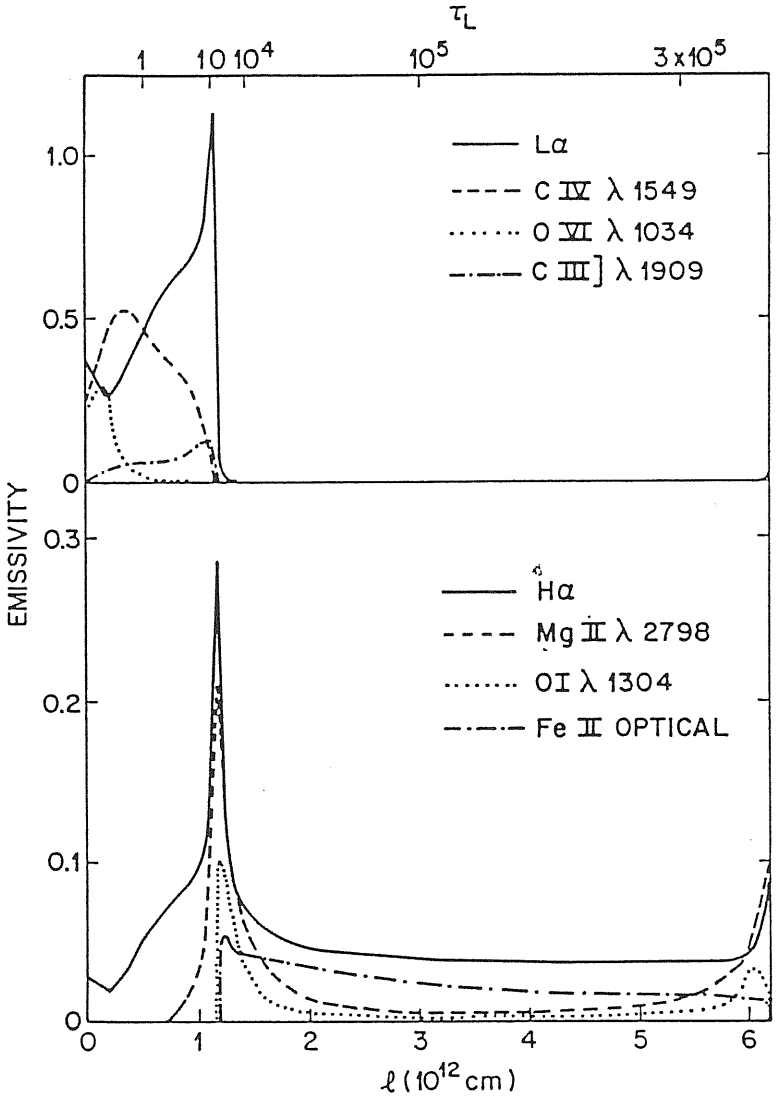

Figure 1.4: Ionization structure of an X–ray heated slab. From: Kwan and Krolik, 1981

remains appreciable collisional excitation of Hα, Hβ competes against collisional excitation of lines of heavy elements for the available energy. Thus the Balmer lines are enhanced where Lyα is saturated, reducing the Lyα/Hβ ratio from the case B to the observed value. In facts, the KK model and its refinements were able to explain for the first time the very low ratio Lyα/H$\beta \approx$ 5 observed.

This problem remains however unresolved, since KK employed a continuum with a too strong X–ray component which is rarely observed. For instance, Zamorani *et al.*, 1981 (see §1 of Chapter 2) found a spectral index $\alpha_{oX} \approx 1.3$, which results in a ratio of the flux at 2 keV over the flux in proximity of the Lyman edge $F_\nu(2keV)/F_\nu(Lycont) \approx 6$) times smaller than the KK continuum.

- The reddening problem: it is unclear whether internal reddening in the BLR gas is able to play a role appreciably in affecting the observed line ratios. Although the observed line ratios seem to generally exclude E(B–V) larger than 0.2, it seems more likely that the dust content is strongly variable from object to object. In the most extreme case, Mkn 739, the UV continuum is detected without the presence of any UV emission line, while the optical spectrum is nearly normal for a Sey–1.5 galaxy (Netzer, Kollatschny and Fricke, 1987; Rafanelli *et al.*, 1989) The problem is made difficult by the lack of any reliable reddening indicator: the sole line ratio HeII λ4686/ λ1640 avoids optical depth effects, but is very difficult to estimate (Netzer, Elitzur and Ferland, 1985; Grandi 1983).

- The FeII problem: photoionization models yield a FeII to hydrogen line ratio about a factor 3 smaller than the average observed one; a better agreement is obtained when very high density ($n_e \geq 10^{12} cm^{-3}$) and large column densities $N_c \approx 10^{25} cm^{-2}$, in order to allow a significant absorption of X–ray radiation in the range between 10 and 200 keV (Collin–Souffrin, *et al.* 1986; Collin–Souffrin, 1988; Wills, Netzer and Wills, 1985). It remains unclear whether the strength of the FeII lines can be *entirely* explained by radiation transfer effects in a dense medium, or whether chemical abundances above solar are necessary (Collin–Souffrin, 1986).

- The presence of optically thin gas is demonstrated by the presence of Lyβ in high redshift quasar spectra, but it is not clear whether optically thin gas emits a considerable contribution to the lines.

  The OI λ8446 line is emitted via a Bowen fluorescence mechanism by gas very optically thick to Lyα (Elitzur and Netzer, 1985). It has the same profile of Hα, which can be emitted both by optically thin and optically thick gas (Morris and Ward, 1989). Only two objects among the 12 studied

by Morris and Ward (1989), Akn 120 and IC 4329A, show profile differences, in the sense that Hβ has a stronger blue wings than OI λ8446.

This implies that usually optically thin gas is not present or it follows the same velocity field as the optically thick gas.

The last two problems and other hints suggest that the observed spectrum cannot be reproduced in terms of a unique emissive medium:

- Gaskell (1982) has found that the high ionization lines (HIL) are systematically blueshifted by several hundred of $km\ s^{-1}$ with respect to the Balmer lines and to the other low ionization lines (LIL); moreover, Ulrich *et al.* (1984) found that various broad lines react to changes in the ionizing continuum with different timescales, providing an other evidence that the excitation level of the emitting gas is kinematically and spatially variable (Mathews and Wampler, 1985). Although the analysis of Ulrich *et al.* (1984) is strictly valid only under the assumption that the lines considered respond in the same way to the continuum changes, the profile differences described in the third Chapter confirm that there is a connection of the ionization levels with the kinematics of the BLR gas.

  The *single cloud* model is inconsistent with these findings, since regions in different kinematical conditions are likely to come from spatially distinct regions (see §1 of Chapter 3).

- It is difficult to explain the observed spectrum in terms of a unique value of the ionization parameter; very high ionization lines NV λ1240 and OVI λ1034 favour $\Gamma \approx 0.03$, while the CIV/Lyα and CIII]/Lyα favour $\Gamma \approx 0.01$. The strength of the FeII lines indicates that Γ should be $\ll 0.01$.

- The $H\alpha/H\beta \approx 2 - 3.5$ ratio would be better explained if dense, optically thick gas is present. If the density is very high, $n_e \sim 10^{12} cm^{-3}$, then the optical depth on the Paschen continuum would led to the selective suppression of Hα, thus decreasing the Hα/Hβ ratio.

- the CIII] line requires a density $\leq 10^{9.5} cm^{-3}$.

A correct treatment of the line formation problem may therefore require that both high numerical and column densities are taken into account. High numerical densities require an adequate treatment of the excited state population balance for a large number of new ionic species (C^{+2}, C^{+3}, N^{+4}, Si^{+4}, Mg^{+2} (Krolik, 1988b) since more and more ground state transitions are thermalized. High column densities imply an accurate treatment of the line transfer. The mean escape probability may not be valid, since the non-local absorption will affect photons coming from a large number of transitions. Large part of this work remains to be done.

These facts have however led Collin–Souffrin (*e.g.* Collin–Souffrin and Lasota, 1989) to propose that the BLR is made up of two spatially distinct regions: a dense region, emitting the bulk of the LIL, and a second region, characterized by the same physical parameter of the standard model, mainly contributing to the HIL. The advantages and the handicaps of this model are discussed in Chapter 2.

1.4 The mass of the central object and the Eddington ratio

Under the assumption that the BLR are inflowing toward the center of the active nucleus, the virialized mass M of the central object can be written as:

$$M = \frac{v^2 R}{2G} \tag{1.4}$$

where v is the velocity of the emitting gas, R its distance to the center, and G the gravitational constant. In practice, this relation can be used in several ways in order to estimate the central mass. Padovani and Rafanelli (1988) computed the mass from the observed highest velocity of the emitting gas. In the framework of infall, the gas should move at the inner radius of the BLR, R_{in}. R_{in} can be deduced by the ionization parameter Γ, and v_{max} by the FWZI on the Hβprofile. Padovani and Rafanelli (1988) and Padovani (1989) found a strong dependence of the Eddington Ratio on the redshift z:

$$\frac{L_{bol}}{L_{Edd}} = 10^{-0.8\pm0.5} \; for \; Sey-1 \; galaxies \tag{1.5}$$

$$\frac{L_{bol}}{L_{Edd}} = 10^{-0.4\pm0.3} \; for \; low \; z \; quasars \tag{1.6}$$

$$\frac{L_{bol}}{L_{Edd}} = 10^{0.5\pm0.4} \; for \; high \; z \; quasars \tag{1.7}$$

This result deeply disagrees with the findings by Wandel and Yahil (1985), who concluded that the derived masses are directly proportional to the observed luminosities of the optical nonstellar continuum. According to their work, all AGN would radiate at $\approx 0.01 L_{Edd}$.

It is not easy to understand why so different conclusions are reached, since both studies apply the same hypotheses regarding the kinematics.

Clearly, the Eddington ratio estimates and its dependence on luminosity may have no physical meaning if the assumption about the kinematics is wrong, or also if the dominant forces responsible of the gas acceleration vary among the objects of the samples with luminosity or with some other relevant (unknown) physical parameter. There is no way at present to overcome these problems.

Regarding the work by Padovani and Rafanelli (1988), several effects may cause an underestimate of the mass, and hence an overestimate of the Eddington ratio: the most important ones are probably related to an underestimate of the FWZI, but it is uneasy to think that the FWZI is selectively underestimated in high– luminosity objects. Moreover, if the dominant motion is rotation instead of inflow the mass increases by a factor of two.

The presence of a thick disc around the central black hole is expected because of the super–Eddington luminosity of high–z quasars. Since anisotropic radiation emission is a direct consequence of this fact, the method employed for computing the bolometric luminosity is not self–consistent with the results.

These sources of uncertainties, taken together, should however not alter the general trend.

Even more severe uncertainties affect the computation by Wandel and Yahil (1985). They used a slightly different form of the equation used by Padovani, which can be obtained substituting $R \approx f_c N_c / f_f n_e$: $M \propto (L_{H\beta}/n_e f_c N_c)^{1/2} v^2$, with the usual meaning of the symbols. They suppose that $f_c \approx 1$ if $L < 2 \cdot 10^{43} erg\ s^{-1} = L_1$ and $f_c \propto L^{-0.2}$ if $L > L_1$ where L is the continuum luminosity at 4000 Å (Mushotzky and Ferland, 1984; Kinney *et al.*, 1985). There is no direct way to confirm this assumption, which in turn strengthens the correlation between mass and luminosity: since $V \propto L^{0.2}$ (Joly *et al.*, 1985) and $L_{H\beta} \propto L$ (Shuder, 1982), we have $M \propto L$, and this *may* account for the result obtained by Wandel and Yahil (1985). Padovani and Rafanelli (1988) instead assumed, in order to compute R, that the product (Γn_e) does not depend on luminosity, and this seems a more likely condition.

The results by Padovani are in agreement with the mass evaluation based on the *Big Bump* emission, described in Chapter 2. Although also the latter method suffers great problems, it allows to obtain the same qualitative dependence on luminosity for the Eddington ratio; hence, in the following, we will assume that *Sey–1 galaxies radiate sub–Eddington, while intermediate and high–redshift quasars radiate near to the Eddington limit, or radiate super–Eddington.*

1.5 Further clues to the nature of the central engine

Excluding Blazars and BAL QSOs, AGN typically show a low polarization degree of the optical and UV nonstellar continuum. Seyfert's continuum is only 2% and 1% polarized in class 2 and 1 respectively. The polarization position angle of the optical continuum is nearly perpendicular to the direction of ejection of the radio axis in Sey–2, while it is parallel in Sey–1 galaxies (Antonucci, 1983; Miller and Antonucci, 1983). If the radio axis lies close to the axis of a central obscuring disc, scattering material would indeed produce polarization at right angles to the axis of the disc. This result has been extended by the important finding

that the spectrum of NGC 1068, the *prototype* Sey–2 galaxy, has a polarized spectrum which is very similar to a Sey–1 type galaxy, with broad permitted lines and FeII emissions. This means that we would infer a much higher optical luminosity NGC 1068 and call it a Sey–1 galaxy, if we would observe it from a direction roughly aligned with the radio axis (Antonucci and Miller, 1985; Miller, 1988). Subsequent work (Miller, 1988) has shown that nearly half of the Sey–2 galaxies observed by Miller and collaborators have obscured broad lines, which are detected only in polarized light. Miller and Antonucci interpret their data suggesting that in the nuclei of Sey–2 galaxies*a thick disc of absorbing material (most probably dense molecular matter) is located beyond the BLR and restricts the view of the continuum source and of the Broad Line Clouds.* Light emerging above the disc encounters hot electrons which scatter the light of the Broad Line into our line of sight.

Further indications on the nature of the *central engine* may be gained considering the effects that the energy output of the AGN can have on the host galaxy. They have become an important subject of investigation in recent times, following the detection of *Extended Emission Line Regions* (EELRs) in many Seyfert, Radio Galaxies, and Quasars. The excitation mechanism has been proved to be due to direct photoionization from the active nucleus in Quasars (Stockton and McKenty, 1987) and Radio Galaxies (Baum and Heckman, 1988; Baum *et al.*1988; Tadhunter *et al.*, 1989; Robinson *et al.*, 1987). In Seyfert galaxies the ionization source is also provided by the active nucleus in many cases (Baldwin, Wilson and Whittle, 1987; Haniff, Wilson and Ward, 1988; Corbin, Baldwin and Wilson, 1988; Pogge 1988, among the most recent works), but it also may be provided *in situ* by hot, young stars (see Heckman 1987, for a recent review), or in a few cases, by shock–heating (for example NGC 6240; Fried and Schulz, 1983). The extent, the kinematics, the excitation conditions and the correlation with the radio morphology of the gas constituting the EELRs, are valuable for probing the mechanism that powers the active nucleus itself. Restricting the attention to EELRs whose gas is photoionized by the active nucleus, the analysis of the EELRs properties has supplied some evidence that *the ionizing continuum is not radiated isotropically*:

- The [OIII] λ5007 emitting gas is extended over a $\sim$ kpc– sized scale, and is located in elongated, cone shaped structures (Pogge, 1988; Haniff, Wilson and Ward, 1988). The elongation axis of the [OIII] emission is *often* aligned with the radio axis (Baum and Heckman, 1988), but for the majority of quasars and radio galaxies the position angle differs by more than 15°. *Ionization maps* reveal also that the axis of the cone shaped structures is often not aligned with the minor axis of the galaxy (Tsvetanov *et al.*, 1989).

- Wilson *et al.* (1988) found an *energy budget problem* for the EELRs. The observed continuum is not able to produce the emission line luminosity in the EELRs. A similar result was also reached by Rafanelli *et al.* (1989),

who found that the high excitation degree observed in the EELRs of Mkn 423 cannot be sustained by the *observed* ionizing continuum. However, they found that, if the continuum is corrected for reddening, the disagreement is greatly reduced.

A possible objection to the anisotropy idea is that, as noted above, there is a great uncertainty in what the real shape of the ionizing continuum would be, but so stated, these findings can be regarded as a compelling evidence in favour of anisotropy in the emission of the ionizing continuum.

The effects outlined above can be related to the intrinsic mechanism of the *central engine* (*e.g.* presence of a thick accretion disc; Acosta–Pulido *et al.*, 1989), but a definite probe remains conditioned to a thoroughly analysis of the role that absorbing or reflecting material, located in proximity of the active nucleus can play in attenuating the ionizing continuum. In Sey–2 galaxies, the presence of an obscuring torus between the BLR and the NLR has been discovered, and this provides a suitable collimation mechanism.

If Sey–1 nuclei radiate sub–Eddington, the presence of a thin accretion disc is expected; a suitable collimation mechanism may be offered by the inflation of the inner disc due to a thermal instability (Pringle, Rees, Pacholczyk, 1973). The situation is however less clear for Sey–1, since they *do not* show EELRs with the high frequency as Sey–2 and radio galaxies do (Rafanelli, 1989).

The paucity of EELRs in Sey–1 galaxies can be explained if the covering factor f_c approaches unity. In this case, most ionizing radiation would be absorbed in the BLR, and would be unable to reach the distances at which the EELRs are observed. This could explain also why the [OIII]λ5007/Hβ (narrow component) ratio is systematically much lower in Sey–1 galaxies than in Sey–2 galaxies.

It is known that low luminosity AGN show more often considerable X–ray absorption than high–luminosity AGN (*e.g.* Turner and Pounds, 1989; Kruiper, Urry and Canizares, 1989); on the basis of the observed soft ($h\nu \leq 1\ keV$) X–ray absorption (see § 1 in Chapter 2), Mushotzky and Ferland (1984) have proposed that f_c depends on luminosity as $\propto L^{-0.2}$. Holt *et al.*(1980) suggest that $N_c \sim 6 \cdot 10^{22} cm^{-2}$ covers $\approx$ 90 % of the source in NGC 4151. $f_c \approx 1$ is consistent with a spherically symmetric geometry, where the absorbing gas covers a large fractional area.

The situation is intrigued by the constancy of the EW of the Balmer Lines with increasing luminosity, since this finding implies on the contrary that the covering factor *does not* depend on luminosity. Moreover, $f_c \approx 0.17$ is necessary for explaining the observed EW of Hβ. The fact that f_c does not vary over the wide range the results by Shuder (1982) apply, means that the geometry of the BLR should be very regular, and a disc or a flattened configuration are the most suitable.

Fabian *et al.* (1986), and Perola *et al.* (1986) moreover state that X–ray absorption is a spherically symmetric configuration is extremely unlikely for the

BLR. These findings, considered together, have led to the idea of a flattened geometry for the BLR. Osterbrock (1979) indeed proposed a *cylindrical configuration* for the BLR, whose plane of symmetry is not necessarily coincident with the plane of the galactic disc (Tohline and Osterbrock, 1982). The finite thickness of the cylinder is due to the vertical turbulent velocity of the BLR clouds. This is necessary for explaining why there are no Seyfert 1 galaxies with broad lines narrower than $10^3\ km\ s^{-1}$. Projection effects and combination of rotational and turbolent velocity thus account for the observed spread in line width among BLO. The origin of the discrepancies in the f_c estimates remains unclear, but some interesting considerations in this regard are also made in the next Chapter.

Chapter 2

Continuum and Line emission from the Accretion Disc

The observations of the ionizing continuum of AGN are briefly reviewed. The importance of the *Big Bump* for supporting the presence of an accretion disc surrounding a central massive black hole are discussed. The physical conditions in the outer region of the disc are exploited, in order to establish whether the disc is able to emit some contribution to the emission line spectrum.

2.1 Observations of the ionizing continuum

There are three major regions of the AGN continuum which have not been observed or observed only in a few objects:

- the millimeter–submillimeter band (0.1 – 1 mm);
- the γ ray domain ($h\nu > 100keV$) (Bassani *et al.*, 1985);
- the Extreme Ultra–Violet (EUV), from $\sim$ 100 to 1000 Å.

The last region will remain unobservable, since it is not possible to eliminate the effects of interstellar absorption in our own galaxy. The only way to overcome this difficulty is to select high redshift objects, extrapolating the observed slope to zero redshift.

Two major facts result from multifrequency observations of AGN:

1. the *average* spectral shape of AGN is described by a power–law:

$$F_\nu \propto \nu^{-\alpha} \tag{2.1}$$

with the spectral index α ranging between $\sim 1 - 1.5$.

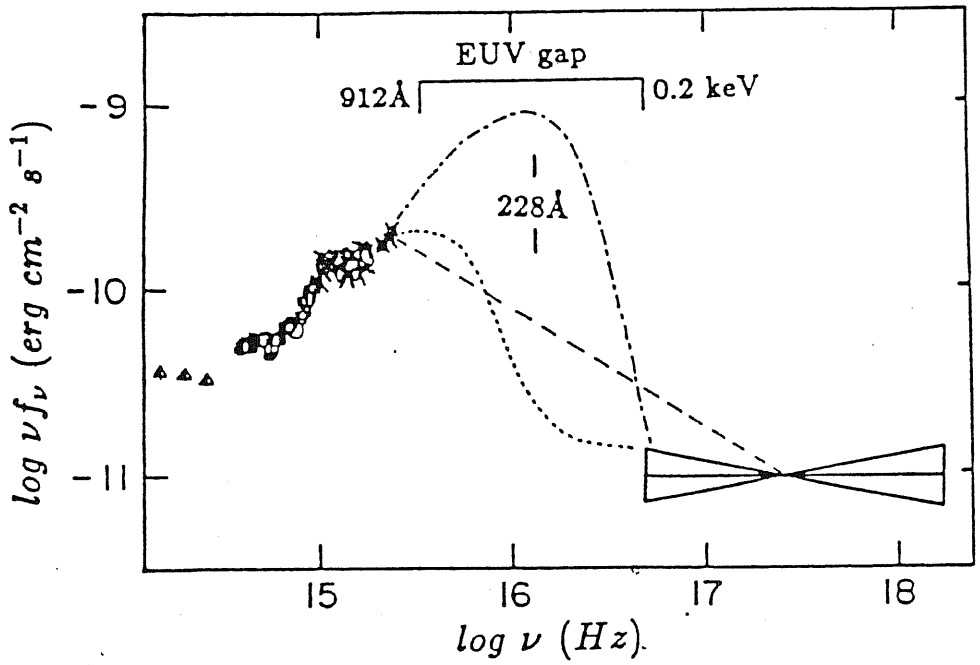

Figure 2.1: The continuum of PG 1501+106 from 2 μm to 7 keV. From: Elvis (1989b).

2. a broad feature is superimposed on the power–law continuum (the *Big Bump*), spanning from $\approx 1\mu$ to the soft X ray range. Malkan and Sargent (1982) and Malkan (1983) argued, before the frequency extension of the Big Bump was fully understood , that it was due to thermal continuum coming from an accretion disc.

3. A *little Bump* is superimposed to the *Big Bump* and to the power–law continuum between 4000 Å and 2000 Å. This feature is due to Balmer continuum emission, blends of high order Balmer lines and blends of FeII lines (Wills, Netzer and Wills 1985). It is interesting to note that the *Big Bump* was discovered because of the continuum flattening around 4000 Å, which is mainly connected to the *Little Bump*, before the contribution of the ultraviolet multiplets of FeII to the *Little Bump* was accounted for.

Figure (2.1) shows the continuum of the QSO PG 1501+106 from the near infrared to the soft X–ray range. Fig. (2.1) emphasizes the importance of the EUV continuum, which is the continuum lying nearest to the ionization edge of hydrogen, and of its correct extrapolation for estimating the *Big Bump* extent.

Although strong blended absorption features revealed in high redshift objects shortwards of the Lyman edge make uncertain the continuum shape shortwards of

1200 Å, present data seem to exclude large change of slope (O'Brien, Gondalhekar and Wilson, 1986, Bechtold *et al.*, 1984).

On the high energy side, The *Big Bump* is connected with the *ultra–soft X–ray excess*, in the cases when this is present (Wilkes and Elvis, 1987), or even with the *soft X-ray excess*. The high energy tail of the whole feature may reach 0.1 keV or 2 keV in the latter case. After the high energy end of the ultra–soft excess is reached, the continuum resumes a slope ≈ 1.

The situation between 0.1 keV and 2 keV is however complicate, since AGN show a wide variety of behaviours (Turner and Pounds, 1989; Warwick, Yaqoob and Pounds, 1989):

- $\sim$ 50 % of the sample show absorption due to a column density $\sim 10^{21} - 10^{23} cm^{-2}$.
- 30 % (one half of the unabsorbed sources show an excess emission); the spectral sensitivity of EXOSAT allowed the detection of objects with soft excess extending past 0.2 keV.
- It is worth noting that low luminosity AGN are more likely to be absorbed. Moreover, Sey–2 show stronger absorption than Sey–1 nuclei. Absorption may occur very close to the center: NGC 4151 varied in the spectral range between 0.1 and 2 keV by a factor of 10 in 5 days.

It is worth emphasizing that the maximum of the *Big Bump* is yet unobserved, since it falls in the unobservable gap between the Lyman Edge and the soft X–ray domain, but there are possible indirect tools for investigating the true shape of the continuum in this range.

2.1.1 Diagnostic line ratios

An alternative method for gaining information about the unobservable EUV spectrum is to employ suitable emission line fluxes and ratios. In Chapter 1, it has been shown that the main emission mechanism for the strongest permitted lines is photoionization followed by recombination. An important part of the ionizing continuum lies in the EUV, and therefore a proper question is to ask whether different parametrizations of the ionizing continuum may induce major changes in the line fluxes, or, inverting the problem, can the relative strength of the observed emission lines be used to indicate the shape of the unobserved ionizing continuum?

The answer to this question is mostly negative (Tarter, Tucker and Salpeter, 1969). At a first order, the relative strength of most optical and ultraviolet lines depends more on the ionization parameter Γ than on the spectral shape of the ionizing continuum. However, the intensity of the Low Ionization Lines (LILs, which include the Blamer Lines, the FeII, OI, NII, NI lines) is very sensitive to the

X-ray continuum, which is the main responsible for the simultaneous presence of low ionization species together with high ionization species in the emission spectrum of Seyfert galaxies and Quasars (Kwan and Krolik, 1981).

Kallman and Krolik (1988) computed the emerging emission line spectrum employing a photoionization code, assuming three different continuum shapes, namely:

1. a broken power–law, of the form $F_\nu \propto \nu^{-1.2}$ for $h\nu < 2keV$ and $F_\nu \propto \nu^{-0.7} for\ h\nu > 2\ keV$;

2. A power–law plus an *10 eV bump*, shown in Figure (2.3), which is a thermal component with $kT_b = 10eV$.

   The normalization has been choosen in order to match the total flux emitted by the power–law of case (1) from 1 Ryd 13,600 Ryd.

3. A power–law plus an *80 eV bump*, scaled as for case (2).

The results are as follows:

- As far as the agreement concerning the *average* emission spectrum is concerned, the *10 eV bump* provides the best fit, although the significativity of the result is uncertain;

- Three line ratios have been found to be useful for evaluating the different spectral shapes:

  1. $OVI\lambda1034/Ly\alpha$;
  2. $HeII\lambda1640/Ly\alpha$;
  3. Fe II lines(2900 Å$< \lambda <$4000 Å)/Lyα.

Generally speaking, the intensities of very high–ionization recombination lines are useful in providing a clue to the shape of the continuum just beyond the ionization edges of the ions which produce the lines, since their strength is roughly proportional to the available number of ionizing photons. They can be used for deducing the continuum shape, when this is not directly observable.

Lα is subject to collisional excitation and deexcitation in the standard conditions of the BLR. Since these processes can cause a variation of the ratio of I($L\alpha$)/I(Ly continuum), where I(Lα) is the intensity of Lα, and I(Ly continuum) is the Lyman continuum absorbed, the above ratios, as Kallman and Krolik clearly stated, can signal only large variations.

The $OVI\lambda1034/Ly\alpha$ ratio is strongly sensitive to the amount of radiation with energy $\geq 55eV$, the HeII continuum, since the ionization potentials for O^{+4} and He^{+1} are quite similar. As shown in figure (2.2), the *80 eV bump* is the

more likely continuum shape for enhancing this ratio. However, the detailed calculations show that no major differences arise for the three shapes.

It is interesting to note that the $HeII1640/Ly\alpha$ ratio is able to distinguish the *10 eV bump* ($HeII1640/Ly\alpha \approx 0.02$) against the other spectral shapes. $HeII1640/Ly\alpha \approx 0.04 - 0.07$ should be for the power–law and $0.06 - 0.11$ for the *80 eV bump*. It is attractive to compare the observed line ratios to the observed ones. The ratio $HeII\lambda1640/Ly\alpha$ deduced from the average spectrum of Sey–1 galaxies published by Veron–Cetty, Veron and Tarenghi (1983) is ≈ 0.01. This value is therefore consistent with the *10 eV bump*.

The FeII multiplets are strongly sensitive to the X-ray continuum for energies above $\approx 4keV$. Considering only the multiplets at wavelengths between 2900 Å and 4000 Å, at the same physical conditions it is found that the efficiency of FeII production decreases from the power–law spectrum to the *80 eV bump*.

Kallman and Krolik therefore proposed a diagnostic diagram involving the following line ratios: $\log(FeII/L\alpha)$ versus $\log OVI\lambda1034/CIV\lambda1549$ (Fig. (2.2). The diagram is unfortunately of limited usefulness: the FeII multiplets in the 3000–4000 Å range are extremely difficult to be measured, since they cover a spectral range which overlaps the classical optical and uv observations techniques, where neither of two is at best.

The important point to be remarked here is that the introduction of a *10 eV Bump* superimposed on the power–law continuum explains the observed strength of the very high ionization permitted lines, whose intensity was too high to be fully accounted for by the usual power–law continua assumed in photoionization calculations (*e.g.* Ferland and Shields, 1985). These results suggest, that *the Big Bump could be a quite common feature in AGN*. It is important to stress that the significativity of the results of Kallman and Krolik (1988) *may* increase if sources absorbed in the soft X–ray range are excluded.

2.1.2 More on the power–law continuum

The continuum for $h\nu \geq 2keV$ is of key importance for the emission of the low ionization lines.

The optical to X–ray (2500 Å to 20 keV; Zamorani *et al.*, 1981) spectral index α_{oX} is a good indicator of the power–law continuum, since there is little contribution from the *Big Bump* at the frequencies where it is computed. α_{oX} is dependent on luminosity, in the sense that the lowest luminosity objects tend to have the steeper ($\alpha \approx 1.4 - 1.8$) spectral index, while the spectral shape in the UV seems on the contrary to be luminosity independent over four orders of magnitude (Reichert *et al.*, 1982; Zamorani *et al.*, 1981).

There is a weak dependence of the spectral index α_{oX} upon the radio properties. Radio loud objects tend to have flatter spectral indexes $\alpha_{oX} \approx 1.0 - 1.4$ than radio quiet ones, $\alpha_{oX} \approx 1.4 - 1.8$, although there is a large scatter in this relation. This effect is a consequence of the flattening of the continuum ($\alpha \approx 0.5 - 0.7$) at 10

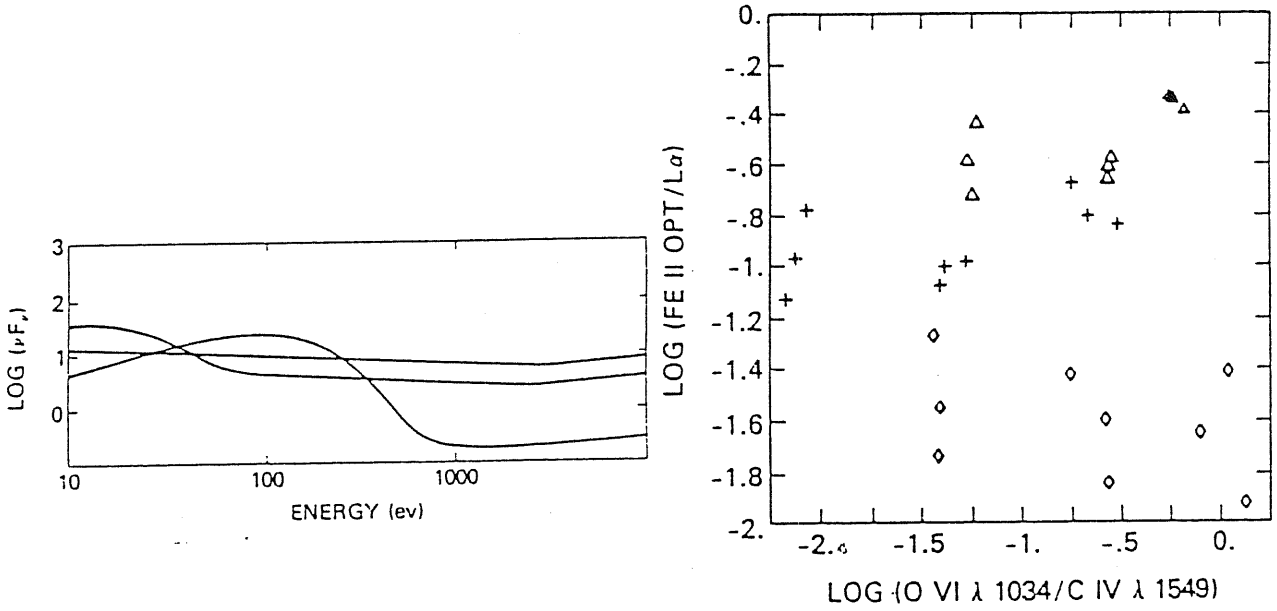

Figure 2.2: A: Assumed shapes of the ionizing continuum; B: diagnostic diagrams. From: Kallman and Krolik, 1982

keV, which is observed in radio–loud but not in radio–quiet AGN. (Mushotzsky, 1982; 1988). Since the FeII emission blends are enhanced by a strong X–ray emission, it becomes unclear why the FeII is strong in radio–quiet objects, which are also the less powerful X–ray emitters (Boroson and Oke, 1984; Boroson, 1989). We shall return to this point in Chapter 4.

2.2 The *Big Bump*

As noted in the previous section, the infrared and optical continuum of Sey–1 galaxies and quasars is typically described, once the effects of reddening have been corrected, by a power–law $F_\nu \propto \nu^{-\alpha}$ with the spectral index α being $\sim$ 1. In the visible and near ultraviolet part of the spectrum (beginning at $\lambda \sim 10000$ Å) an excess emission is superimposed to the continuum described by the power law. The excess emission (*Big Bump*) may extend up to the soft X–ray domain, and comprise the soft X ray excess.

It was firstly noted that:

- the flux emitted in the *Big Bump* is too large to be powered by photoionization due to the power–law continuum, and it should therefore be regarded as an independent component;
- a Planck function provides a satisfactory fit to its spectral shape.

From the theoretical point of view, the Shakura and Sunyaev (1973) model predicts that an optically thick, geometrically thin accretion disc emits a spectrum of the form:

$$L_\nu \propto \nu^{1/3} exp(-h\nu/kT_b) \tag{2.2}$$

where T_b is the temperature at $R \sim 5R_g$. The temperature as a function of R is given by:

$$T_b \approx 1.6 \times 10^5 (\frac{L}{10^{46} erg\ s^{-1}})^{1/4} (\frac{R_0}{5R_g})^{-1/2} (\frac{M}{10^8 M_\odot})^{-1/2}\ ^\circ K \tag{2.3}$$

For reasonable values of M, and L, a substantial part of the spectrum may fall in the far UV or in the unobservable EUV.

These facts led Shields (1978) and Malkan and Sargent (1982) to suggest that the *Blue Bump* is *thermal emission coming from a geometrically thin, optically thick accretion disc.* This explanation is very appealing, since it offers the first possibility to look directly at the *central engine* of AGN, and it would allow an estimate of the central mass M (in solar masses) and of the accretion rate $\dot{M}$ (in solar masses per year). A lower limit to the accretion rate can be given by the relation:

$$\dot{M} = \frac{L_{opt/uv} + L_X}{c^2 \eta} \tag{2.4}$$

where $L_{opt/uv} + L_X$ is the total *Big Bump* luminosity, and η is the efficiency of the conversion of gravitational energy into electromagnetic energy. More precisely, in the framework of the standard Shakura and Sunyaev (1973; hereafter SS) model, we can write:

$$logM + log\dot{M} = \frac{3}{2} log\ F_\nu - \frac{1}{2} log\nu + \frac{3}{2} log(4\pi D^2) - 29.285 \tag{2.5}$$

$$\frac{1}{2}(39.189 - logM + \frac{1}{2} log\dot{M}) = log\nu_{max} \tag{2.6}$$

(Bechtold *et al.*, 1987), where D is the luminosity distance of the quasar, ν_{max} is the frequency of the maximum emission. The quantities on the right side of the equations above are all determined by the observations, so that it is in principle possible to independently estimate M and $\dot{M}$.

The connection of the *Big Bump* with the ultra–soft X–ray excess leads to $\nu_{max} \simeq 16$ and hence to temperature estimates of the order $\sim 1 \cdot 10^6\ ^\circ K$, which imply that the disc radiates at a super–Eddington rate, and therefore an inconsistency problem with the thin disc assumption arises.

Nevertheless, the possibility that the soft excesses originate from the inner region of the accretion disc seems likely. Turner and Pounds (1989) noted that soft X– ray excess is strongly variable, but that its variations are uncorrelated with the variability of the hard X component above 2 keV. The doubling timescale

of the X continuum was $\sim$ 10 hours, consistent with the dynamical timescale of an accretion disc at 5 R_g for a $\sim 10^7 M_\odot$ black hole.

The hypothesis that the ultra–soft X excess is due to the *Big Bump* is strengthened by the fact that BL Lacs objects, whose *Big Bump* is less prominent or absent, also lack the ultra–soft excess, and the power–law provides a good fit the continuum up to 1 keV (Urry *et al.*, 1988). Moreover, Mc Dowell *et al.* (1989) found a positive correlation between the intensity of the UV bump and the intensity of the soft X–ray excess, which strongly suggests that the two features have a common origin.

The problem may be solved, if the black–body assumption is released, and continuum opacity due to electron scattering is taken into account (Czerny and Elvis, 1987). This is justified by the break-down of the approximation of infinite optical thickness in the inner part of the disc, where the disc structure is determined by the radiation pressure (*case A* of SS), and electron scattering may become the main source of opacity in the highly ionized plasma. Electron scattering produces a flattened modified black body spectrum, and becomes dominant over true absorption processes at frequencies grater than ν_0:

$$\nu_0 \simeq 6.3 \times 10^{12} k/hT^{-3/4}\rho^{-1/2} \tag{2.7}$$

The departure of the spectrum from a simple sum of Black Bodies becomes relevant if a substantial part of the energy is emitted at frequencies higher than ν_0, i.e. if the maximum of the black body spectrum occurs at frequencies $\nu_{max} = 3.9kT/h \geq \nu_0$.

Expressing the density ρ as a function of the disc parameter, employing the case A of SS, where radiation pressure and electron scattering dominate, we obtain:

$$\rho = 3.3 \times 10^{-7} \dot{M}^{-2} M^{1/2} \alpha^{-3/2} T^{-2} \tag{2.8}$$

Substituting (3.5) in (3.4), and setting $\nu_0 = 3.9kT/h$, the temperature at which electron scattering becomes important is:

$$T_{es} = 3.0 \cdot 10^3 \dot{M}^{-4/11} M^{1/11} \alpha^{-3/11} \tag{2.9}$$

The resulting temperature T_{es} is $\simeq 13000°K$ if $M = 10^8 M_\odot$, if $\dot{M} = 10 M_\odot yr^{-1}$, and $\alpha = 0.1$. A correction applied to this value for the presence of bound–free processes, leads to $T_{es} \simeq 26,000°K$. This analysis shows that at frequencies above $\nu_{es} = kT_{es}/h \simeq 15.0$ the black-body approximation fails, and that the effects of electron scattering must be considered. Henceforth, for the high energy tail of the spectrum a more refined model is necessary. Equation (2.2) may be employed only for frequencies below ν_{es}, and since equation (2.3) can not be used, only an estimate of the product $M \cdot \dot{M}$ can be obtained.

The most recent attempts to fit the *Big Bump* are due to Czerny and Elvis (1987) and Sun and Malkan (1988).

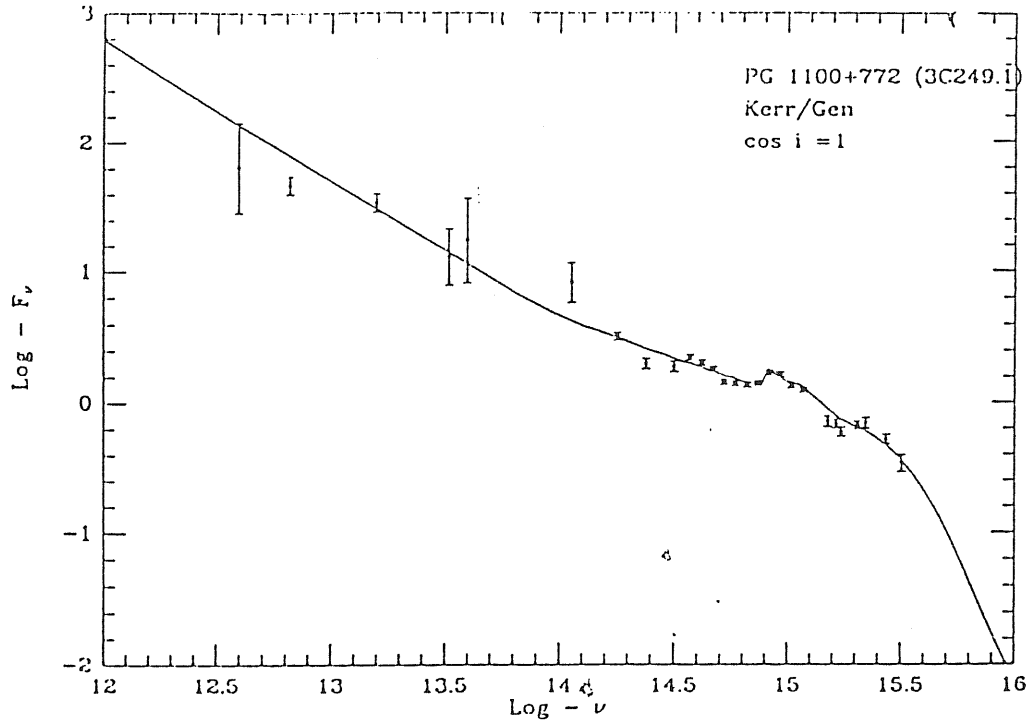

Figure 2.3: Model fit of 3C249.1. From: Sun and Malkan (1988)

Czerny and Elvis (1987) show that the spectral fit of the quasar PG 1211+143 requires a bolometric luminosity $L_{bol} \sim 2L_{Edd}$, if the effects of electron scattering are considered, thus reducing, although not completely solving, the problem of the supercritical luminosity.

Sun and Malkan (1988) employed non–LTE stellar atmosphere models in order to account for the electron scattering opacity. The assumption of a Kerr black hole in their work further reduces the super–Eddington problem, since the efficiency of accretion may be as high as 40 %. It introduces a strong dependence on inclination, due to gravitational redshift, Doppler boosting and gravitational focusing. The last two effects produce an enhancement of the most energetic radiation for discs which are seen nearly edge-on, since radiation is bended along the plane of the disc, in a opposite sense of the effect of a geometrically thick accretion disc. The gain due to this refinement is however questionable, since the description of the vertical structure of the disc by mean values (as the SS model does) does not determine the shape of the disc with the accuracy which is necessary for including self-shadowing effects in the inner part of the disc.

Sun and Malkan (1988) are able to fit with good agreement the overall spectral shape of some quasars and low luminosity objects spanning over 6 decades in frequency, from the far infrared to the soft X–ray range ($\log \nu \sim 12 - 18$, see Fig (2.3)).

One of the most interesting results of Sun and Malkán (1988) is that Seyfert galaxies are accreting at a small fraction of the Eddington limit, while intermediate and high redshift quasars are accreting at rates near to their Eddington limit. This finding, that fully justifies the thin α–disc assumption for Seyfert galaxies, is consistent with the unified scheme for AGN proposed by Begelman (1985), and with the estimates of M and $\dot{M}$ deduced employing a very different method by Padovani and Rafanelli (1988) and Padovani (1989), and removes some of the discrepancies which arose from earlier studies.

However the use of stellar atmosphere models is not entirely satisfactory, since appropriate values of the surface gravity for accretion discs are lacking, and the actual model leads to a Lyman edge in absorption. More refined models, as that of Laor and Netzer (1989) suggest that the Lyman edge should on the contrary be in emission.

On the other side, observations of Lyman edges are difficult tasks, since they can be observed only in high–redshift quasars with $z > 2.5$ (Baldwin and Smith, 1983; Antonucci, Kinney and Ford, 1988), or with IUE in quasars in intermediate redshift quasars ($0.3 < z < 0.8$). Lyman edges are a common feature in approximately more than half the quasars, but they do not seem an *universal* feature. Among the quasars that show indication of absorption shortwards to the Lyman limit, many show the Lyman discontinuity to be significantly blueshifted with respect to the quasars indicating that this feature is neither intrinsic to the quasar nor due to the BLR (Baldwin and Smith, 1988; Ulrich, 1989) As a consequence, it is still unclear whether observations of the Lyman edge in quasars are decisive or consistent with the model predictions.

An other possibility, based on an interesting physical scheme has been analyzed by Band and Malkan (1988). They assume that the *blue bump* (*i.e.* part of the long wavelength tail of the *Big Bump*) is thermal in origin, and that the ultra–soft excess is due to inverse Compton scattered radiation from the blue bump rather than from the synchrotron source which is assumed to be responsible for the power–law component, as in the standard Synchrotron-Self Compton (SSC) model. The fit of the AGN spectra is satisfactory in the range between $log\nu \sim 12 - 18$, but the inferred value of $L_{acc}/L_{Edd} \sim 0.2 - 0.4$ for low luminosity objects seems to be fairly high.

Despite the results of the models based on accretion disks are very encouraging, alternative explanations have been proposed for explaining the *Big Bump*.

For instance, the *big bump* can be explained in the framework of a *complete* nonthermal model (O'Dell *et al.*, 1986; Stein, 1988). Relativistic protons interacting with the ambient thermal medium lead to production of $\Pi^{\pm}$ and Π^{0}, that will decay to $e^{+}e^{-}$ pairs and γ rays. The $e^{+}e^{-}$ could be responsible of the *Big Bump* radiating an additional synchrotron component in the strong magnetic field in the vicinity of the supermassive black hole.

Very recently, Guilbert and Rees (1988) have proposed that very dense ($n_e \sim 10^{11} - 10^{15}, N_c \sim 10^{24}$) clouds, passing at $\sim 20R_g$ from the black hole can be

responsible of the thermal emission associated to the *Big Bump*. Lightman and White (1988) argue that the resulting spectrum is consistent with the observation of NGC 4151 and 3C273.

Recent advances in soft X–ray observations make the actual situation even more intriguing. The observations of photoelectric absorptions (*e.g.* the K-shell Fe absorption edge at $\sim$ 6.4 keV) are important for testing the geometry of the BLR, since they provide an indication of the covering factor f_c of the absorbing matter, under the assumption that clouds are disposed in a spherically symmetric geometry. A key point in favour of the disc hypothesis was that photoelectric absorption was not observed, despite $\sim$10 % of the flux between 2 and 500 keV should be absorbed in order to account for the strength of the observed low ionization lines (see the next section). Ulrich (1989) reports in her review that recent GINGA observations are *consistent* with partial covering (60 % to 30%) of the source by gas of column density $N_c \sim 3 - 6 \cdot 10^{24} cm^{-2}$. The Fe fluorescent line at 6.4 keV was detected in all the three Seyfert for which the observational results are known. However, observations of a larger sample is necessary to decide whether the absorption is due to clouds bypassing the vicinity of the hole, or to the edge of a cold disc. In this respect, it is interesting to note, that GINGA observations showed that a strong luminosity enhancement between 2 and 10 keV in NGC 4151 caused a *decrease of the column density by a factor 2, but leaving the covering factor* $\sim$ *0.9*. This is more consistent with a stable geometry rather than a variation in the absorption due to Poissonian fluctuation in the number of clouds covering the source.

From the theoretical point of view, much work remains to be done. No model developed until now is entirely satisfactory. In particular, models based on stellar atmospheres calculations are very probably not applicable to the inner regions ($R \sim 10^2 R_g$), where the UV radiation is emitted. At the same time, observational data are up to now insufficient to rule out any of these models, and therefore major refinements of the model are not justified. Unfortunately, the peak of the *Big Bump* fails in the EUV, where observations are uneasy also from space–borne instrumentation. In the near future however, X–ray spectroscopy with SAX and AXAF (see *e.g.* Holt 1988) would allow to reveal any absorption feature with unprecedented resolution in the X-ray domain. Simultaneous observations in the optical and in the UV with HST and in the X–ray domain will give us also a *synoptical* view of the AGN continuum, allowing to put more severe constraints on the shape of the EUV continuum.

At the present stage, we can in addition note that the accretion disc idea gives an elegant explanation to *the Baldwin effect*, which will be discussed in the next paragraph.

2.3 The Baldwin effect

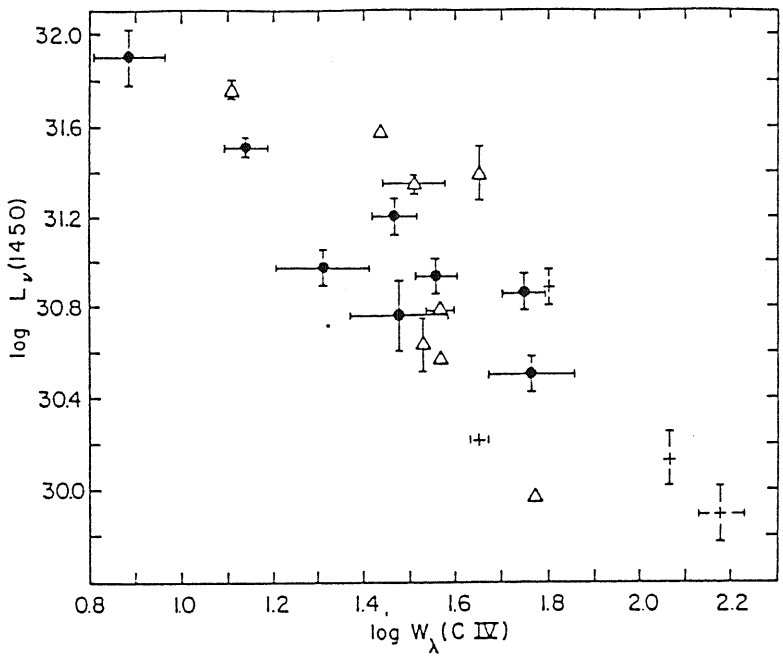

Figure 2.4: The *Baldwin effect*: the anticorrelation between CIV EW and quasars luminosity. From: Baldwin (1977)

One of the most relevant effects in the AGN spectra is perhaps the decrease of the Equivalent Width (EW) of the most prominent ultraviolet emission lines (CIV λ1549 , MgII λ2800) with increasing luminosity (Baldwin, 1977; Baldwin *et al.*, 1978). This effect (also called the *Baldwin effect*) becomes relevant for luminosities $L_\nu(1450\ \text{Å}) \geq 30$ (Fig.(2.4).

The decrease in the EW of the UV lines can be explained in several different ways.

Mushotzky and Ferland (1984) proposed that the covering factor f_c decreases with luminosity, and hence a smaller fraction of the ionizing continuum is intercepted by the BL clouds, leading to a reduction in the strength of the emission lines. Assuming that f_c is nearly constant, the effect can be otherwise accounted for by a decrease of the ionization parameter.

An alternative explanation, due to Netzer (1985), suggests that the most luminous objects do have a more relevant thermal component in the UV (i.e. a stronger *Big Bump*) superimposed to the power–law continuum.

Netzer (1985) proposed that the anticorrelation between the Quasars luminosity and the CIV λ1549 equivalent width is due to the increasing contribution of the *Big Bump* with increasing luminosity. An optically thick geometrically thin accretion disc presents a different viewing angle to the line of sight, thus a range of apparent luminosity for a given disc luminosity. Magnitude limited surveys should suffer a bias toward the highest luminosity objects and hence select objects whose disc is seen nearly face–on. The ratio L_R/L_{1550}, where L_R are respectively the specific luminosity at $\lambda \sim 7000$ Å, and at $\lambda \sim 1550$, gives an indication of the relative prominence of the *big bump* over the power–law continuum, i.e. of the inclination of the accretion disc. The correlation between the L_R/L_{1550} ratio

and the equivalent width of the CIV λ1549 line provides a first support to the Netzer idea. Moreover, the *Baldwin effect* does not affect the EW of the Balmer lines as expected, since at wavelength $\lambda \sim 7000 - 5000$ the contribution of the big bump is not appreciable.

A preferred disc orientation may be related with the velocity field of the emitting gas. Richstone, Ratnatunga and Schaffer (1980) find a weak anticorrelation between the EW of CIV and the CIV width, but their result is very uncertain and is not confirmed by an analysis of the Osmer (1980) and Wampler *et al.* (1984) samples. In light of the results by Collin–Souffrin (see next section), it should be more interesting to search for a correlation between the Balmer Line widths and the (L_R/L_{1550}) ratio. Another observational test to be pursued is a search of any anticorrelation between the FeII emission strength and the *Big Bump* prominence.

A first test was performed in the work of Netzer (1985). Netzer's model predicts that the probability $P(EW)$ of observing a given equivalent width EW of the CIV line is $\propto EW^{-2}$. Netzer compared the observed EW distribution from the samples of Wampler *et al.* (1984) and Osmer (1980), with the distribution computed convolving the expected distribution $P(EW) \propto EW^{-2}$ with a gaussian *broadening function.* The mean value of the gaussian corresponds to the minimum CIV EW observed. He found that the agreement between the two distributions is good, provided that the gaussian has a dispersion $\sigma \approx 10 - 14$. This model is highly simplified, but if correct it supports the hypothesis that much of the *Big Bump* in quasars is indeed produced by an accretion disc (Filippenko, 1988b).

Netzers' explanation of the Baldwin effect is certainly appealing but it remains to clarify whether other effects – like an increase in the BLR mean distance from the central object and a decrease of the covering factor (and/or of the ionization parameter) play a major role (Ferland and Mushotzky, 1984).

2.4 Line formation in the outer regions of an accretion disc

Till now we have tried to answer whether the observations of the continuum support the presence of an accretion disc. *On the basis of the previous evidence, we can rely on the assumption that the accretion disc is indeed present.*

Under this assumption, the question addressed in this section will be:

- Is the accretion disc able to contribute to the emission of the broad lines, specifically to the Low Ionization Lines (LIL)?

An attempt to answer to this question will be given in the standard framework of the SS model. As shown in Appendix A, the *standard* SS model describes the radial structure of a thin accretion disc, *e.g.* the behaviour of the central temperature, numerical density, column density, opacity and geometrical thickness

as a function of the radius R, once the accretion rate $\dot{M}$, the black hole mass M, and the parameter α are specified. However, an important warning should be issued before going on: the disc temperature T_{disc} and density ρ_{disc} are not very sensitive to M, $\dot{M}$, and α. This is a direct consequence of the approximations with which the SS model was built up. Therefore, a great care should be used in analyzing the estimates of the quantities M, $\dot{M}$, with the possible exception of α, that can be estimated on the basis of the ultraviolet variability. These remarks apply to the considerations of the preceeding section, as well as the present one: the following analysis, due to Collin-Souffrin (1987), Collin–Souffrin and Dumont (1989), Dumont and Collin–Souffrin (1989a,b) is in fact strongly *model dependent.*

In Appendix A it has been remarked that the disc structure depends weakly on the dimensionless parameter α. Since α does not enter the expression of the UV luminosity, nothing can be said on the structure of the disc from the features observed in the *Big Bump.* However, the inner part of the disc, where the radiation pressure dominates the gas pressure are unstable over thermal time scales (Pringle, Rees, and Pacholczyk, 1973). The thermal time scale τ_{therm} is $\propto 1/\alpha\omega$, where ω is the local Keplerian angular velocity. If the thermal instability is responsible for the variability observed in the UV continuum in Seyfert galaxies, Siemiginowska and Czerny (1989) argued that it is possible to derive informations on the value of α by observation of the folding time scale of the UV variability. They found that $0.01 \leq \alpha \leq 0.1$, a value consistent with the thin disc hypothesis.

Let us now analyze the physical relevant for having a substantial contribution to the LIL and particularly to the Balmer Lines from a thin disc.

For the numerical density we have:

$$n = 1.3 \cdot 10^{11} (\frac{M}{10^9})^{-2} \dot{M} (\frac{T}{10^4})^{-3/2} \alpha^{-1} \tag{2.10}$$

$$N = 6.9 \cdot 10^{26} (\frac{M}{10^9})^{-1/2} \dot{M} (\frac{T}{10^4})^{-1} \alpha^{-1} \tag{2.11}$$

Thus, the disc region where the density is suitable for LIL emission $n_e \approx 10^{12}$ to $10^8\ cm^{-3}$ lies at $\approx 10^4 R_g$, where R_g is the gravitational radius of the Black Hole.

The gravitational energy release at distances R$\gg R_g$ is given by:

$$D(R) \approx \frac{3GM\dot{M}}{8\pi R^3}\ erg\ cm^{-2}\ s^{-1} \tag{2.12}$$

Since the typical energy emitted in Hα and Hβ is $\sim 10^{42} erg\ s^{-1}$, it is clear that the emission of an accretion disc (integrating over the disc surface for $R > 10^4 R_g$, we get a total disc luminosity $L_{disc} \sim 5 \cdot 10^{40} erg\ s^{-1}$, for $L \sim 0.1 L_{Edd}$ and $M \approx 10^8 M_\odot$) cannot be responsible for the whole emission in the Balmer lines, unless an *additional, external source of heating is present* (Collin–Souffrin, 1987).

An additional requirement for the production of emission lines from the disc is that the temperature increases in the vertical direction. The SS model gives

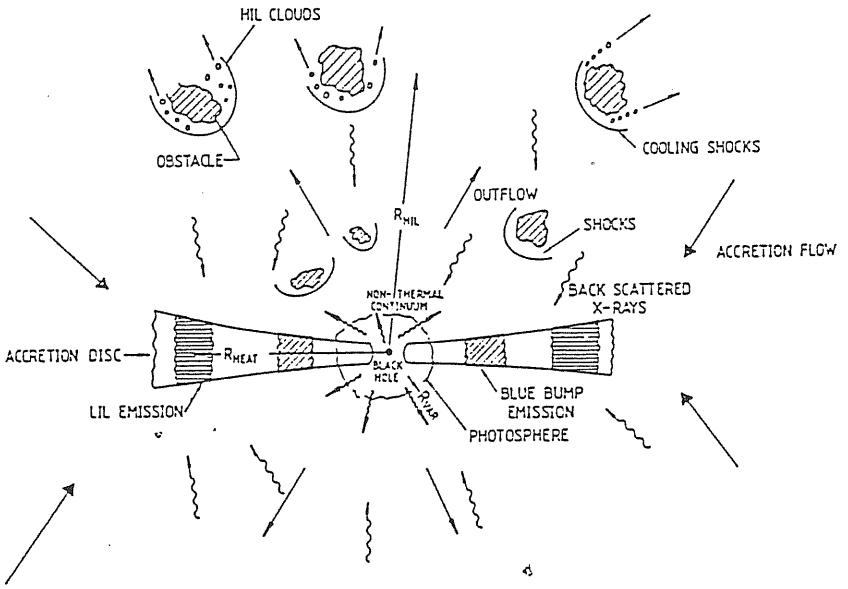

Figure 2.5: The geometry of the Collin–Souffrin model

the radial behaviour of the central and surfaces temperatures, T_c and T_σ. Both scale as $\propto R^{-3/4}$, but T_σ is always $< T_c$, in the inner region where the disc is optically thick (note that the column density decreases with increasing radius). As a consequence, *absorption lines* should be expected from the inner part of the accretion disc.

An external radiating source can on the other side completely alter the vertical temperature gradient. Therefore, the disc should be able to see part of the ionizing continuum, either directly or after being scattered, for producing emission lines. The first possibility seems unlikely, since the covering factor of the disc should be very small. The second one appears more plausible. Several mechanisms have been proposed in order to account for the reflection of the ionizing radiation toward the disc, among others scattering due to the highly ionized gas above the disc, or reflection by the BL clouds moving over the disc (see Fig.(2.5)).

Before discussing in detail the models by Dumont and Collin–Souffrin (1989a; 1989b), it is important to emphasize that the *standard model* of the BLR reviewed in Chapter 1 fails to explain several observed features. First, the presence of the $CIII]\lambda 1909$ requires electron densities $n_e \sim 10^9 cm^{-3}$, while the FeII and Balmer decrement would require densities $\sim 10^{11} cm^{-3}$ and higher. The LILs are better explained if they come from a relatively dense ($n_e \geq 10^{11} cm^{-3}$), at low temperature ($T \approx 6000°K$), Compton or collisionally heated medium of large column densities ($N \sim 10^{25} - 10^{26} cm^{-2}$; Collin–Souffrin, 1982). On the contrary the most prominent HIL are better explained in terms of the parameter deduced for the standard *heuristic model.* These facts led Collin–Souffrin (1987), Netzer

(1985), Smith and Raine (1980), Mardaljevic *et al.*, (1986) to suggest that the BLR are made up of two emittive media.

Collin–Souffrin (1987) and Dumont and Collin–Souffrin (1989a) have been able to prove that a low ionization spectrum should indeed be produced by the disc, once a suitable model for the external illumination has been provided. They consider two possibilities:

- the illuminating sources are two point sources located symmetrically at a height A above the black hole; the physical meaning of this model becomes clear if we consider for instance that part of the continuum is reflected by cloud constrained in a jet along the disc axis (*Point Source Model*, PSM). An approximate parametrization to the PSM is given by:

$$F_{inc} = \beta \frac{L_{bol}}{4\pi} \frac{A}{[R^2 + A^2]^{3/2}} \tag{2.13}$$

  where β is the fraction of the continuum scattered toward the disc. For large radii, ($R \gg A$) the illuminating flux decreases as R^{-3}, while it is constant for $R \ll A$. A is therefore an important parameter for determining the disc emissivity.

- disc illumination is provided by a scattering medium above the disc, which redirects part of the ionizing continuum emitted in the innermost part of the disc toward the outer disc region (*Diffuse Model* , DM). The DM can be parametrized by:

$$F_{inc} = \beta_1 \frac{L_{bol}}{4\pi R^2} (\frac{R_{min}}{R})^g \tag{2.14}$$

  where g is an index whose value is between 0 and 1, and R_{min} is to be identified with the radius of the central source. In this case, the proportion of flux scattered toward the disc is β_1/g.

Dumont and Collin–Souffrin (1989b) proved that both line profiles and line intensities are only *weakly* dependent on the illumination model.

Collin–Souffrin and Dumont (1989a) have moreover demonstrated that, if the continuum extends to $\approx 500keV$, it is able to penetrate and Compton heat a column density $N_c \approx 10^{25} cm^{-2}$ to a temperature of $\approx 7 \cdot 10^3\ ^\circ K$. Two different regions should be considered:

- an optically thick region, for $R < R_{25} \approx 10^4 R_g$, where the X–ray heating cannot affect the internal structure, and is dissipated in the outer layers. A strong external radiative heating is thermal unstable and can lead to the formation of a corona.

- for $R > R_{25}$ the disc has a larger central temperature than in the absence of external radiation and emits an atomic line spectrum in the visible and ultraviolet range (Collin–Souffrin and Dumont (1989)

In the latter region, the ionization parameter is in agreement with the expected values for the FeII emission ($\Gamma \ll 10^{-2}$):

$$\Gamma = 0.007\beta\alpha(\frac{T}{10^4})^{3/2} \ll 10^{-1} \tag{2.15}$$

where $\beta \approx 0.1$ is the fraction of the continuum scattered toward the disc.

The vertical ionization structure for $\Gamma \ll 10^{-2}$, e.g. in the radiatively heated zone for $R \geq 10^4 R_g$, consists in a thin ionized zone (HII region), limited to the surface layers, and in a deeper PIZ; the fraction of radiation emitted in the HIL and LIL depends on the proportion of continuum absorbed in the PIZ and in the HII regions, which is $\propto N(HII)/N(PIZ)^{1/3}$.

Since the column density $N_c \approx 10^{25} cm^{-2}$ is very large, the column density of the PIZ depends much more on the shape of the spectrum in the X–ray range rather than on the ionization parameter (Kwan and Krolik, 1979; 1981; Halpern and Grindlay, 1980; Dumont and Collin–Souffrin, 1989b), and we expect that the ratio I(HIL)/H(LIL) is $\ll 1$, provided that the continuum follows a flat enough power-law spectrum, with $\alpha \leq 1$, *up to 500 keV*.

Collin–Souffrin and Dumont (1989a,b) found moreover that the equivalent width of the line produced by the disc *are in good agreement* and can equal the observed ones. The disc can also give a *partial* contribution to the total line emission, according to the fraction of continuum scattered toward the disc for a fixed bolometric luminosity.

The line ratios are in agreement with the LIL observations. The $Ly\alpha/H\alpha$ ratio is smaller than observed, since Lyα originates in different regions. Results on line profiles, for the first time computed together with a precise evaluation of the emissivity based on a photoionization code, are described in the next Chapter.

The Collin–Souffrin model offers the advantage of solving the classical *energy budget* problem for the BLR and to reduce the extent of the so–called *[OIII] problem* for line emission by a keplerian disc.

2.4.1 The energy Budget problem

Netzer (1985) noted that a substantial part of the total broad line flux is emitted in the small bump, which is formed by thousand of FeII lines and by Balmer continuum. Taking into account this contribution, Collin–Souffrin and Lasota (1988) suggest that:

$$< F(Ly\alpha)/F(H\beta) >= 6 < F(HIL)/F(Ly\alpha) >= 3 \tag{2.16}$$

$$< F(LIL)/F(Ly\alpha) >= 5 \tag{2.17}$$

Netzer (1985) stressed that his photoionization calculations provide a value of the $Ly\alpha$ flux which is not too much different from the case B value ($\approx 1 - 1.5$ (Kwan and Krolik, 1981; Kwan, 1984; Mushotzky and Ferland, 1984); hence the

problem resides in a selective enhancement of the Balmer line and in the LIL, rather than in a suppression of the Lyα photons.

Netzer proposed that the internal reddening plays a major role for explaining the *energy budget* problem of the BLR. Collin–Souffrin (1986; 1988) pointed out that the presence of reddening would enhance the *Fe II problem* (see Chapter 1, for references). Present photoionization codes fail in accounting for the observed strength of the optical and UV FeII multiplets with respect both to the Balmer lines and to Lyα. If a substantial reddening affects the observed line ratios, the HIL should be preferentially absorbed, since they are mainly emitted in the UV. Thus, the reddening correction would enhance the HIL in comparison to the LIL, but at the same time it would enhance the ratio between the optical FeII strength and Hβ.

So the FeII/Hβ problem is worsened by reddening. Although it may be not correct to treat the reddening effects in such a general way as Collin–Souffrin does, and they should computed before the observed and theoretical line ratios are compared, it seems unlikely that internal reddening is determinant in solving the *energy budget* problem. The *energy budget* problem is readily accounted for once it is assumed that a substantial fraction ($\sim$ 10%) of the hard X–ray flux ($h\nu > 2$ keV) is selectively absorbed by the disc, which has column density $N_c \geq 10^{25} cm^{-2}$). On the contrary, the BL clouds ($N_c \sim 10^{22} cm^{-2}$) are transparent to the hard X–ray flux.

This suggests also a first observational test:

- the LIL intensity should correlate with the intensity of the *Big Bump*. This occurs because both LIL emissivity and the *Big Bump* intensity are anisotropic and stronger when the disc is seen face-on. No observational data are available on this point, also due to the difficulties of collecting reliable data on the *big bump* for a large sample of objects.

2.4.2 The [OIII] problem

A problem for the disc geometry arises because of the Keplerian velocity field, which implies that $v^2 \propto r^{-1}$. If the ionization parameter remains constant with the distance from the center, as the similar profiles of CIV λ14549 and CIII] λ1909 would indicate (at a zero–order accuracy), we have $n_e \propto r^{-2} \propto v^4$. Hence, assuming a ratio $\approx$ 10 between the innermost and the outermost velocity of the disc, and a maximum density of $\approx 10^{9.5}\ cm^{-3}$ (the critical electron density of CIII]λ1909), the density at the outer rim of the disc should be $\approx 10^{5.5}\ cm^{-3}$. This value is less than the critical density of the [OIII]$\lambda\lambda$4959,5007 lines, and therefore a broad component of [OIII]$\lambda\lambda$4959, 5007 should appear (Shields, 1978; Calvani, Marziani and Padovani, 1989). This problem is controversial, since broad wings on the long wavelength side of [OIII]λ5007 have been observed in some objects (Pelat and Alloin, 1982; Van Groningen, 1983), but this result is limited to a

few objects, and still uncertain. The *[OIII] problem* is alleviated if we assume that only the low ionization lines are emitted by the disc. In this case, the density at the inner edge of the disc region that radiates the lines ($R_{in} \approx 10^4 R_g$), is $n_e \geq 10^{11}\ cm^{-3}$. Also if a disc extension to $R_{out} \approx 10^6 R_g$ is required to avoid the central dip in the Balmer profile, no broad wings for the [OIII] will arise. Moreover, it should be considered that the [OIII] broad wings may be also emitted in a region intermediate between the classical BLR and NLR (see e.g. Krolik, 1989), since several indications, reviewed by Wilson and Heckmann (1985) and by Marziani (1986), point in favour of a *smooth* continuous range of physical properties between the BLR and NLR.

2.4.3 A problem for the Collin–Souffrin model

A source of concern for the Collin–Souffrin models is the insurgence of self–gravity for very extended discs around the supermassive black–hole, which are on the other side–necessary to *fill in* the central dip in the line profile. The Shakura and Sunyaev (1973) model allows to write the ratio of the disc self gravity to the vertical component of the black hole gravity as a function of the adimensional accretion rate $\dot{m}$, *e.g.* the ratio between the accretion rate and the Eddington accretion rate, the central mass M, the α parameter, and the external radius of the disc:

$$Q = \frac{2\pi\Sigma}{Mz/R^3} \approx 7.8 \cdot 10^{-6} \alpha^{-7/10} \dot{m}^{2/5} \left(\frac{M}{10^8 M_\odot}\right)^{13/10} \xi^{27/20} \qquad (2.18)$$

where $\xi = G/M$. (Chen and Halpern, 1989). Thus, for values of these parameters appropriate for AGN ($\alpha \approx 0.1$, $\dot{m} \approx 0.1$, $M \approx 10^8 M_\odot$, the disc becomes self gravitating at radii $R \approx 10^3 R_g$, comparable to the radii at which the disc is able to emit the lines.

Self gravity can lead to the fragmentation of the outer regions of the accretion disc. This effect may provide a mechanism for cloud production. If clouds are formed near to the plane of the disc, they may experience ionization by a continuum which may be quite different from that of the clouds supposed to pass above the disc. Netzer (1987) has examined a configuration in which the continuum is due to an anisotropic disc contribution in the UV and to an isotropic X–ray component. Physically, the X–ray component may be due to the emission of a hot corona surrounding the inner region of the disc.

He found, in agreement with Collin–Souffrin, that the clouds located at higher inclination, moving close to the plane of the disc, and experiencing a stronger X–ray continuum relative to the UV continuum, emit the bulk of the low ionization lines, whether clouds at low i emit the bulk of the HIL. Thus, *with the sole support of the findings of Collin–Souffrin on line emission, it is not possible to discriminate between a* true *disc model and line emission from a flattened* cloudy *BLR.* A way for overcoming this problem is an analysis of the kinematics of the emitting gas.

Chapter 3

Dynamics of the Broad Line Region

In this chapter, the main concern will be the structure and the dynamics of the *Broad Line Region* (BLR). The observational data and suitable methods for data analysis are reviewed at first; then models based on various velocity fields are described, and a first comparison with observations is done. Last, the difficulties of the standard BLR model are stressed. The hypothesis that the outer regions of the accretion disc contributes to the BLR is introduced on the basis of dynamical considerations.

3.1 Observations of Line Profiles

Observations of emission line profiles in *Broad Line Objects* (BLO) show:

- Lyα is symmetric to within 10 %, that is to the uncertainties involved in subtracting fainter emission lines from its red wing; this finding holds in the great majority of AGN. The profile CIV λ1549 shows is often symmetric, but blue– ward asymmetries are also observed.

  The Lyα profile is more centrally peaked and has more extended wings than CIV λ1549. As a consequence, the FWHM of Lyα is generally smaller than that of the CIV λ1459 line. CIV is also broader than other lines coming from lower ionization potential, specifically MgII λ2800. This suggestion (Wu, Grady and Boggess, 1984) is confirmed by a comparison of the FW10%I for the CIV and Hα and Hβ lines (Osterbrock, 1985), but it is not always true for CIII] λ1909 (Wilkes, 1984). Wu, Grady and Boggess (1983) moreover claim that the profile differences are more evident for Seyfert galaxies than for QSOs, but this result remains controversial (Wilkes, 1989).

- After the profiles have been cleaned of other contaminating lines (e.g. mainly of FeII λ4924, λ5018 in the wings of Hβ), it does not seem that

there is a preferred asymmetry in the broad emission (Shuder and Osterbrock, 1982; De Robertis, 1985). The majority of the profiles are symmetric but both blueward and redward asymmetries are present. This situation contrasts with the observed asymmetries of the Narrow Lines, which are mostly blueward asymmetric. The opposite asymmetry is observed only in a minority of objects (Whittle, 1985; Whittle *et al.*, 1986; Wilson and Heckman; 1985). Profile asymmetries can be explained by different physical mechanisms, in the framework of different geometries and will be discussed more extensively in the next section.

- The difference between the radial velocity of the centroid of the Balmer lines and the systemic radial velocity of the underlying galaxy does not show a net trend. The mean displacement is $+200$ km s^{-1}, but both redshifts and blueshifts are present (Sulentic, 1989). Discrepancies between the redshift of the peaks of low and high ionization emission lines are instead observed. In high redshift objects, MgII λ2798, OI λ1304 and CII λ1335, lines coming from ions in a low ionization stage, are redshifted by an amount up to $\approx$ 1000 km/s with respect to some high ionization lines, like CIV λ1549 (Gaskell, 1982). This finding, also known as the *Gaskell effect*, will be discussed more thoroughly in Chapter 4.

It has already been remarked that the relative intensities in the emission line spectrum are similar in the different AGN classes at least at a first order accuracy. The only exception is represented by the FeII lines, which are very weak or absent in the radio loud objects, and whose strength is strongly variable from object to object. Broad Line profiles are often different in Radio quiet and radio loud object, since:

- Radio loud objects show, with respect to radio quiet objects: broader, *box–shaped* BL profiles, with a strong Narrow Component which let them resemble more the profiles of Sey–1.5 than that of Sey–1 galaxies; they show not infrequently irregularities and *lumpinesses* (Osterbrock, 1978; Grandi and Osterbrock, 1978; Miley and Miller, 1979).

Emission line profiles are similar in low and high luminosity AGN, but there are some intriguing differences:

- QSOs have roughly logarithmic profiles, i.e. $F(\lambda) \propto log(\lambda - \lambda_0)$, as predicted by the radiation pressure driven wind model (Blumenthal and Mathews, 1979), whose shape do not appear to be variable (Baldwin, 1975; Wilkes, 1984). Among Sey–1 galaxies, there are several objects whose shape is *certainly* not logarithmic, but also logarithmic profiles are commonly observed. It is not possible to give a more precise statement about the frequency of observation of the different shapes.

- In some Seyfert galaxies Hβ and HeII λ4686 are significantly wider than Hα (the average ratio FWHM (Hα/Hβ) $\sim$ 1.16) indicating that the ratios Hα/Hβ and HeI λ5876 increase from the center to the far wings of the line (Shuder, 1982). This means that the the physical conditions of the emitting gas are dependent on the velocity, since these profile ratios necessitate either of an increasing density n_e, an increasing Γ, or an increasing Lyα optical depth with increasing velocity. If Hα/Hβ is equally sensitive to the changes in n_e and Γ, then larger velocities occur at smaller radii, because of the relation between n_e, Γ, and R. This behaviour is consistent with rotation or infall, and cannot be easily explained by outflow, unless the clouds are instantaneously accelerated to a terminal velocity at the point of their formation.

  Shuder (1984) extended his work to some low redshift QSOs, at higher luminosities than that of the Seyfert 1, and found that the differences between the profiles of Hα, Hβ, HeI are less pronounced.

- The onset of a P–Cygni profile occurs in some of the most luminous quasars (Turnshek, 1984), called Broad Absorption Lines (BAL) QSOs. BAL QSOs are a tiny fraction ($\approx$ 10%) of all known QSOs. In BAL QSOs the dominant absorption lines are intrinsic to the QSO. They show strong resonance absorption lines, primarily Lyα and CIV λ1549, but also SIV, NV, OIV, very broad and extending continuously from the emission line redshift blueward to velocities exceeding 10^4 km/s. Such lines are often described as P–Cygni profiles in analogy to similar features seen in stars which are ejecting material (Weedman, 1986). There is indeed little doubt that matter is outflowing in BAL QSOs, but the absorption is due to gas which is in very different physical condition compared to the BLR emitting gas.

On the basis of the present data, it is not clear whether there is *significant* dependence of the profile features on luminosity. Since it has been stressed that some differences in the line profiles occur, the covering factor *may depend* on luminosity, low and high luminosity objects radiate at different Eddington regimes, and there are evidences for inflow in low–luminosity AGN, while in some most luminous objects the presence of outflowing matter seems certain, it is legitimate to *suspect* that different kinematics may be at play in Sey–1 galaxies and QSO. We however remark that the state–of–the–art does not allow even a *tentative* conclusion.

In the following, we will use a certain care to generalize findings proved on different object classes, and we will underline each time that these extrapolations become necessary because of data paucity.

3.2 Line asymmetries

In the previous section we have noted that broad line profiles are often asymmetric. In this section, we discuss the physical information deducible from line asymmetries.

We refer to line asymmetries defining an *asymmetry index*. The asymmetry index is given by the difference of the width in the longwavelength and shortwavelength side of the line peak, at a fixed fractional intensity. Hence

$$(A.I.)_{X\%} = \frac{(AR - AB)_{X\%}}{(AR + AB)_{X\%}} \tag{3.1}$$

The asymmetry index can be computed at different fractional intensities, in order to have a quantitative description of the line. The line centroid, computed at a large fraction of the peak intensity, may be considered as an independent measure, related to the shift of the peak position of the line.

Several physical mechanisms can give rise to asymmetries in the line profiles:

1. optical thickness effects in a line (as is the case for Lyα and, probably, for Mg II λ2798 (CK; Wills, Netzer and Wills (1985)). Profile asymmetries arise provided that a significant radial component is present in the cloud motion;

2. dust opacity also affects the profiles. It is relevant to know where the dust is located, *i.e.* whether it is associated with the broad line gas or with the intercloud medium (ICM). The last possibility seems unlikely, due to the high temperature of the ICM, and will not be further considered (see below). Dust content in the broad line gas appears to be moderate, since $E(B-V) \approx 0.1 - 0.2$, but it seems to be strongly variable from object to object, as stressed in Chapter 1;

3. geometrical shielding of one kinematical component can give also rise to profile asymmetries, in the case that the unhidden component moves radially;

4. gravitational effects can deeply affect the line shape; they are extensively discussed in Chapter 4 in the framework of a disc geometry;

5. electron–scattering; asymmetries can arise in an expanding medium if the electron scattering optical depth τ_{es} is larger than unity $\tau_{es} > 1$ (Auer and van Blerkom, 1972). This is not the case for the BLR gas.

For instance, an enhancement of the blue side of a given emission line can arise if the gas is infalling, and dust is present on the cloud side not exposed to the radiation field. The emission coming from clouds withdrawing the observer will be preferentially suppressed, and hence create a blue–ward asymmetry. The same

asymmetry can also arise if the cloud system is outflowing, and the clouds are embedded in absorbing material. Hence the analysis of an observed asymmetric profile at a given time is insufficient to fix the direction of motion even if the hypothesis of predominantly radial motion is made. More ambiguous indications result if also the geometry remains to be established.

3.3 Emission Line Variations

Broad line variability has been revealed in a wide range of time–scales, particularly in BLRG and Seyfert galaxies. In NGC 4151 the shortest time scales τ_{var} are of the order of days (Antonucci and Cohen, 1983). A time–scale ranging from few days to 1 month is also reported for some objects. Most observations refers to the time scale of one or few years, but it is not clear whether this is a typical time scale or it is an effect of the temporal sampling.

It seems established that line fluxes variation correlates with continuum fluxes variation (de Bruyn, 1980). This fact provides an additional confirmation of the idea that photoionization due to the nonthermal continuum is the main source of heating for the Broad Line gas, and that the gas is optically thick in the Lyman continuum. However, most observations refers to the optical continuum, which is not part of the ionizing continuum, but which seems fortunately to vary in phase with the ultraviolet continuum. Less clear is the behaviour of the optical to X ray continuum: the X-ray emission undergoes rapid flares on time scales of days and a few hours, and there is no information on how the spectral shape may change between the X–rays and the optical regions. This information would be of very great importance, since most lines have different temporal responses to the different continuum changes.

The response of the broad emission lines to changes in the continuum is of interest because under certain conditions it is possible to determine the velocity field of the BLR.

The relevant time scales in this respect are:

1. the recombination time scale, $\tau_{rec} = (n_e \alpha_B)^{-1}$, where n_e is the BLR electron density, and α_B is the recombination coefficient estimated from case B of the recombination theory. This is the time scale for establishing ionization equilibrium of any volume element of the BLR;

2. the light travel time, estimated in case B, is

$$\tau_{LT} = 5 \frac{(\frac{L(H\beta)}{10^{42} erg\ s^{-1}})^{1/3}}{n_e^2 f_f}\ light\ days \qquad (3.2)$$

where L(Hβ) is the Hβ luminosity and f_f is the filling factor (Osterbrock, 1974);

3. the characteristic timescale of the continuum variation τ_{var}.

The line variations delay the continuum ones by an inappreciable amount of time in most low–luminosity objects (de Bruyn, 1980; Peterson *et al.*, 1982), leaving the EW of the emission lines nearly constant. This result is consistent with having $\tau_{var} \ll \tau_{LT}$. When observed, time delays may reach a few decades, providing a hint to the geometry and to the extension of the BLR. τ_{var} must be comparable to τ_{LT} in order to have detectable time–dependent structures:

- if $\tau_{var} \ll \tau_{LT}$ changes in the continuum are so slow that the line flux would be always proportional to the continuum flux, and there would be no variable structure in the lines.

- If $\tau_{LT} \ll \tau_{var}$, the continuum would vary so rapidly that only a thin shell of BLR gas would reflect the continuum level at a given time. In this case the total line flux would appear to change little as the continuum varies, and changes would be difficult to detect (Osterbrock, 1985).

The implication of the line profile variability for analyzing the velocity field are described in detail in the following sections. Here the most basic observational facts on flux and profile variations are recalled.

1. In QSO the net changes in emission lines generally preserve the original profile (Zheng *et al.*, 1987; Zheng, 1989). The present data are insufficient for providing data on time delays, since the temporal sampling is very sparse; more frequent observations are desiderable.

2. profile shape variations of permitted lines are commonly observed in Seyfert galaxies. Profile variations show a great variety of morphologies. In NGC 5548 the total line fluxes changed significantly accompanying a continuum outburst in 1984, without any change in the profile (Peterson, 1987). Pure broadening of the CIV λ1549 line was also observed in NGC 5548 without instaurating any asymmetry (Gregory, Ptak and Stoner, 1982). Variations in the wings have been frequently registered. For instance, Mkn 279 displayed a strong variation in the red wing, while the blue wing remains nearly unchanged (Peterson *et al.*, 1982). Variations in the blue wings of the sole hydrogen line were observed in NGC 1275 and NGC 4151 (Pronik, 1987 and references therein), and seems to be more common than variation in the red wings.

   NGC 4151 underwent one of the most remarkable observed changes: the Broad Component nearly disappeared from 1974 to 1984 (Penston and Perez, 1984), leaving an emission line spectrum similar to that of a Sey–2 galaxy. Broad wings of the Balmer lines of NGC 7469 decreased in the period 1975–1980, without any variation in the core and in the *intermediate* wings;

3. the degree of variation of line fluxes is dependent on the Balmer series number, in the sense that higher order lines change more rapidly. As a consequence, also the Balmer decrement is time dependent (de Bruyn, 1980; Phillips, 1978; Schulz and Rafanelli, 1981);

4. the onset and the variation of additional BL components is also observed.

   Ulrich *et al.* (1984) noted the presence of two *satellite* components around the CIV λ1549 line, which were visible when the continuum level is low and situated $\sim$ -30 and $\sim$ 40 Å from the center of the CIV line (Fig. (3.1)). Their intensity is variable on time scales of months, but do not *strictly* correlate with changes in the continuum. The peak wavelength of the two satellite lines is constant since 1981. (Ulrich *et al.*, 1984; 1985; Clavel *et al.* 1987). This feature bears some resemblance with the presence of two broad components, respectively blueshifted and redshifted by $\sim$ 2000 km $s^{-1}$to the center of Hβ, discovered in NGC 5548 by Peterson *et al.* (1987) and Stirpe, de Bruyn, and van Groningen (1988). The flux in both the blueward and the redward component does not seem to be correlated with the continuum variation, but the red component seems to vary in a different way than the blue one (Peterson, 1988). This fact argues against the suggestion that the two satellite components are emitted in a disc–like geometry, as was instead proposed by Stirpe, de Bruyn and van Groningen (1988). These components can be enhanced due to trapping of the Broad Line gas in jet–like geometry by the radio emitting plasma (Whittle *et al.*, 1988).

   A similar effect has been proposed for explaining the presence of both a blueshifted and redshifted system of lines in the optical spectrum of SS433 (*e.g.* Zwitter *et al.*, 1989, for a recent review);

5. different lines responds to the continuum changes on different timescales; restricting the attention to NGC 4151, one of the most observed objects, Antonucci and Cohen (1983) found that, while the higher order Balmer lines and the He II λ4686 responded very rapidly to the continuum change,on time scales less than 1 month, only part of the broad Hα component varied, with time scales up to the length (15–months) of their investigation. This implies that gas at distances larger than 1 light–year also contributes to the BLR. Ulrich *et al.* (1984) reached similar conclusion from the monitoring of the variations of the CIV λ1549, CIII] λ1909, and Mg II λ 2800 lines. The time delay of the CIV variation with respect to the non– stellar continuum was of approximately 13 days, while Mg II varied with a lag of 25 days. CIII] varied less, if at all.

   This could suggest that the emitting regions for the three lines are located at different distances from the central source.

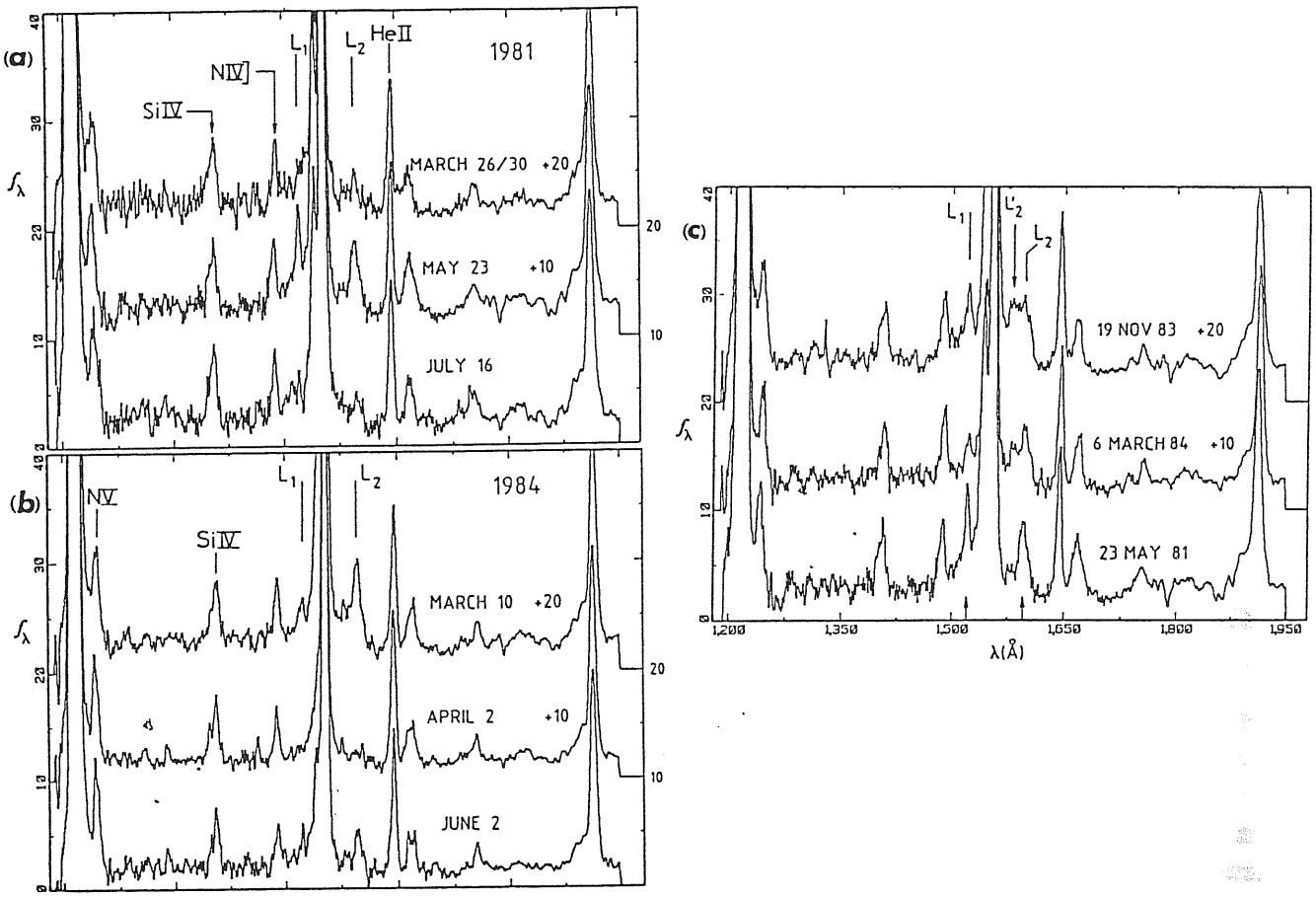

Figure 3.1: The structure of the CIV λ1549 line in NGC 4151. The *satellite* lines are labeled with L_1 and L_2 From: Ulrich *et al.*, 1985

The interpretation of the data in the last item for analyzing the structure of the BLR is straightforward *only* if all these lines respond in the same way to the changing ionization parameter. This does not seem appropriate (e.g. Mushotzky and Ferland, 1984), and hence a more refined analysis is required. The hint to the BLR structure we can gain from the observations of large time delays is that *the system of emitting clouds is not disposed in a spherically symmetric configuration.* In this case, the emission lines would respond *immediately* after the continuum brightening.

3.4 Variability and the determination of the velocity field

The most powerful method for obtaining informations on the velocity field of the BLR is provided by the reverberation–mapping technique outlined by Blandford and McKee (1982). This method is as yet unemployed, for two basic reasons:

1. the method requires extremely good temporal sampling and also very low noise in the data;

2. the objects for which the method is applicable ($\tau_{var} \approx \tau_{LT}$) are only a minority.

The first difficulty can be overcome by coordinated observational campaigns, that can provide equally–spaced temporal sampling of a selected sample of objects, and are currently underway.

Present detectors allow very high–signal to noise spectroscopy, but a considerable source of error both in the estimates of the line fluxes and line profiles remains the arbitrary placing of the continuum underlying the emission line. We can hope however to have a set of suitable data in the near future.

In the following, the basilar features of the method will be described according to Blandford and McKee (1982), with particular reference to the observational aspects.

The hypotheses under which the method works, are:

- the gas is optically thick to the ionizing radiation;

- the amount of emitting gas is constant. Variations of gas amount can affect the emissivity, but they are expected on a time scale $\geq \tau_{dyn} = R/v \sim 10^7 s$, much larger than the rise time for continuum flaring ($\sim 10^4 s$).

- the variation of the ionizing continuum should be isotropic that is the observer should see the same variation as the line emitting element.

Provided that these hypotheses are satisfied, the goal is to obtain the one dimensional velocity distribution function and the emissivity. The BLR can be regarded as a linear system which outputs a line of luminosity $L_l(v,t)$ in response to an input continuum $L_c(t')$, with $t' \leq t$, since the observer sees emission from gas excited by the ionizing source at all previous time. The system should therefore be described by a transfer function:

$$L_l(v,t) = \int_{-\infty}^{+\infty} dt' L_c(t') \Psi(v, t-t'). \tag{3.3}$$

The transfer function would be too noise to be of practical use, so its shape will be analyzed employing a set of moment functions:

$$\Psi^{(n)}(t) = \int_{-\infty}^{+\infty} dv v^n \Psi(v,t) \tag{3.4}$$

$\Psi^{(0)}$ is proportional to the line intensity emitted following a continuum flash; $\Psi^{(1)}$ to the gas velocity and $\Psi^{(2)}$ to the velocity dispersion. The moments can be computed for suitable kinematical models and their behaviour compared with the moments computed on the basis of the observational data. This would allow to get at least qualitative information on the velocity field. In Fig. (3.2) the temporal behaviour of $\Psi^{(0)}$ $\Psi^{(1)}/\Psi^{(0)}$, $\Psi^{(2)}/\Psi^{(0)}$ is shown for some selected models. The model labeled by ROD (*Radially Outward Decelerated*) assumes that clouds are created at a certain distance R_0 from the ionizing source, with a velocity w_0 asymptotically decreasing outward, $w_0 \propto R^{-1/2}$. In model ROA (*Radially Outward Accelerated*) clouds are injected at zero velocity and then smoothly accelerated to a terminal velocity w_0. In the last case, the dependence of the acceleration on the distance is the same as in the radiatively–driven outflow models for optically thick clouds, and the observed profile would be logarithmic.

The onset of asymmetries in the time–dependent profile would allow to determine whether the gas is inflowing or outflowing. For inflow, $\Psi^{(1)}$ is initially positive since the material between the source and the observer would give rise at first to a redshifted emission; $\Psi^{(1)}$ becomes negative when the far side is dominant. The ratio $\Psi^{(2)}/\Psi^{(0)}$ gives information whether the gas moving faster is located nearer or further from the center. If the gas moving faster is located nearer to the center, as in the case of infall, the maximum of $\Psi^{(2)}$ should occur instantaneously after the continuum flash.

In Fig. (3.2) the same moment ratios are shown for models ISO, which stand for a spherically symmetric cloud system with a Maxwellian velocity distribution, and with a velocity dispersion increasing inward according to a keplerian law (a situation that seems rather unphysical), and for a keplerian velocity field in a thin accretion disc, labeled with DISK, for three different inclinations. Relativistic effects are neglected. In a steady–state, the line profile emitted by a disc is symmetric. It is very important to stress that the profile *should remain symmetric* also when the line responds to the continuum change.

Two main differences arise from the case of the cloud shell:

- the response of the line is delayed by an amount of time $\tau_{del} = R_0(1-\sin(i))$, where R_0 is the distance beyond which the bulk of the line is emitted, and i is the disc inclination (see Appendix B);
- the time dependent–profile would be characterized by a initially small value of the moment ratios $\Psi^{(1)}/\Psi^{(0)}$, $\Psi^{(2)}/\Psi^{(0)}$, since the velocity of the gas initially responding is transverse to the line of sight.

3.5 Dynamical models for the BLR

It has been previously recalled that broad emission line profiles of some Seyfert–1 galaxies and most QSOs are logarithmic in shape. This means that the specific luminosity L_λ at a given wavelength λ, for wavelengths not too close to the peak wavelength of the line, λ_0, can be written as:

$$L(\lambda - \lambda_0) = C \cdot \log \mid \lambda - \lambda_0 \mid \tag{3.5}$$

where C is a normalization constant.

In this section we analyze whether it is possible to obtain logarithmic profiles under the assumption that a system of clouds is moving radially under the effects of radiation pressure and/or gravity. The equation of motion for a single cloud is:

$$m_c \frac{du}{dt} = -\frac{GMm_c}{R^2} + \frac{n\alpha}{M_p}\frac{h\nu}{c} m_c \phi + \rho A_c(\hat{u} - u) \mid \hat{u} - u \mid \tag{3.6}$$

where m_c is the cloud mass, M is the mass of the central object, M_p is the proton mass, ρ is the cloud density, R is the distance between the BLR and the central object, $\mid \hat{u} - u \mid$ is the relative velocity of the cloud to the intercloud medium (assimilated as an outflowing wind), A_c is the cloud surface exposed to the radiation field, ϕ is a factor > 1 which takes into account the effects of metals on the radiative acceleration. The second term on the right is the radiative acceleration, the third is the drag force due to the rapid motion of the cloud in the hot intercloud medium (*ICM*). The presence of a confining medium of low density and high temperature (if pressure equilibrium between clouds and intercloud medium applies) is necessary, since the BLR clouds are not self gravitating (see *e.g* Mathews and Capriotti, 1985). The first term is the gravitational force, which will be considered negligible in the cases of radiatively driven outflow.

Let us consider the emission line profiles expected to arise from: a steady–state system of (1) optically thin and (2) optically thick clouds, where the acceleration source is due to the pressure of radiation from a centrally located continuum source, with mass M. The two cases differ because the radiative acceleration assumes different forms in the case of optically thin and thick clouds.

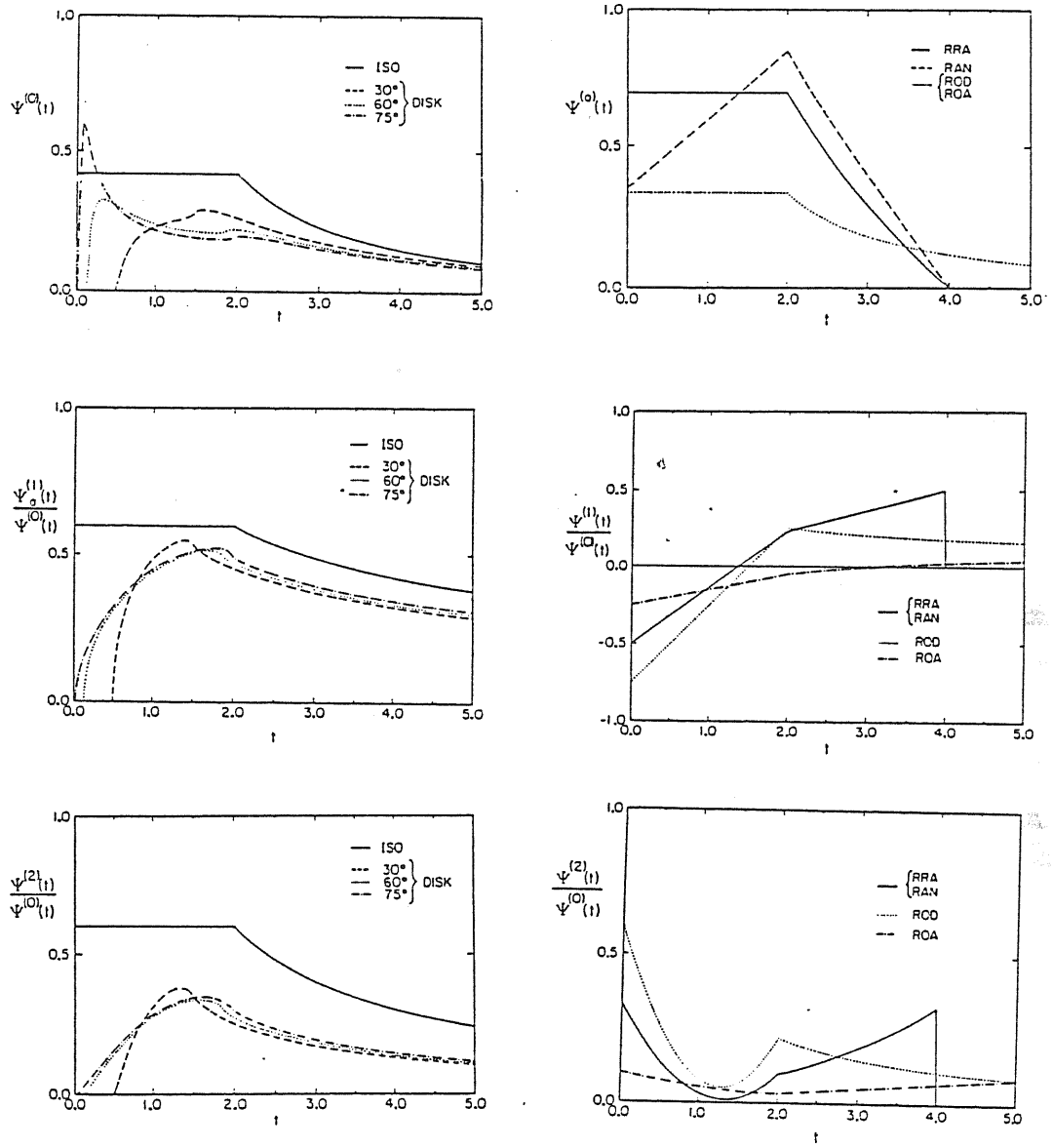

Figure 3.2: Temporal behaviour of the transfer function moments. From: Blandford and McKee (1982)

1. In the optically thin case, the radiative acceleration is given by:

$$a_{rad} = n_g \int_{\nu_0}^{\infty} \frac{\kappa_\nu L_\nu}{4\pi R^2 \rho c} d\nu \tag{3.7}$$

where n_g is the number density of hydrogen atoms in the ground state κ_ν the cross section for hydrogen photoionization. The ionization balance allows to write $a_{rad} = \alpha n_e h\nu_c / m_p c$, where α is the recombination coefficient for hydrogen, ν_c is the weighted mean frequency of the ionizing photons. Substituting in the equation of motion, neglecting all terms except that due to the radiative acceleration:

$$dr = \frac{m_p c v dv}{\alpha n_e h \nu_c} \tag{3.8}$$

In order to compute the line profile, we need to compute the integral given in Appendix B (Eq.(B.2)). The cloud emissivity j_c is given by $\alpha_{eff} n_e^2 h\nu_l V_c$, in the optically thin case. In the steady state hypothesis, the number density of clouds is:

$$n_c = \frac{dM}{dt 4\pi R^2 v m_p} n_e V_c \tag{3.9}$$

$\frac{dM}{dt}$ is the rate at which the material is carried outward by the radially moving clouds. Hence,

$$n_c j_c R^2 dR = \frac{\nu_l}{\nu_c} \frac{\alpha_{eff}}{\alpha} \frac{dM}{dt} \frac{c}{4\pi} dv \approx const \cdot dv \tag{3.10}$$

if α_{eff}/α does not vary much from cloud to cloud. Thus, the profile can be written as:

$$L(\lambda - \lambda_0) \approx const \int_{\max v(R_1), |\lambda - \lambda_0| c/\lambda_0}^{v_{max}} \frac{dv}{v} \tag{3.11}$$

(Capriotti, Foltz and Byard, 1980; Blumenthal and Mathews, 1974). Blumenthal and Mathews (1974) considered the case in which clouds form at rest ($v(R_1) = 0$) from thermal instabilities in the intercloud medium:

$$L(\lambda - \lambda_0) = const \log\left(\frac{v_{max}\lambda_0}{|\lambda - \lambda_0|}\right) \tag{3.12}$$

2. The case of a cloud optically thick to the ionizing radiation is formally identical to the thin case. The radiative acceleration is given by:

$$a_{rad} = \frac{A_c \int_{\nu_0}^{\infty} L_\nu d\nu}{4\pi c R^2 M_c} \tag{3.13}$$

Table 1

	thin		thick	
	in	*out*	*in*	*out*
ϵ_l	$\alpha_{eff} n_e h\nu_l V_c$		$\frac{A_c}{4\pi R^2}\frac{\alpha_{eff}\nu_l}{\alpha\nu_c}\int_{\nu_0}^{\infty} L_\nu d\nu$	
a	$\alpha n_e \frac{h\nu}{m_p c} - \frac{GM}{R^2}$	$\alpha n_e \frac{h\nu}{m_p c}$	$\frac{A_c \int_{\nu_0}^{\infty} L_\nu d\nu}{4\pi c R^2 M_c} - \frac{GM}{R^2}$	$\frac{A_c \int_{\nu_0}^{\infty} L_\nu d\nu}{4\pi c R^2 M_c}$

(see Table 1 for a summary), where A_c is the surface area of the cloud exposed to the radiation field, and M_c the mass of the cloud. j_c can be estimated from the condition of ionization equilibrium:

$$j_c = \frac{A_c}{4\pi R^2}\frac{\alpha_{eff}\nu_l}{\alpha\nu_c}\int_{\nu_0}^{\infty} L_\nu d\nu \qquad (3.14)$$

where the meaning of the symbols is the same as above. Employing the condition of steady state one obtains, for the integrand function of Equation (B.2):

$$n_c j_c R^2 dR = \frac{\nu_l}{\nu_c}\frac{\alpha_{eff}}{\alpha}\frac{dM}{dt}\frac{c}{4\pi} dv \approx const \cdot dv, \qquad (3.15)$$

which is identical to the case of the optically thin clouds. Hence, in both cases, a logarithmic profile results, under the assumption of steady state outflow of a system of isotropically emitting clouds. As a consequence, on the sole basis of the profile shape, it is not possible to distinguish between optically thin or optically thick gas.

We now consider the case of infall. In equation (3.2) the first and second term of the right hand side should be considered. In the optically thick case, the gravitational acceleration is $a_{grav} = -GM/R^2 \propto R^{-2}$ and the radiative deceleration scales as $\propto R^{-2}$ (see Table 1), since it depends only on the optical thickness. The steady state equilibrium condition yields: $n_c j_c R^2 dR = const \cdot dv$, and hence a logarithmic profile results. In the optically thick case, the radiative deceleration is independent on the distance, so at a certain R it can dominate the gravitational term. It is therefore unclear whether an optically thin cloud would be able to fall in.

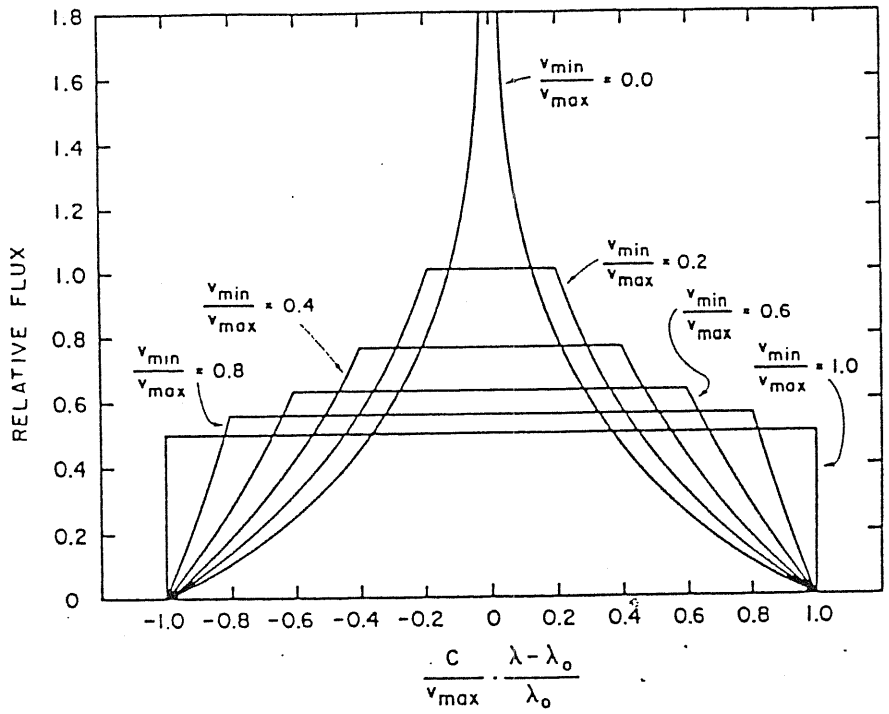

Figure 3.3: Normalized profiles for an expanding spherical shell of isotropically emitting clouds. From: Capriotti, Foltz and Byard (1980)

Releasing the steady–state hypothesis, CFB considered two kinematical scenarios:

1. a shell of outflowing optically thick clouds, for which $n_c = const$ and $v = v_2(R/R_2)$, where R_2 is the outer radius of the shell, and v_2 is the expansion velocity at R_2. In this case, the resulting profile is:

$$L(\lambda - \lambda_0) = const \cdot \log(\frac{R_2}{R_1}) \; for \; v(R_1) > \mid \lambda - \lambda_0 \mid / \lambda_0 c \qquad (3.16)$$

$$L(\lambda - \lambda_0) = const \cdot \log(\frac{v_{max}\lambda_0}{c \mid \lambda - \lambda_0 \mid}) \; for \; v(R_1) < \mid \lambda - \lambda_0 \mid / \lambda_0 c \qquad (3.17)$$

   The resulting profile is shown in Fig. (3.3). The flat–topped part of the profile results from the presence of an inner edge R_1, that contributes as an infinitesimal shell outwardly expanding at $v_{min} = v(R_1)$; in the case $v_{max}/v_{min} = 1$, the whole shell reduces to an infinitesimal thickness, and the profile has also box–shaped wings.

2. a shell where each individual cloud has obtained random velocities, with velocity dispersion v_D, and moves ballistically outwards. If all accelerations

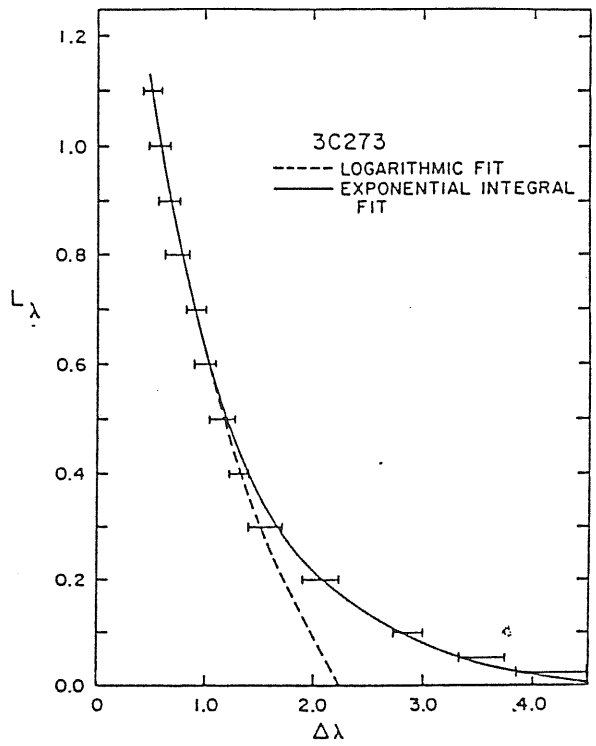

Figure 3.4: 3C273 profile fits. Dashed line: logarithmic profile. Solid line: first exponential integral. From: Capriotti, Foltz and Byard (1980)

are negligible, the clouds will move of radial uniformly accelerated motion, with $v \propto r$. The line profile can be described as:

$$L(\lambda - \lambda_0) = const \int_{\Lambda}^{\infty} \frac{e^{-y}}{y} dy = const \cdot E_1(\Lambda) \qquad (3.18)$$

where $y = (v/v_D)^2$ and E_1 is the first exponential integral. As Fig. (3.4) shows, the exponential integral gives a profile, which is quite similar to the logarithmic in the line intermediate wings, but which is more extended in the far wings. CFB were able to fit the profiles of the quasars 3C273 and PKS 1217+02.

These models however are based on many simplifying assumptions: they are computed for a pure hydrogen clouds, and no optical depth effects have been considered; the screening of clouds by other clouds was not taken into account. The dynamical pressure term is very important for cloud survival, as it will be further analyzed in the last section, but it was always considered negligible, and therefore neglected. Also the problem of cloud formation is not taken into account.

Considering that the emitting clouds are optically thick to Lyα, Lyα is emitted predominantly be the illuminated surface of the cloud. If the clouds move radially, then Lyα has a strongly asymmetric profile, in net disagreement

with the observation. *Thus, radial outflow and inflow do not account for the observed Lyα symmetry.*

We have recalled that there is some evidence in favour of gravitational infall. Perhaps the most elaborate model supposing gravitational acceleration of the clouds is the parabolic–orbital model by Kwan and Carroll (1982, hereafter KC; Carroll and Kwan, 1985). The profile of a spherical distribution of clouds orbiting a central object in nearly parabolic orbit is analyzed. Each cloud is supposed to be in pressure equilibrium with the intercloud medium. Two important effects are considered: (1) the line emission in each cloud is anisotropic for Lyα; (2) the clouds change their shape during infall. This is a direct consequence of the pressure equilibrium hypothesis. The column density remains constant trough the motion $N_e \approx 5 \cdot 10^{22} cm^{-2}$, is estimated on the necessary condition that the gravitational force should be at least equal or larger than the wind force, in order to allow the start of the infall motion. The cloud is initially very optically thick. As the cloud approaches the center, it is compressed mainly along the direction toward the central object and becomes highly flattened. Close to the central source, the cloud will break up into many smaller clouds, because of the different angular momenta of its constituent parts. After the pericenter is reached, the cloud fragments move outward, and eventually expand. When the outermost part of the BLR is reached, the cloud becomes optically thin to the ionizing radiation. The KC model has many appealing points of strength, since:

- It is able to reproduce a fairly symmetric Lyα profile, since the presence of both in– and outflowing motions alleviates the asymmetry expected when optically thick clouds move predominantly in one of the two ways.
- Computed line profiles are roughly logarithmic, although large deviations are expected in the line core and far wings, as it is often observed.
- The computed Lyα profile shows strong wings and a more centrally peaked core.
- The presence of both optically thin and optically thick is foreseen, although the bulk emissivity is due to optically thick material, as expected.
- The profile differences between He I λ5876 and Hβ, MgII and Hβ and CIII] λ1909 and CIV λ1549 are reproduced, assuming isotropic emission for these lines (Carroll and Kwan, 1985).

Among the most important uncertainties, the evolution of the clouds on their trajectories plays the major role. Several instabilities and the drag effects appear to conspire for cloud disruption.

3.5.1 Formation and disruption of clouds

Due to the motion across the *intercloud medium* the cloud will experience a dynamical pressure $P_{dyn} = \hat{\rho}\hat{u}^2$, which acts directly on the irradiated surface. As a consequence, the cloud is compressed by a factor ~ 2 or 3 in the radial direction, and will assume a *pancaked* shape. One of the main concern on the BLR cloud model regards the physical processes leading to the cloud formation and disruption. A system of clouds sweeping out from the nucleus requires the presence of a source of gas, located near to the center, whose origin is unclear. At the same time, it seems unlikely that clouds are formed by thermal instabilities of the intercloud medium as suggested by Krolik, McKee and Tarter (1981), since the instabilities would require implausibly large finite initial perturbation amplitudes (Mathews and Ferland, 1984; Mathews and Doane, 1989).

A variety of instabilities can lead to the cloud disruption on a time scale much smaller than the dynamical timescale (Blumenthal and Mathews, 1979; Mathews and Capriotti, 1985; Mathews, 1986). Disrupting forces can considerably lessen the spatial extent and hence the total optical depth of the clouds; as a consequence emission lines from optically thick regions (MgII, FeII, etc.) cannot be produced. The effects of instabilities are therefore undesiderable in the framework of the cloud model. The Raileigh–Taylor instability arises if BLR clouds are accelerated *solely* by the RAM pressure of a medium of lower density, as the ICM is ($\rho \approx 10^8\ g\ cm^{-3}, T \approx 10^8\ ^\circ K$). For the standard BLR condition, one can show that the cloud disruption results before the ICM is able to accelerate the cloud (Mathews and Blumenthal, 1977; Mathews and Capriotti, 1985; Mathews, 1986):

$$\frac{\tau_{RT}}{\tau_{dyn}} \approx 10^{-3} \tag{3.19}$$

Radiation gradient can reduce or eliminate the R–T instability, but it is cause of new sources of instabilities.

Considering an ideal cloud that approaches internal hydrostatic equilibrium in response to the environmental forces and move in radial orbits as they emit observed line profiles, the main instabilities are:

- unbalanced gas pressure within a cloud would drive lateral flow, that destroys the whole cloud in a time (Mathews and Vielleux, 1989):

$$\tau_{lf} = < \frac{\delta P}{P_0} >^{-1/2} \frac{r_t}{c_s} \ll \tau_{dyn} \tag{3.20}$$

  where c_s is the sound speed of the cloud, δP is the overpressure originating within the cloud, and P_0 is the pressure of the ICM. Mathews and Vielleux (1989) have demonstrated that *outflowing* clouds can be stabilized by radiation pressure, but *inflowing* clouds are most unstable to this effect.

- Cloud rims, in the *pancake* geometry, are subjected to a stronger radiative acceleration than the central part of the cloud, since the radiative acceleration is inversely proportional to the column density. As a consequence rims are pushed away from the clouds;

- the radiation pressure in Lyα or Mg II may exceed the gas pressure and may have a destabilizing effect.

Summarizing, emission line clouds are hence significantly eroded by lateral flows. The fate of the optically thin cloud debris and their contribution to the line profiles is still unclear.

Even deeper difficulties arise if a disc of rotating clouds is considered. The cloud collision time is:

$$\tau_{coll} = \frac{1}{n_c \pi r^2 u} \tag{3.21}$$

Considering that the number density of clouds n_c can be rewritten in term of the covering factor $f_c \approx (\pi/3) n_c r^2 R$, and that the dynamical time scale in this case is given by the orbital period $\tau_{dyn} = \tau_{orb} \approx 2\pi(R^3/GM)^{1/2}$, we have $\tau_{coll} \approx \tau_{orb}/6\pi f_c$. Since $f_c \approx 0.1$, clouds should collide in about one orbital time. Cloud–cloud collision would heat the gas at $T \sim 10^8$ $^\circ K$ and hence destroy the cloud. Moreover, a confining intercloud medium would be necessary also for a disc of radiating clouds. Keplerian shear and Poynting–Robertson shear would lead, also in the hypothesis of an ordered, collisionless system to the destruction of the clouds in one orbital time (Mathews, 1982; Mathews and Capriotti, 1985). Hence, if the disc geometry is applicable to the BLR (as it will be discussed in Chapter 4), a disc of discrete clouds seems most unsuitable, and only *a disc continuously filled with gas should be considered.*

If this is the case, no confining medium is required, and the problems related to the clouds formation and survival are automatically solved.

3.6 Keplerian kinematics for the BLR?

Before going on, we want to analyze whether the accretion disc around the massive black hole may extend up to the BLR distance from the central source.

3.6.1 The distance of the BLR to the central object

In chapter 1, a first order of magnitude estimate of the distance of the BLR from the central source has been computed on the knowledge of the ionization parameter Γ. The optimal method for evaluating R is however to cross–correlate the measurements of the continuum and line fluxes. The cross correlation between the line and continuum fluxes can be computed as a function of the time delay

τ:

$$\mathcal{K}(\tau) = const \cdot \int dt[F_l(t) - \mathcal{F}_l][F_c(t-\tau) - \mathcal{F}_c] \qquad (3.22)$$

where the subscripts $_l$ and $_c$ refer to the line and the continuum respectively , F(t) is the observed flux at time t, and $\mathcal{F}$ are the sample means.

If the BLR gas is disposed in a shell, the line emission from material closest to the central source will respond most rapidly and with the largest amplitude to continuum variations. Thus the peak of the line continuum cross–correlation function will indicate a light–travel time typical of the inner parts of the line emitting region.

Gaskell and Sparke (1986) deduced dimensions of the inner edge of the BLR $\sim$ 6 light days ($\approx 0.005pc$) for Akn 120 and $\sim$ 10 light days for Mkn 509. These values are below any previous estimate and would imply highly non–standard conditions for the BLR (e.g. very high density, $n_e > 10^{11} cm^{-3}$ in order to preserve $\Gamma \approx 0.01$). These results have been extensively criticized (see *e.g.* Krolik 1988; Edelson and Krolik, 1988; Netzer and Maoz, 1989), since both the quality of the present data and the temporal sampling seem to be inadequate to the application of the method.

Therefore, great care should be used in applying these results. On the other side, the observed variability time scales indicate only that the size of the BLR is $R \leq 2$ light months in Akn 120 (Peterson *et al.*, 1985; Alloin, Boisson and Pelat, 1988) and is ≤ 30 light days in NGC 4151 (Ulrich *et al.*, 1984; Peterson *et al.*, 1985).

It is worth noting that the estimated distance ≤ 1 light month $\approx 2600 R_g$, is consistent with the dimension of the outer regions of the accretion disc, and is in agreement with the distance of the region suitable for low ionization emission line formation, as widely stated in the previous Chapter.

3.6.2 Disc profiles: first considerations

We note that lines emitted by a gaseous disc are also an appealing possibility for solving the *Lyα symmetry* problem. It is therefore important to analyze whether an accretion disc can also produce logarithmic profiles.

For treating the disc case, we do the phenomenological assumption that the surface emissivity j_σ has a power–law dependence on the radius: $j_\sigma \propto R^{-a}$.

Under this assumption, the integral of Eq. (2.9) in Appendix B may be rewritten as:

$$L(\lambda - \lambda_0) \propto \int_1^{v_{max}/\beta} \frac{y^{2a-5}}{(y^2-1)^{1/2}} dy \qquad (3.23)$$

(van Gröningen, 1983), where $y = (R/R_0)(\lambda/(\lambda - \lambda_0)(1/\sin i)$. The shape of the line profile for some values of a is shown in Fig.(3.5).

It is interesting to note that the profile becomes bell–shaped for $a > 2.5$; the case $a = 2.5$ is the most noticeable, since an analytical solution for the profile

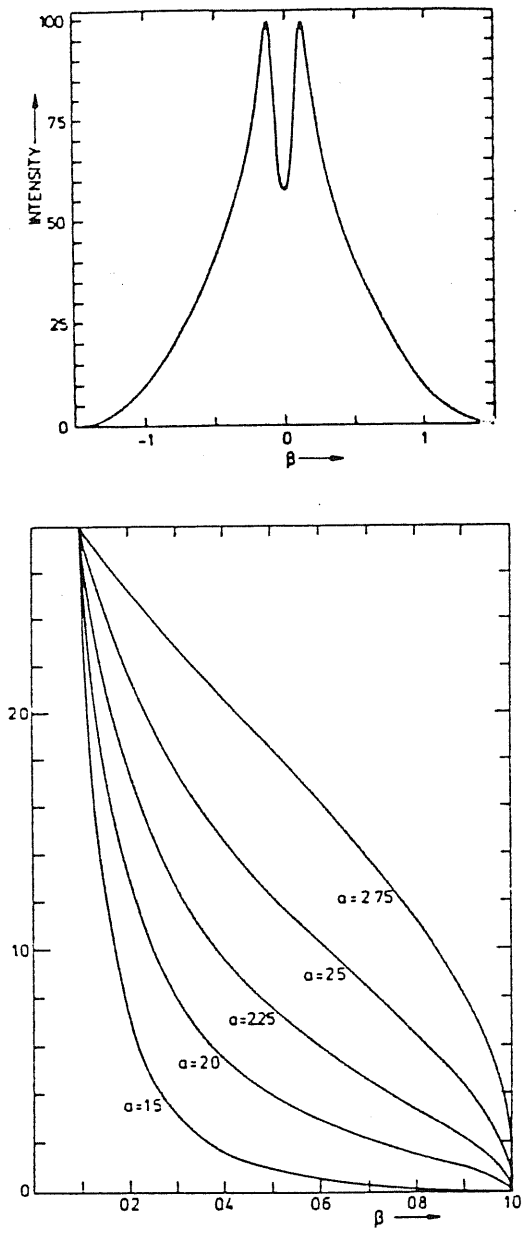

Figure 3.5: Profile shapes of a line emitted by a disc for some values of the power–law index a of the surface emissivity. From: Van Gröningen (1983)

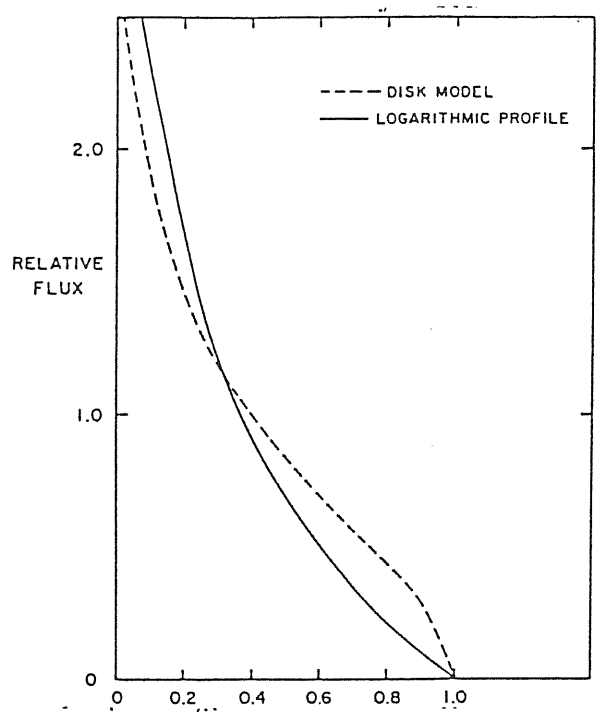

Figure 3.6: Logarithmic profile and disc profile. From: Capriotti, Foltz and Byard, 1980

can be computed:

$$L(\lambda - \lambda_0) \propto \log(1/\beta + \sqrt{1-\beta^2}) \tag{3.24}$$

where $\beta = (\lambda - \lambda_0)/\lambda \cdot (c/v_{max} \sin i)$. CFB state that this is the best approximation to a logarithmic profile that can be emitted by an accretion disc; differences from a true logarithmic profile can be as high as 20 % in the line wings (Fig.3.6).

3.7 Conclusions

From the observational point of view, it is important to emphasize that:

- observations of stationary profiles give *often* a somewhat ambiguous information on the BLR kinematics;
- profile variability observations can in principle allow the determination of both the geometry and the kinematics of the BLR. Present data are till now very sparse and lack the necessary requirements for applying reverberation techniques.

From the theoretical point of view we have that:

- dynamical models based on radial motion succeed in explaining the logarithmic profile shape, but they fail in accounting for the Lyα symmetry;

- the parabolic–orbital model is appealing, but clouds instabilities may restrict its validity;
- disc models provide gas at a suitable distance from the central source without any confinement or drag problem. They explain readily symmetric profiles and symmetric variations (see also the next Chapter) but they fail in fitting the logarithmic profile shapes.

From the previous analysis it appears that *no kinematical model is entirely satisfactory for explaining the profile observations of the BLR.* There are some hints that a Keplerian disc *may* solve some classical difficulties of the BLR kinematics. We shall thus reanalyze the observations in the next Chapter and investigate whether the hypothesis that the disc emits the Balmer lines gives some real advantages.

Chapter 4

BLR kinematics and rotation

Before going on and deepening the discussion about the kinematics of the BLR, we wish to recall some basilar findings reviewed or proved in the preceeding Chapters. First, accretion onto a massive black hole is good explanation for the power source of AGN. Second, there are many *indirect* evidences, mainly based on the AGN continuum, in favour of the presence of an accretion disc; considered separately, they remain *circumstantial*, but taken together they *strongly support* the accretion disc hypothesis, although at the present time some alternative models are also plausible. Third, the ultimate refinements of the models elaborated by Collin–Souffrin and collaborators have shown that a thin accretion disc is able to emit a low ionization line spectrum, provided that part of the X–ray continuum can reach the outer region of the disc. Forth, the outer regions have the same distance from the central source of the ionizing continuum as that *measured* for the BLR. Fifth, there are some relevant problems in the *standard* dynamics of the BLR that could be alleviated with the assumption that the outer disc regions emit the BL, and namely: the symmetry of Lyα , the stability of the emission line profiles and the problems related to the clouds survival. Therefore, from the theoretical point of view, it is legitimate to lookout for a contribution to the Balmer lines due to the accretion disc. That contribution is *not* self evident in the observed emission line profiles: only a very limited number of AGN show emission line profiles that directly remind an accretion disc, as we shall discuss below. In the hypothesis that this contribution is indeed present, we have therefore to discuss:

1. whether an additional kinematical component may mask or hide some of the features expected from a rotational component, and how we can bring it out, or

2. whether the suggestion that an accretion disc is responsible for the BL should be relaxed.

Two approaches are appropriate: a statistical one and a detailed analysis of selected emission line profiles.

4.1 The statistical approach

One of the classical objections to the accretion disc idea is the paucity of AGN with relatively *narrow* Balmer lines. If the bulk emission in the Broad Balmer lines is due to gas moving in a disc, *narrow* broad profiles ($FWHM \sim 1000\ km\ s^{-1}$), would be expected if the accretion disc is observed face–on. A few Seyfert galaxies with *narrow* broad lines have been identified (Osterbrock and Pogge, 1985), but their limited number (≈ 10) do not alleviate the problem. In the case of radio loud objects, Browne *et al.* (1982),and Orr and Browne (1982) have suggested that different type of radio loud AGN (namely core dominated and extended radio sources) are explained by a projection effect. In their scheme, the flat spectrum compact core component is emitted by an unresolved symmetrical jet, and is relativistically beamed with a Lorentz factor γ, while the steep spectrum extended component is the emission due to the unbeamed lobes. They define the parameter:

$$R = \frac{Flux\ density\ of\ beamed\ compact\ core}{Flux\ density\ of\ unbeamed\ components} \tag{4.1}$$

The parameter R depends upon the angle θ between the line–of–sight and the direction of motion of the approaching side of the compact core. According to Orr and Browne (1982) all core dominated quasars are normally double lobes whose axes are pointing close to the line–of–sight, while all normal double–lobed quasars are just unaligned core–dominated ones.

The parameter R versus the FWHM of Hβ is shown in Fig. (4.1). There is clearly a paucity of very broad profiles at large values of R. The corresponding *narrow* Hβ profiles imply that the line emission is constrained in a plane perpendicular to the radio axis (as in a rotating thin disc). The disc inclinations for the different values of R and Hβ FWHM are shown on the right side of Fig.(4.1). This approach has however been criticized since:

- the number of core dominated objects is too large to be consistent with the beaming factor $\gamma \approx 5$ found by Browne, and would imply that the beaming is into a large angle ≈ 2 *sterad* (Phinney, 1985);
- the profiles in radio quite objects (which are viewed in random directions) resemble those in core–dominated galaxies, but never that in small R galaxies. This would suggest that the lobe dominated galaxies have intrinsically unusual profiles (Miley and Miller, 1979; Heckman, 1983).

Nevertheless, an additional, albeit indirect confirmation of the interpretation of Wills and Browne (1986; Wills and Wills, 1986) is provided by the weakness of FeII Lines in lobe dominated objects (see e.g. Phillips, 1978; Wills, Netzer and Wills, 1985; Boroson, 1989). If the FeII lines are mainly emitted by the accretion disc, Collin–Souffrin (1987) has stressed that the FeII emission should correlate with the disc inclination, being stronger when the disc is seen face–on

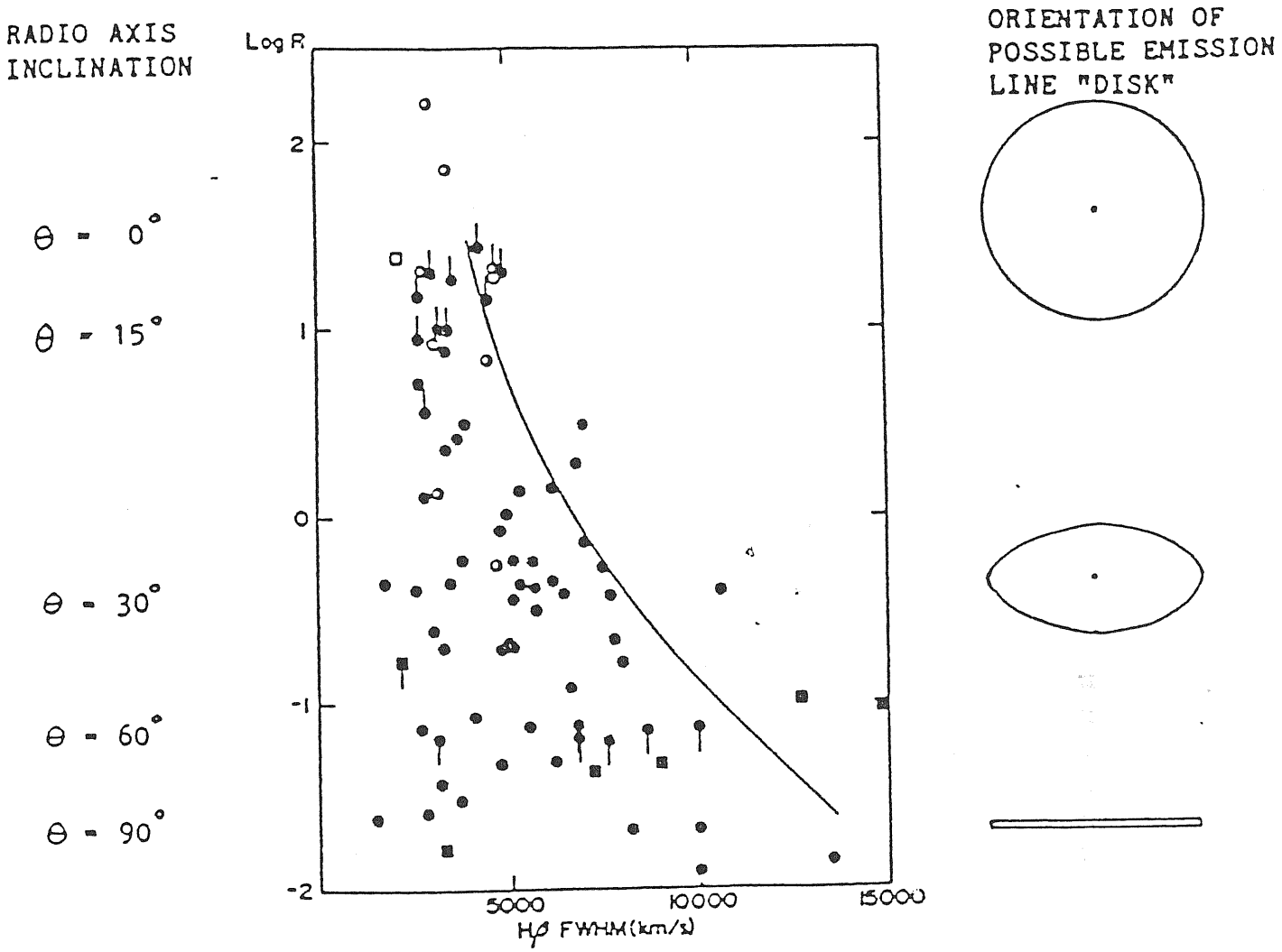

Figure 4.1: The correlation between the parameter R and the FWHM of Hβ.
From: Wills and Wills (1986)

(large R, small width), and this is exactly what is observed. It should also be very interesting to control whether there is a significant sample correlation with the inclination deduced from the prominence of the *Big Bump*.

The large width found for pole–on discs imply a large random motion component. Large vertical velocity dispersion is expected for instance in a *thick accretion disc*. A flattened BLR would provide also a suitable explanation. The finding we want to point out that the correlation found by Wills and Browne (1986) is *consistent with a strong rotational component*. The presence of a wide range of widths for a given R suggests however that *this component may not be self–evident in the line profiles, of the single AGN*.

So, let us look in more detail to the profile analysis. We restrict our attention to Hα and Hβ, unless otherwise stated.

4.2 Emission line profile expected from an accretion disc

The numerical computation of the emission line profiles expected for a thin accretion disc are described in Appendix B, also with the inclusion of relativistic effects. In this section, we want only to recall the underlying physics. The inner radius of the disc is at the last marginally stable orbit. The disc may extend up to the outer radius of the BLR, and even further. As outlined in the previous Chapter, the bulk emissivity for the LIL is at $R \approx 10^4 R_g$. In this region, gravitational effects are negligible, so we consider first a *non–relativistic* disc.

The gas in the disc moves approximately at the local Keplerian speed:

$$v_\phi = \sqrt{\frac{GM}{R}} \tag{4.2}$$

The maximum velocity v_{max} will occur at the inner edge r_{in} of the disc. In this case r_{in} *is the radius where the disc begins to radiate the line*. The velocity v_p is the velocity at the outer edge r_{out} of the accretion disc. v_p is also the velocity shift of the two peaks of the profile from the symmetry center of the line. Hence the ratio

$$\frac{v_{max}}{v_p} = (\frac{R_{out}}{R_{in}})^{1/2} \tag{4.3}$$

is not dependent on the disc inclination i, and gives a first estimate of the relative (to R_{in}) extension of the disc.

The value of v_{max} is half the value of the line FWZI. However, since $v_{obs} = v'_\phi \sin i \cos \phi'$ [1], the observed FWZI strongly depends on the disc inclination. For

[1] Φ is an azimuthal angle defined in the plane of the disc. See Appendix B for a most extensive discussion of the disc geometry. In the following, we set $\cos \phi' = 1$, since we are interested in the maxima of radial velocity variations

$i \longrightarrow 0$ the observed profile would approach a Dirac function; in practice it will reduce to the turbolence profile, which should be much narrower than the ones expected at large disc inclinations.

The size of the disc can also be estimated from luminosity arguments (Perez, 1987; Mathews, 1982). If the disc is fully ionized, the Strömgren depth is equal to its geometrical thickness h. Thus, $V(HII) \approx \pi R^2 h = \pi R^2 c\Gamma/\alpha n_e$ where α is the effective recombination coefficient, and

$$R \approx 10^{18}(\frac{L_{H\beta}}{10^9\ erg\ s^{-1}})(\frac{10^{-2}}{\Gamma})(\frac{10^9 cm^{-3}}{n_e})^{1/2} cm \approx 3 \cdot 10^4 R_g \tag{4.4}$$

for a black hole mass $M = 10^8 M_\odot$, and which is in roughly agreement with the previous estimates.

The central mass, or an upper limit to it, can be computed from the third Kepler law:

$$M = \frac{v_p^2}{G} R_{out} \sin^2 i \leq \frac{v_p^2}{G} R_{out} \tag{4.5}$$

and

$$M = \frac{v_{out}^2}{G} R_{in} \sin^2 i \leq \frac{v_{out}^2}{G} R_{in} \tag{4.6}$$

The sole measure of the FWZI can thus determine the value of the adimensional mass ratio M/R.

A keplerian disc will emit lines with a fairly distinctive profile:

- A direct consequence of the keplerian velocity field and of the finite extension of the disc is the onset of a double peaked line core, as if the line were self absorbed. Since double peaked profiles are only rarely observed in AGN, the profile should be filled in, implying that R_{out} is large. If we assume that the central dip is hidden by the Narrow Component (NC) of the same line, the width of the NC set the an upper limit for $v_p \approx 300 km/s$. Hence an estimate of R_{out} for a mass of $10^8 M_\odot$ and $i = 45°$ gives $R_{out} \approx 2 \cdot 10^6 R_g \approx 6 \cdot 10^{19}\ cm$.

- The profile is markedly smooth and symmetric; asymmetries are present only:

  1. if the disc is not uniformly illuminated. This possibility is not unlikely (e.g. Luminet, 1979), but it has not been considered yet in detailed studies;
  2. if relativistic effects are relevant. Relativistic effects are discussed in the next section.

  If neither of these effects operates, also during the response to a continuum change the profile remains symmetric (e.g. Blandford and McKee, 1982).

- The shape of the profile wings can be described by a power–law; this is a result of the phenomenological choice of a power–law dependence on the radius for the emissivity (e.g. $\epsilon(R) \propto R^{-\alpha}$, van Groningen (1983)), but it is also confirmed by the computation of Dumont and Collin–Souffrin (1989b). Suitable values of the power–law index are $3 \leq a \leq 5$.

In Chapter 3 we have discussed some functional forms expected for different kinematical models and suitable for explaining the line wings: if the gas is constrained in radially accelerated outflowing clouds, the profiles result logarithmic for a wide range of physical scenarios; in the case of ballistic outflow the profile is fitted by a first–exponential integral function. Van Groningen compared the observed functional forms in a sample of Seyfert–1 galaxies. He considered also a gaussian shape in addition to the previous functional forms. A Gaussian function may represent the profile due to turbolent motion; for instance, a *narrow* gaussian profile is expected if the line is emitted in a thin accretion disc seen almost face on. The comparison between observed and computed profiles is not an easy task. First, the Hβ must be cleaned for the presence of FeII emission, which affects particularly its red wing. Second, the fitting procedure depends strongly on the placement of the underlying continuum, which is usually the main source of error in measuring line fluxes and Equivalent Widths, and it remains somewhat arbitrary. As shown in Fig.(3.3), the logarithmic and exponential integral profile differ only in the far wings; hence an overestimate of the continuum would reduce *any* exponential–integral profile to a logarithmic shape. As a consequence the sample of Van Groningen comprises only 12 carefully selected objects, for which the fitting procedure is particularly easy, and cannot be readily extended to a larger sample. He found that nearly half of the observed profiles are of power–law form, with a power–law index $\approx 3 - 3.5$. This does not ultimately prove the disc hypothesis, but is *consistent* with it. It is known that the computed emission line profiles *strongly* depend on the radial behaviour of the emissivity. The profiles of a line emitted in an accretion disc, in the typical conditions of AGN, should therefore be self–consistently computed coupling the velocity field to the emission condition of the gas, through the solution of the transfer equation. These calculation have been performed by Collin–Souffrin and Dumont (1989), and Dumont and Collin–Souffrin (1989a; 1989b).

Collin–Souffrin and Dumont (1989b) isolate 5 different computed profile types (see Figure (4.2)), in the case that relativistic effects are negligible:

- double peaked, U-shaped profiles, typical of small disc radii;
- double profiles with round tops occurring even for large disc radii in the *Diffuse Model* (DM) with g=1;
- single peaked profiles with shoulders, occurring in the DM, for g=0.5 and large disc radii. The shape of the shoulders differs from line to line in the same model;

- single profiles with 2 components of comparable intensity: a narrow core, and a broad component, in the *Point Source Model* (PSM), at large disc radii;

- in the case of very large radii, a single peaked regular profile occurs. Profile wings can be described by a power–law, $L(\lambda - \lambda_0) \propto (\lambda - \lambda_0)^{-4}$

As a direct consequence, the resulting profiles are not necessarily *double peaked*: if the disc radius is large enough ($R \geq 10^4 R_g$), the profiles are generally single peaked, possibly with small shoulders. The relevance of this findings for supporting the idea that the accretion disc is the main emitter of the low ionization lines is however bound to the detailed fit of the observed profiles, and this work remains to be done.

4.3 Line asymmetries in the disc geometry

In this section, we will analyze the effects that the relativistic corrections introduce in the line profile. We limit however the discussion to the most important physical aspects of the problem; a detailed account of the emission line computation is given in Appendix B. Consider for now a gas element moving around a central massive object in a circular Keplerian orbit. A photon emitted by the gas at wavelength λ_{em} will be observed at λ_{obs}, because of the effects of the Doppler shift:

$$\lambda_{obs} = (\frac{\lambda_{em}(1 - \beta \cos\theta)}{\sqrt{1-\beta^2}} \approx \lambda_{em}(1 + 1/2\beta^2 - \beta\cos\theta) \tag{4.7}$$

where $\beta = v/c$, $\cos\theta = \cos\phi' \cos i$, θ is the angle between the velocity vector of the emitting element and the line of sight, i is the disc inclination, and of the gravitational redshift:

$$\lambda_{obs} = \lambda_{em} \frac{1}{1-\beta^2} \tag{4.8}$$

These relations imply that the position of the line centroid is independent on the disc inclination. The profile FWZI has the same dependence on inclination as in the non–relativistic case, $FWZI \propto 1/\sin i$. Gas elements located nearer to the central object will suffer a stronger gravitational and transverse redshift than elements located further out. Hence a redward asymmetry of the line, that will become stronger toward the line wings, since the gas moving faster is also located nearer to the central object. The presence of Doppler boosted radiation tends on the contrary to create an enhancement of the peak in the blue side of the line (Mathews, 1982; Chen, Halpern and Filippenko, 1989).

The computation of profiles resulting from a relativistic accretion disc performed by Chen Halpern and Filippenko (1989) have been extended to small inclination angles (Calvani, Marziani, and Sulentic, 1989a). The procedure followed in the latter work is exactly the same as that outlined by Chen Halpern

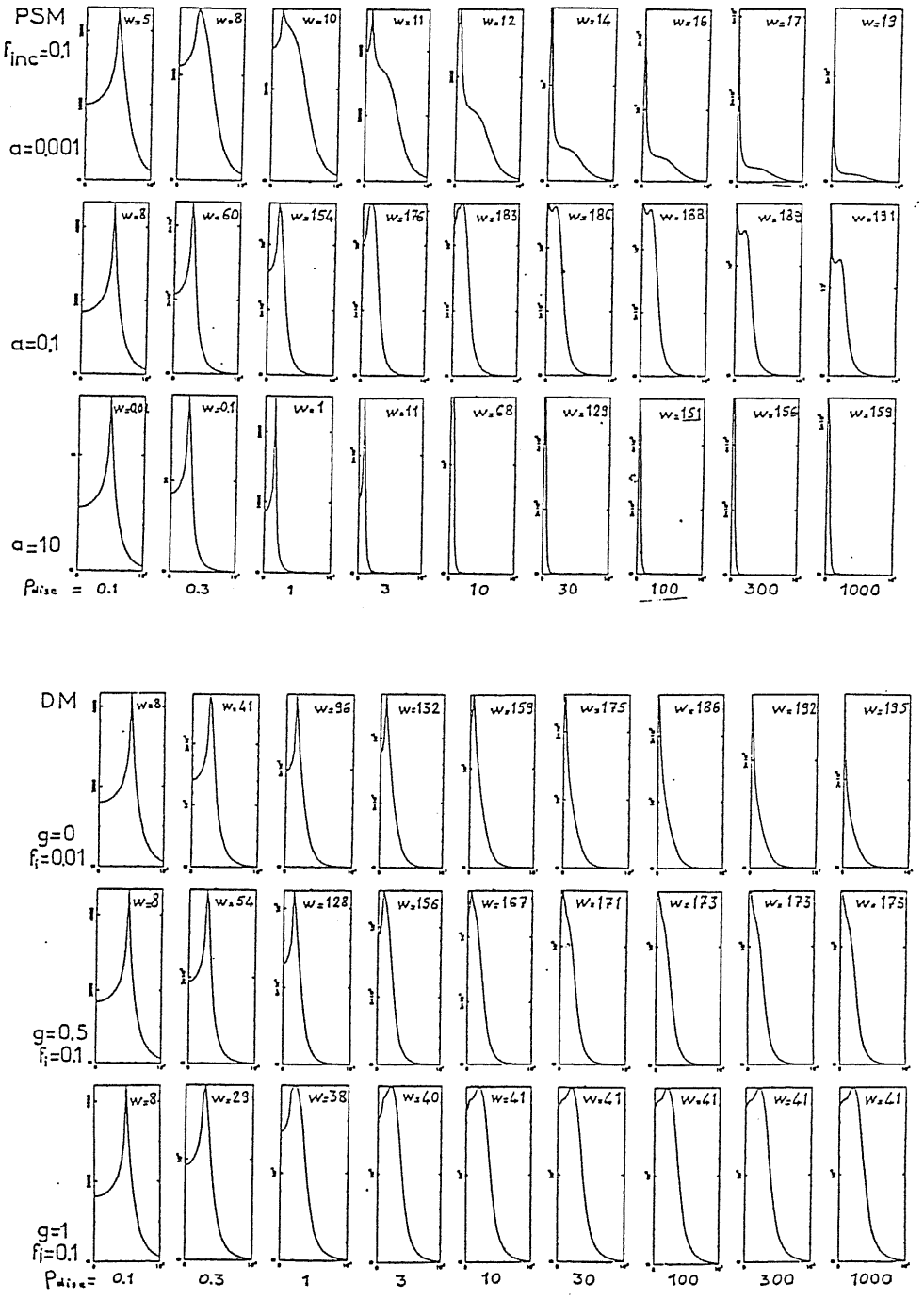

Figure 4.2: Hα profiles obtained for different values of the disc radius (in $10^4 R_g$ unit), and for $a = 0.001, 0.1, 10$ in the PSM and for $g = 0, 0.5, 1$ in the DM. From: Dumont and Collin–Souffrin (1989b)

and Filippenko (1989; see also Appendix B). A power–law radial dependence of the surface emissivity has been used, and no local broadening was considered.

For $i \leq 65°$ and $R_{out} \approx 2000 R_g$, a double horned profile results. For $i \approx 85°$, an additional, slightly redshifted peak begins to be appreciable in the central dip of the profile. This term is due to light bending and increases when smaller radii ($R_{in} \approx 100 R_g$) are considered.

In Fig. (4.3) a very interesting example is shown: $R_{out} = 10^4 R_g$, $R_{in} = 100 R_g$, $i = 85°$; we see that the central dip has been completely filled in. The central peak present only in the case of an optically thick disc, is due to light bending and is redshifted with respect to the rest wavelength of the line by an amount which corresponds to the gravitational plus transverse redshift of the innermost emitting disc regions. The Doppler boosted peak is located approximately at 6100 Å, hence it is blueshifted by 460 Å with respect to the rest wavelength. Although the overall shape bears some resemblance with observed profiles, blueshifts of this order of magnitude have not yet been found (to my knowledge). If the relativistic optically thick disc is considered, we thus expect that:

- the peak wavelength is approximately coincident with the rest wavelength, if the disc is very large, or redshifted by

$$\Delta z \approx \frac{3}{2} \frac{GM}{c^2 R} \tag{4.9}$$

  corresponding to the sum of *gravitational and transverse* redshift.

  The mass required to produce a redward displacement $c\Delta z \approx 400\ km\ s^{-1}$ (which is for instance observed in Akn 120, see below) of the Balmer Lines is thus

$$M \approx 1.5 \cdot 10^7 R_d M_\odot \tag{4.10}$$

  where R_d is the distance from the BLR to the central object in light days. Since current estimates of the BLR size for Arak 120 range in the interval 6 – 30 light days, the value of the mass is 100 – 500 times the minimum mass of $\sim 10^6 M_\odot$ due to the Eddington limit (Osterbrock, 1985).

- Calvani, Marziani and Sulentic (1989b) are attempting to fit selected profiles in order to analyze whether the observed asymmetries can be accounted for by relativistic effects. The work is still in progress and will not be discussed here. Generally speaking, peaks blueshifted by $\sim$ few Å or $\sim$ tens of Å remain difficult to be explained even invoking relativistic effects (see for instance the case $R_{in} = 100\ R_g, R_{out} = 1600\ R_g, i = 25\ °$ in Fig.(4.3)): only the case of very extended disc $R_{out} \sim 10^4 R_g$, and with $R_{in} \geq 500 R_g$, is suitable. We remark that in this case the profile would be highly peculiar.

Therefore, if a rotational component is indeed present, it seems more likely that it dominates *profiles with line peak at rest wavelength or redshifted; if gravitational redshift plays a role, the redward displacement would increases toward the line wings.*

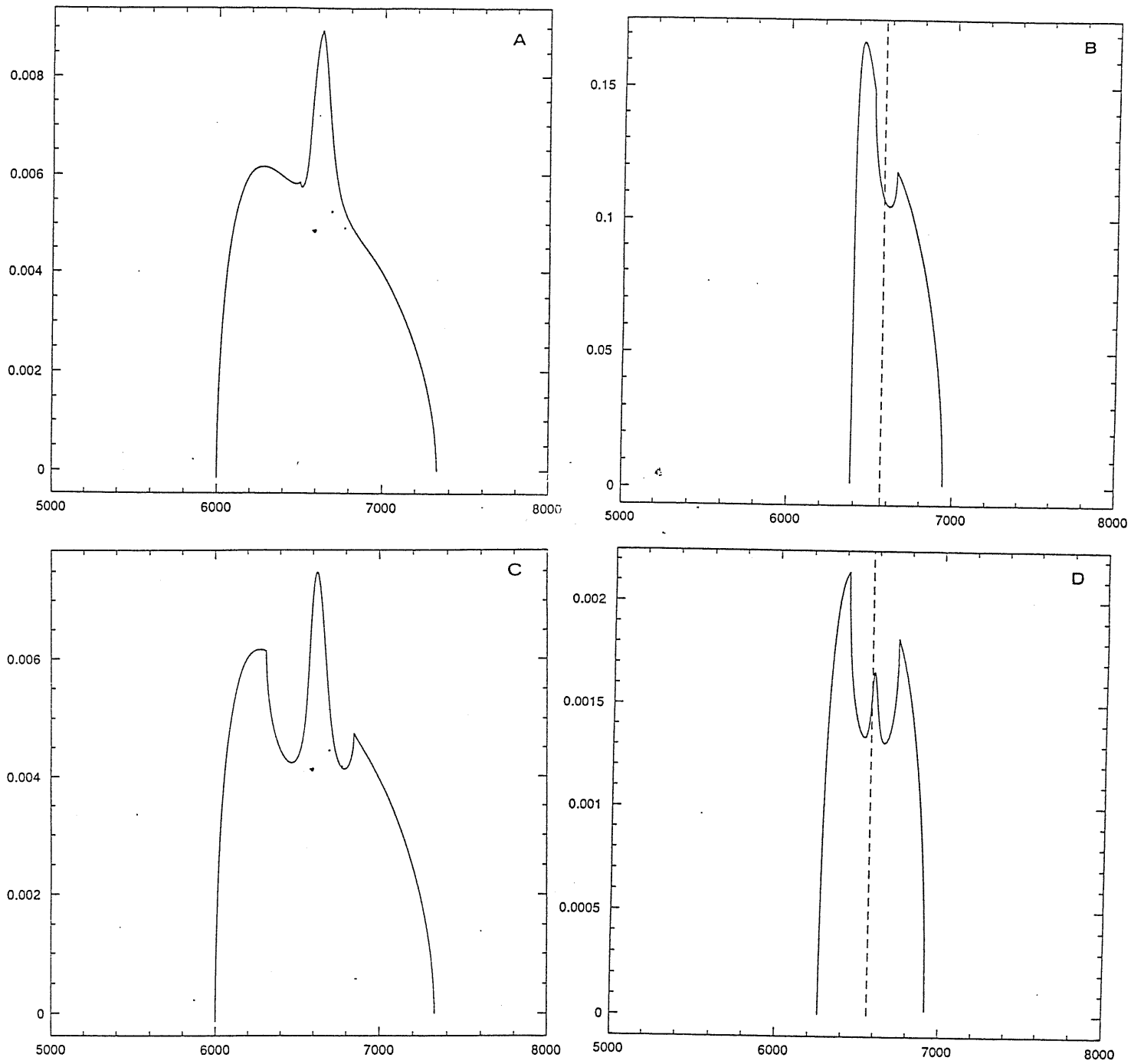

Figure 4.3: Hα profiles for a relativistic accretion disc. A: R_{in} = 100 R_g, R_{out} = 10000 R_g, i = 85°; B: R_{in}=100 R_g, R_{out}=1600 R_g, i = 25°; C: R_{in}=100 R_g, R_{out}=600 R_g, i = 85°; D: R_{in}=400 R_g, R_{out}=1800 R_g, i = 85°.

The most extensive work on the redshifts of the broad Balmer lines is due to Sulentic (1989). A reliable rest frame of reference is provided by the narrow lines. NL usually do not have radial velocity differences larger than 200 $km\ s^{-1}$ (in the most extremes cases) with respect to systemic velocity of the underlying galaxy (Wilson and Heckman, 1985 and references therein). However Sulentic' sample encompasses objects which belongs to nearly all AGN classes; the arguments of Chapter 1 stress, that one should split the sample in at least two subclasses of different luminosity.

Among 61 objects, Sulentic (1989) found that:

1. Nine objects show symmetric and unshifted profiles;
2. 35 objects show a measurable wavelength shift relative to the NLR (from 120 to 1900 $km\ s^{-1}$), with redshifts slightly more common than blueshifts;
3. a shifted profiles is very unlikely to show a blue asymmetry (red asymmetries are eight times more common);
4. more than half of the profiles are asymmetric;
5. red asymmetries are three times more common as blue ones.

The results are also shown in Figure (4.4). They do not have a unique immediate interpretation. It is very interesting however to note that in the histogram where the values of the line centroid at 1/4 of the maximum intensity are reported, redshifts are much more common than blueshifts. Since it is known that the most rapidly moving gas is located in the innermost BLR (Shuder, 1982), it should be appealing to consider the predominance of redshifts as due to gravitational redshift. Clearly, the presence of *blue* and red peak displacement and red asymmetries remains to be explained. Hence, if we *assume* that a rotational component plays a major role *at least two kinematical components should be invoked to explain the generality of the observed features.*

The presence of two components for the BLR is supported by the so–called Gaskell effect (Gaskell, 1982). Gaskell found that in intermediate redshift quasars the centroid of the HIL (like Lyα, CIV, N V) is systematically blueshifted by $\sim 600\ km\ s^{-1}$ (the blueshift can reach 1000 $km\ s^{-1}$ in the most extreme cases) with respect to the NL and to the low ionization lines (Mg II, the Balmer lines). The work by Junkkarinnen (1989) does not confirms the Gaskell effect. She selected a sample of quasars at $z \approx 1.3$, thus higher than the mean $z \approx 0.5$ of the Gaskell sample, in order to be able to measure the centroid of the [OII]λ3727, that gives the reference frame, CIV λ1549 and Mg IIλ2800 lines, and found that the CIV is at the same redshift as the NL. On the contrary, MgII is redshifted by $\approx$ 400 km $s^{-1}$with respect to the NLR. These findings are intriguing, since they support the suggestion of two different emitting regions for the CIVλ1549

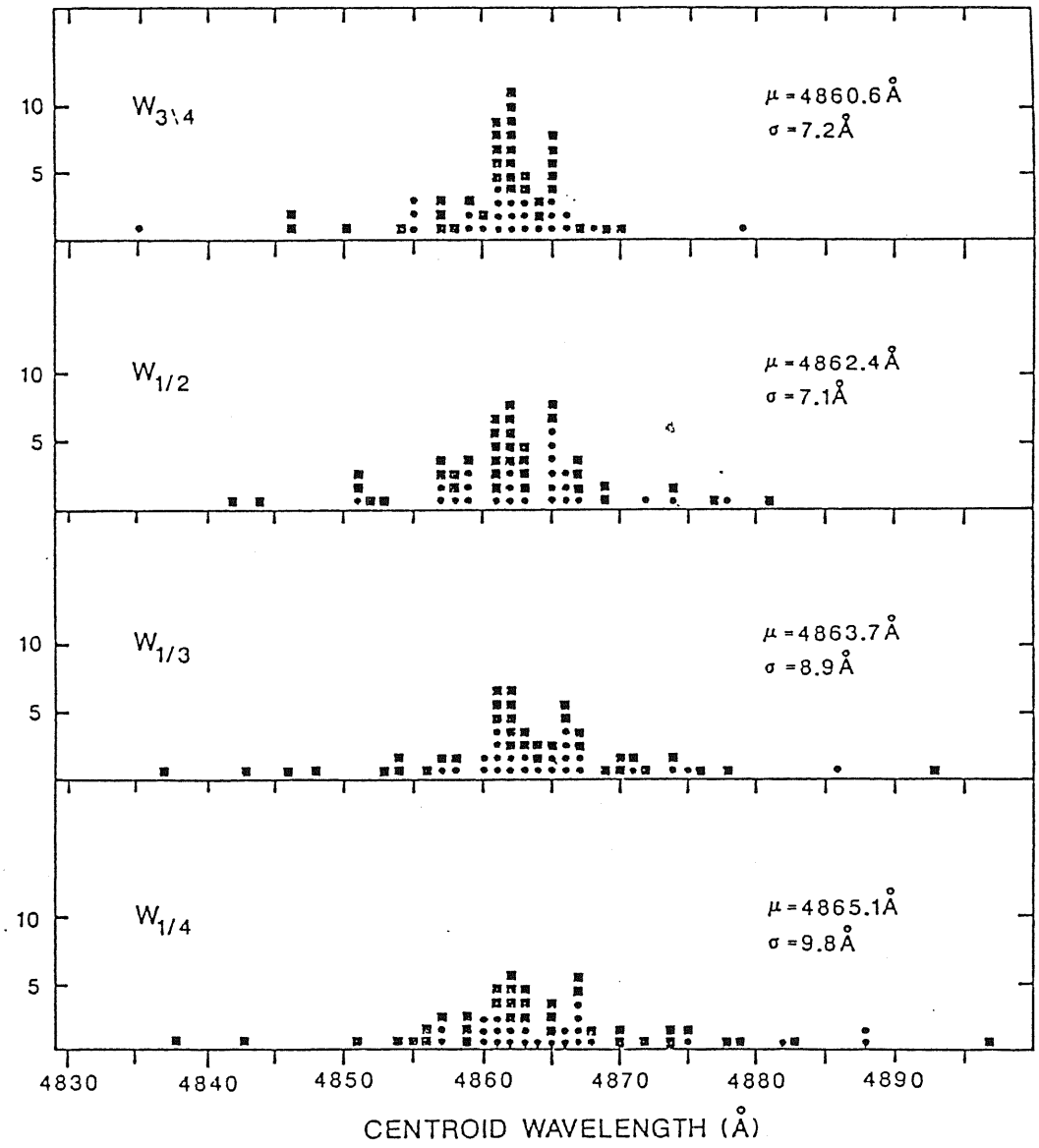

Figure 4.4: Broad line centroid at different fractions of the peak intensity. From: Sulentic (1989)

and Mgλ2800, but they do not reconcile with the details of the Gaskell findings and lack any direct explanation.

Unfortunately, there is no clear indication whether the *Gaskell effect* depends on AGN luminosity. For low redshift objects, the HIL lie in the ultraviolet range and are only observable with IUE. The IUE instrumental setup does not allow a very precise wavelength calibration (the uncertainty is $\approx$ 800 km $s^{-1}$and is of the same order of the effect we want to measure) and hence a study of this effect in these objects is not feasible. The situation will improve only with the launch of Space Telescope.

Moreover, apart from the *Gaskell effect*, the need for two BLR emitting media arises from the explanation of the low ionization spectrum.

Under the assumption that at least part of the Broad Lines is emitted by the disc, how can the disc contribution be hidden? First, if the HIL are systematically blueshifted with respect to the LIL in the way Gaskell states also in low luminosity AGN, the gas emitting the HIL should give a considerable contribution also to the Balmer Lines. Hence, if a *blueshifted* (*by several hundred km* s^{-1}) component is superimposed to the contribution of the disc, a blueshifted peak may arise.

Van Gröningen (1983; 1984) has shown that the additions of a second component due to gas constrained in a jet geometry to the contribution of the accretion disc fits the Hα profile of Mkn 374 very well.

If the disc collimates the jet and is opaque to the radiation emitted by the BL clouds in the jet, the *Gaskell effect* can be explained by a combination of the radial motion of the clouds plus disc obscuration. An other possibility is for instance, that BL clouds in the jet emit the bulk of the HIL, and that the disc is responsible for the LIL. Also in this case, the *Gaskell effect* is accounted for.

Smith and Raine (1985) have moreover exploited the possibility that the formation of clouds results from the interaction of a nuclear wind driven by radiation pressure, and by a thermally driven wind coming from an accretion disc (*duelling wind* model). They were able to reproduce the logarithmic shape of the line wings and account for the observed variability of NGC 4151. Clouds after their formation move from the surface of the disc ballistically outwards.

Mardaljevic, Raine and Walsh (1988) considered the contribution of the disc to the line emission. This *duelling winds* model has the advantage that the relative contribution from clouds and disc is in principle determined and not a free parameter. MRW point out that the disc contribution can be hidden, and may become dominant only in exceptional cases. In figure (4.5) the comparison between the observed profiles, the disc and the cloud contribution is shown for III Zw 2; despite the disc contributes for $\approx$ 65 % to the line profile best fit, a detailed analysis of the profile shape would not give a response immediately consistent with the accretion disc hypothesis.

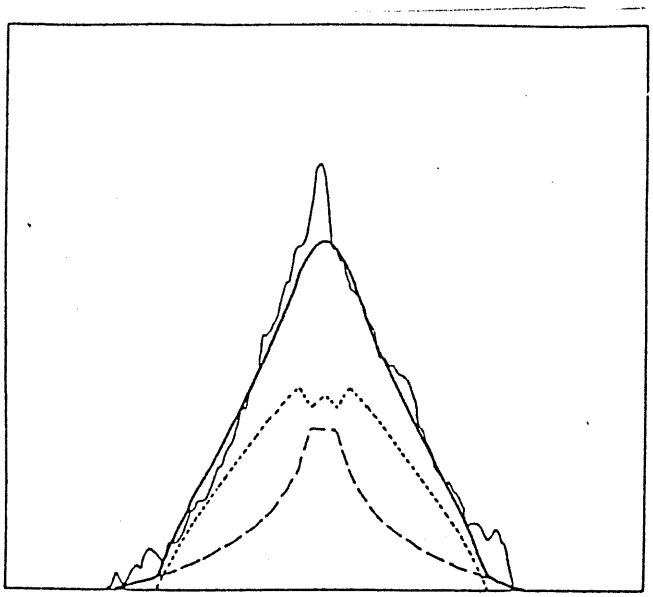

Figure 4.5: Multicomponent fit to the Hβ profile of III Zw 2. From: Mardaljevic, Raine and Walsh (1988)

4.4 Accretion discs or binary black holes?

In a few objects (Akn 120, 3C390.3, see the discussion on each object below), a double–peaked profile indeed occurs. The most plausible explanations are:

1. the line is emitted by gas moving in a Keplerian velocity field;
2. the line is self absorbed;
3. the structure in the line profiles is due to light travel time effects as a result of variability in the ionizing continuum (Capriotti, Foltz, and Peterson, 1982);
4. there are two broad line components, *e.g.* two systems of clouds constrained in a jet–like configuration;
5. they are due to *two spatially distinct* BLR; the displaced peak is due to one whole BLR moving by up to several thousand km $s^{-1}$with respect to the BLR located in the host galaxy. The secondary BLR is due to a secondary black hole moving with it (Gaskell, 1983; 1988).

We consider the last idea at first. As pointed out by many speakers at the *Heidelberg Conference on Dynamics and Interaction of Galaxies*, held at the beginning of June (see *e.g.* Kormendy 1989 and van den Berg, 1989), galaxy merging seems to be a common phenomenon. If we accept the view that at the center of every galaxy lies a massive black hole, merger remnants should harbor – at least in some phases of their existence – a binary black hole. The early stage

of a merger can give thus two spatially resolved AGN in the same galaxy: Mkn 266 is without any doubt a binary active nucleus (Hutchings 1989) and Mkn 78 may be a good candidate (de Robertis, 1987; Marziani, 1986). Arp 102b has been considered as a possible candidate (the emission line profiles of this object are discussed in detail in the following section), since it is an elliptical galaxy strongly interacting with a spiral companion. If there are two orbiting BLR , the relative motion should led to an appreciable profile variation. The Kepler third law allows to write the orbital period P as:

$$P = 2.7 \frac{M}{10^8 M_\odot} \left(\frac{v \sin i}{5000\ km\ s^{-1}} \right)^{(-3)}\ yr \qquad (4.11)$$

where i is the inclination angle of the orbit with respect to the plane of the sky, M is the mean mass of binary system, and $v \sin i$ is the observed radial velocity. Halpern and Filippenko (1988) monitored the position of the blue hump for 5 years. They noted that the measurements are consistent with a constant wavelength at $\approx$ 6612 Å, which means a velocity of 4980 km s^{-1}in the frame of the galaxy. The accuracy of their measurements was about 200 km s^{-1}, that is $\approx$ 4 % of the radial velocity. Hence, the phase displacement of the two orbiting bodies should be less than $\Delta\Phi \approx 2 \arccos 0.96 \approx 32°$, which constraint the orbital period to a value larger than $\approx$ 55 yr. Equation (4.11) sets therefore a lower limit to the mass of $2 \times 10^9 M_\odot$. This value seems unlikely, since Arp 102b is a low luminosity object. Since low luminosity objects radiate at $\approx 0.01 L_E$, it is reasonable to assume that the mass is $\leq 10^8 M_\odot$.

It is important to stress that the double–peaked profiles observed in 3C390.3, 3C382, Akn 120 (see below) are not consistent with the profile shape that should be observed in the case of a binary active nucleus. Low velocity gas will orbit the center of mass of the binary, thus producing a single core. A double peak is expected on the line wing, where high velocity gas, orbiting close to each black hole, will contribute; the separation between the two peaks is comparable to the relative orbital speed of the binary system, so their separation would not be so wide as in the case of Arp 102b and 3C390.3 In light of these arguments, the hypothesis of a binary BLR should be discarded for these objects.

4.5 The detailed study of a selected sample of objects

The data on the profile of the Balmer lines, coupled with the UV line fluxes and profiles, and with the radio data, often provide enlightening clues to the nature of the BLR.

An observing program for the analysis of the Balmer line profiles is carried out at the Asiago Observatory and at the European Southern Observatory by myself.

Journal of Observations

Object	Date	U.T.	E.T.	Res. FWHM (Å)	Spectral range (Å)	Detector
Akn 120	Dec. 22, 1987	30^h12^m	45^m	≈ 3.5	4050–5350	ESO 1.52 m + B&C + CCD RCA
3C 390.3	Jul. 5, 1989	24^h34^m	50^m	≈ 4	6020–7160	Asiago 1.82 m + B&C + CCD Thompson
Arp 102b	Mar. 24, 1989	27^h02^m	50^m	≈ 4	5880–7020	Asiago 1.82 m + B&C + CCD Thompson

The immediate goal is to get high–resolution (Resolution $\approx$ 2 Å FWHM), high signal–to–noise ratio spectra of a sample of suitable Sey–1 and BLRG, for analyzing whether Balmer emission line profiles are dominated by a rotational component. The sample selection criteria are quite etherogeneous, and encompass most features expected for accretion disc profiles, evaluated on low resolution scans.

Among others, the presence of *structures* that led to suspect a double– peaked profile. Moreover, I selected a more homogeneous sample of objects on the basis of the relative prominence of the Big Bump.

Here the results for three objects (Arp 102b, 3C390.3, Akn 120) are presented in a very preliminary way. The Journal of Observations is given in Table 1. The procedure followed in the data reduction will be described elsewhere.

4.5.1 Arp 102b

Arp 102b is an elliptical, low luminosity ($M_V \approx$ -18) radio galaxy. The Balmer line profiles are almost unique (see Fig. (4.6)). Chen, Halpern, and Filippenko (1989) have shown that a relativistic accretion disc provides a very good fit to the profile (see also Appendix B), particularly if a local broadening source is introduced (Chen and Halpern, 1989) (see Fig.(4.7)). According to these authors, the inner region of the disc forms an ion torus, whose hot corona produces the X–ray radiation, which is backscattered toward the outer, thin regions of the accretion disc. The best fit is obtained for $R_{in} = 125R_g$ and $R_{out} = 500R_g$.

The centroid of the BC is redward displaced with respect to the Narrow Component of Hα , by $\Delta v_r \approx 560\ km\ s^{-1}$. If this is due to gravitational redshift plus transverse redshift, as is expected for the relativistic accretion disc, the resulting black hole mass is $M \approx 3.26 \cdot 10^7 R_d\ M_\odot$, where R_d is the distance between the central objects and the emitting region. This value is consistent

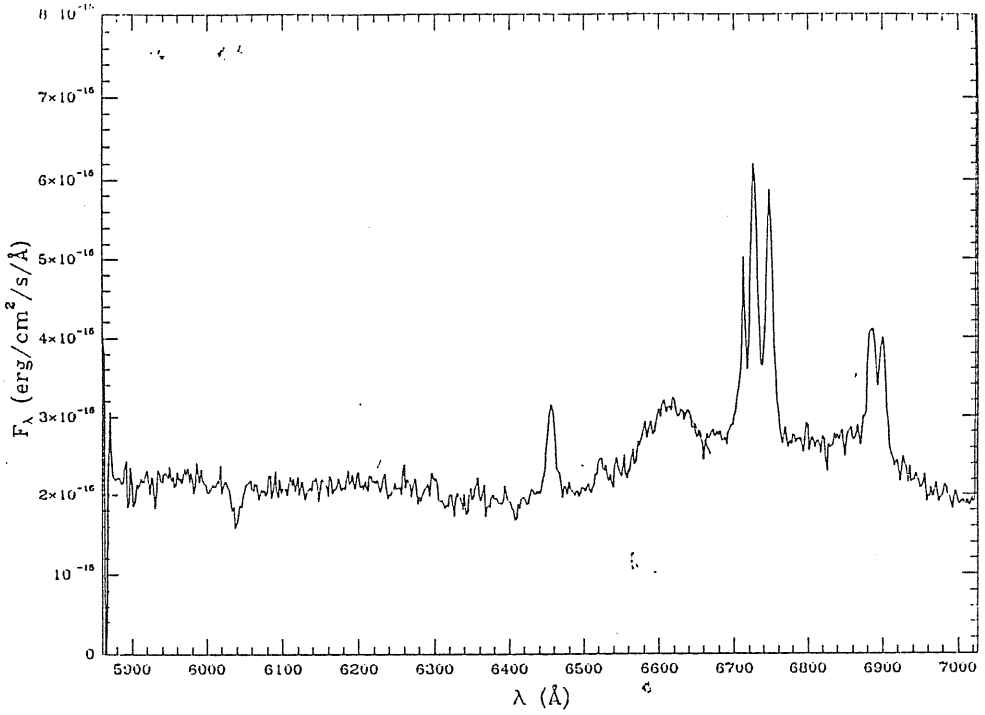

Figure 4.6: Arp 102b

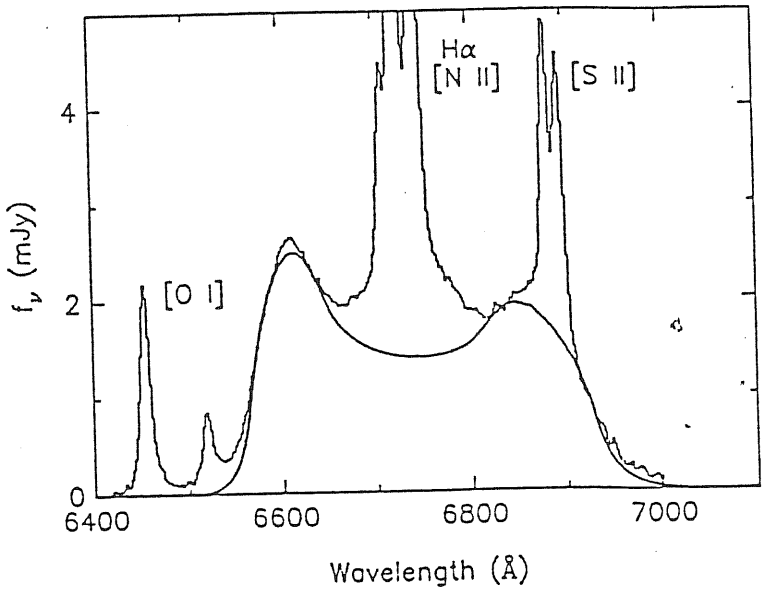

Figure 4.7: Accretion disc fit to the Hα profile of Arp 102b: From: Chen and Halpern (1989)

with the estimate made from the 3^{rd} Kepler law.

We measured the Hα/Hβ (Broad Component) ratio on the Asiago spectra: Hα/H$\beta \approx$ 10, with the flux emitted in Hα being $\approx 4 \cdot 10^{-13} erg\ s^{-1} cm^{-1}$. The high Balmer decrement suggests that the BLR suffer strong internal absorption.

Lyα was the sole line detected in the UV spectrum, but the width of Lyα is probably less than that of the Balmer lines. The flux due to the Lyα broad components is $\approx 1.4 \cdot 10^{-13} erg\ cm^{-2} s^{-1}$, giving a ratio of the *broad* Lyα/H$\beta \approx$ 3.5, which is typical of the values found in AGN. This points out against a peculiarity in the Lyα emission.

It is intriguing however that there is no evidence of CIVλ1549 in the spectrum obtained by Chen, Halpern and Filippenko (1989).

Moreover the fitted profiles do not reproduce the whole BC of Hα. There is a partial contribution of Hα near to the NC, suggesting that another component contributing to the BLR is present.

Taking into account these facts, it is worth emphasizing the role that internal absorption may play in selectively suppressing the emission of a BLR component. The extent of the problem is unclear, but this problem should be settled before applying any model–dependent consideration to the data. In this case, the absence of appreciable CIVλ1549 emission could suggest that the BLR gas emitting the HIL is *hidden* or *absorbed.* However, if a strong additional BC were superimposed on the profiles observed for Arp 102b, two shoulders should appear in correspondence of the peaks, and to my knowledge no similar resulting profiles have yet been published.

As Chen, Halpern, and Filippenko (1989) stressed, for the values of R_{out} and R_{in} reported above, light travel time is of order of $10^5 s$, so that short term variations on time scales of days are possible in response to variations of the central X–ray source. An independent confirmation of the rotating disc hypothesis may thus be provided via the reverberation mapping technique (Blandford and McKee, 1982).

4.5.2 3C390.3 ≡PKS 1845 + 79

3C390.3 is a radio galaxy with double–peaked Balmer line profiles (Fig.(4.8)). The possibility that the BL are emitted in an accretion disc has been extensively analyzed by Perez *et al.* (1987) and by Perez (1988).

They note that the central dip did not change radial velocity since the first spectra of the galaxy were taken, $\approx$ 17 yr ago. This make self–absorption due to an high–density bypassing cloud an unlikely explanation, since it is difficult that a bypassing cloud producing the absorption would remain at a constant v_r for such a long lapse of time.

The large and small scale radio structures, and the continuum energy distribution which shows the presence of a faint *Big bump* component, indicate that

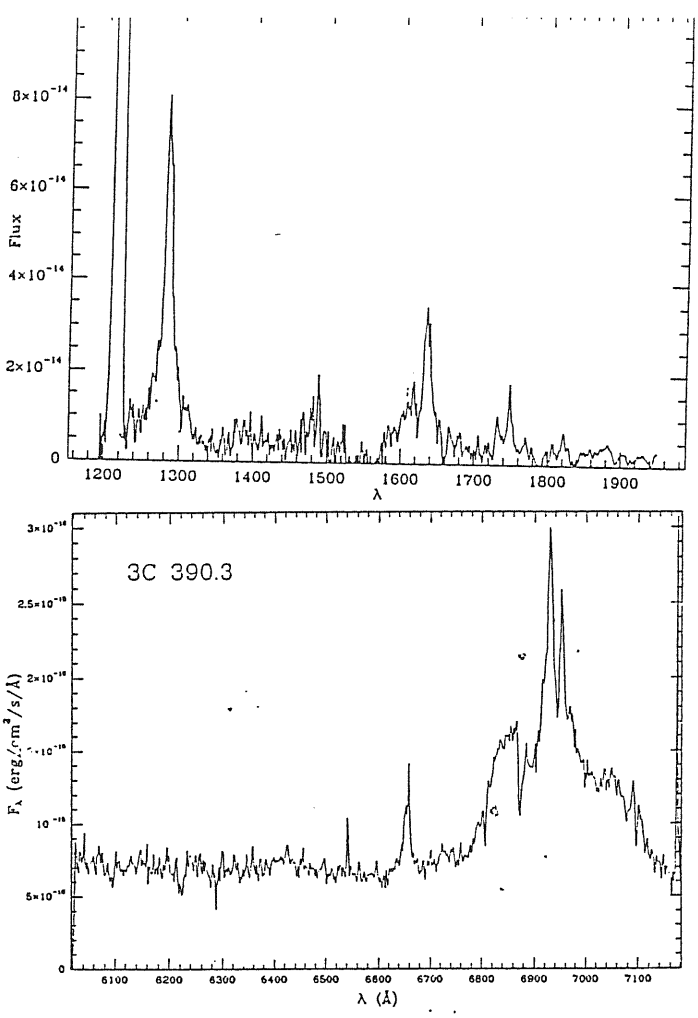

Figure 4.8: Optical and Ultraviolet spectra of 3C390.3

the emission is being collimated by a disc of intermediate inclination ($i \approx 60°$ (Perez *et al.*, 1988).

Despite the central the radial velocity of the central dip remains constant, 3C390.3 is a strongly variable objects. Variation in the continuum and in the profile shape has been observed on time scales of several months – 1 years. The spectroscopic variability is consistent with a high and low status (without any assumption of true periodicity).

Gaskell (1988) has pointed out that asymmetric variation of the double peak is shown in the spectra by Oke (1987), and he claims that this should rule out the accretion disc hypothesis. A visual inspection of all scans reproduced by Perez (1988), in the low and high photometric status, does not confirm any asymmetric variation in the peaks, within the confidence allowed by the quite low signal–to–noise ratio that affects the low state observations.

However, we note in our spectrum, that the red wing of Hα, beyond the red peak, is much stronger than that reported by Perez (1987). This *may* be due to infalling gas in a flattened geometry, and it is difficult to be explained in a *pure* disc geometry. Another severe difficulty to the accretion disc idea is that the centroid of the BL (evaluated as the mean radial velocity of the two peaks) is *blueshifted* by $\approx 540\ km\ s^{-1}$ with respect to the NC of the same line. Relativistic effects cannot readily explain a blueshift of a few hundred $km\ s^{-1}$;

however, due to the strongly asymmetric shape of the computed profiles from a relativistic accretion disc, it should be interesting to test whether a good fit can be performed also in this case (*e.g.* Figure (4.3B)).

The IUE spectrum, retrieved from the Ultraviolet Low Dispersion Archive (ULDA) is shown in figure (4.8). Lyα is much narrower than the Balmer Lines, suggesting that the BC is very weak compared to the NC, and contributes only to the line wings. These findings remind Arp 102b, but in this case the CIVλ1549 is present, with a profile very similar to that of the Balmer lines. This may suggests that different mechanisms are at work in the case of 3C390.3.

The profile of Hα and Hβ 3C390.3 and in 3C382 (the latter has been not discussed in detail here since the broad line profiles are similar in a qualitative way to those of 3C390.3, and the line shifts measurements give the same trend) can be explained if we consider that the observed *structures* are consistent with bipolar outflow, as originally suggested by Miley and Miller (1979).

The *double peaks* could be due to two BL clouds systems trapped in the radio plasma ejection, and outflowing on the opposite sides of the nucleus. This explanation avoids the problem related to the *blueshift* of the centroid of the two peaks. Whittle *et al.* (1988) have recently discovered that there are sub–components of the NLR and EELRs whose kinematics differs from the kinematics of the galaxian gas, is present and is *strictly related* to the radio lobes. The presence of subcomponents is responsible for *lumpinesses* in the [OIII]λ5007 profile, that sometimes let the integrated profile resemble a *double–peaked* one.

4.5.3 Akn 120

Akn 120 is reported to vary both in the continuum and the line emission (Schulz and Rafanelli, 1981; Alloin, Boisson and Pelat, 1988; Alloin *et al.*, 1989; Peterson *et al.*, 1983; 1985). According to Alloin, Boisson and Pelat (1988) it is possible to define a *low* and *high* activity spectrum and its related broad line profiles. These authors noted that difference line profiles, obtained when Akn 120 was in the low and high state, appear as *two–peaked* profiles with underlying broad wings (see Fig. (4.10)), and they interpreted this feature as a signature of a disc structure, whose emission is *triggered* during the maximum activity phase. This conclusion seems perfunctory, since:

- the red peak of the difference spectrum is stronger than the blue one, a circumstance which is not easy to understand in a disc model;
- the profile later changed in a way which is inconsistent with the disc model. The *blue* side of Hβ is strengthened in the spectrum taken on Dec. 22, 1987 (a "third" component has been switched on?, see Figures (4.9) and (4.10)) at ESO. The continuum level and the relative strength of Hβ and [OIII]λ5007 suggest that Akn 120 at the time of my observations was in a intermediate levels between the low and high state considered by Alloin,

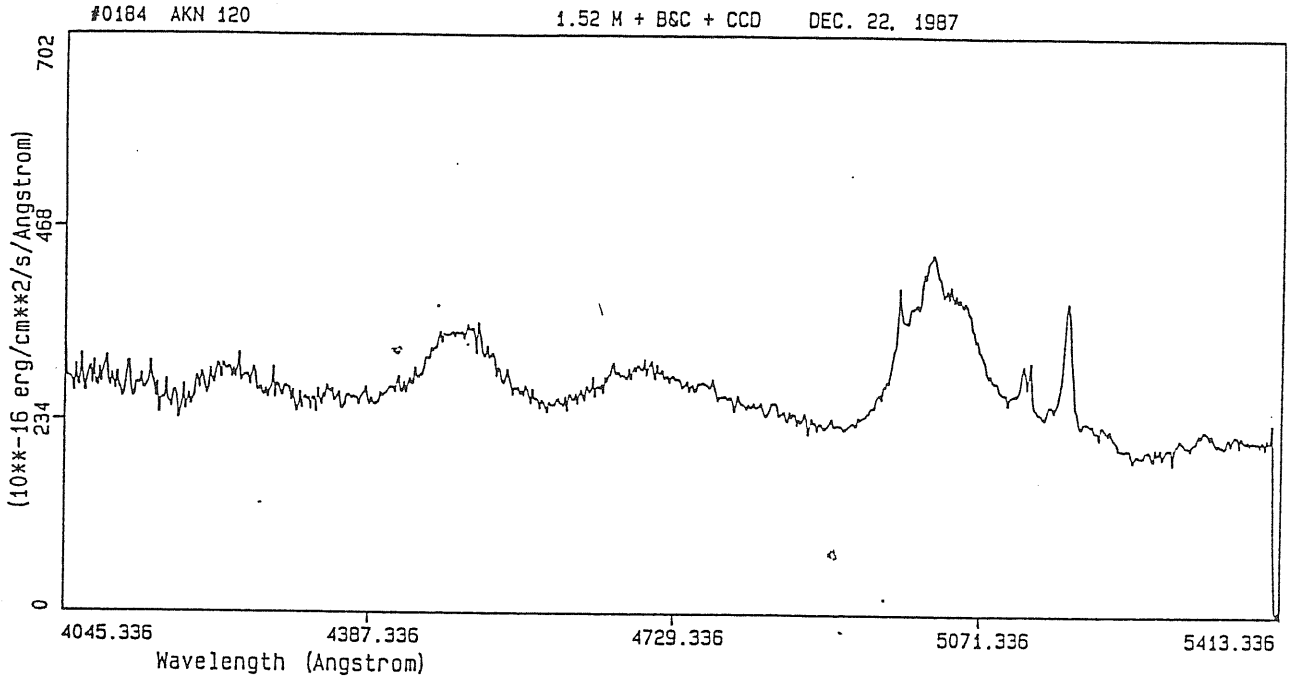

Figure 4.9: Spectrum of Akn 120

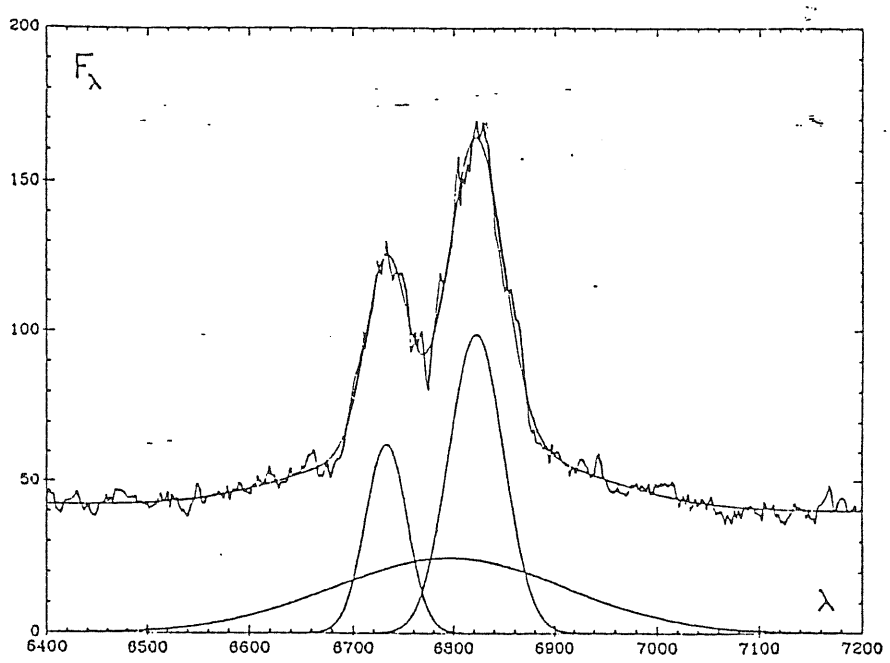

Figure 4.10: Difference profile of Hα for Akn 120. From: Alloin, Boisson, and Pelat (1988)

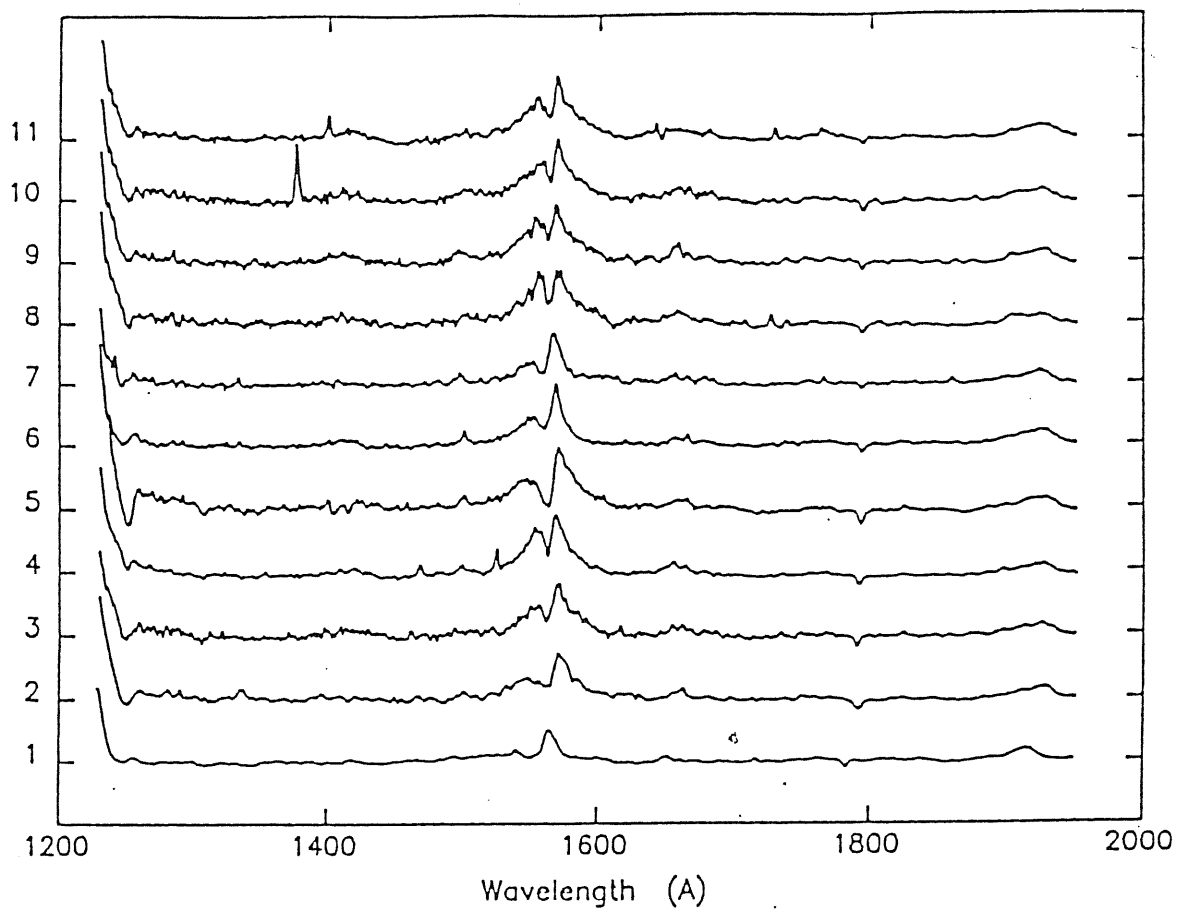

Figure 4.11: CIV profiles of NGC 3516 at different epochs. From: Voit *et al.*, (1987)

Boisson and Pelat (1988). Hence *the onset of the new component does not correlate with the continuum strength.*

This finding is perhaps one aspect of a more general phenomenon. Voit *et al.* (1987) report the presence of a variable *absorption feature* in the CIVλ1549 of NGC 3516. See Fig. (4.11)); observations labeled with progressive numbers span a temporal basis from 1978 to 1984. The absorption feature is variable on a timescale of $\sim$ 10 days. The blueshifted peak appears to be more strongly variable than the red one, and this is very difficult to council with the accretion disc idea. A similar conclusion holds also for the Stirpe, de Bruyn and van Gröningen (1983) report on the variability of NGC 5548.

4.6 Summary and Conclusions

4.6.1 Presence of the accretion disc

The idea that an accretion disc is present around the central black hole in AGN is supported by the following evidence:

1. accretion discs and massive black holes are expected at the center of active nuclei for explaining their enormous energy output (*e.g.* Rees, 1984).

2. the thermal emission due to an accretion disc provides a satisfactory fit to the *Big Bump*;

3. accretion discs provide a suitable explanation for the *Baldwin effect*;

4. accretion discs offer a nice explanation to the low ionization spectrum and to the *energy budget* problem of the BLR;

5. accretion discs are consistent with the beaming of the UV and X radiation;

6. accretion discs do not need any confining medium and may provide a reservoir of matter for the BLR clouds.

Ultimately, the *Big Bump* remains the most powerful argument in favour of the presence of the accretion disc. Other arguments listed above are *consistent* with the accretion disc idea, but they cannot used as a *probe*.

It is intriguing that the last instrumental improvements in X–ray spectroscopy, give *some* support to alternative explanations: an ensamble of dense, cold clouds could reprocess the non–thermal continuum and create a feature resembling the *Big Bump*. In this case, short term variability ($\sim$ few days) is expected.

On the other side, there are some tests that could be performed for the accretion disc hypothesis. There are some parameters that should correlate with the accretion disc inclination i. Choosing a sample of radio loud AGN, we have that:

- the ratio L_R/L_{1450} should correlate with the relative prominence of the *Big Bump* and hence with the disc inclination; since the *Big Bump* is strongly variable, an *time averaged value* of the ratio should be used.

- The parameter R should also correlate with i.

It should be very interesting to analyze whether the inclinations deduced from the two parameters are in agreement. An additional check may be provided by a study of the time delay of the Balmer Lines to variation in the ionizing continuum, since this would allow to estimate $R(1 - \sin i)$. Last, also the FeII strength should correlate with the *Big Bump* strength.

4.6.2 The accretion disc as part of the BLR

The situation is less clear for the problem of the disc contribution to the BLR. Summing up, the *Pro* and *Contra* for the hypothesis that the accretion disc emits the BL are:

Against:

1. There is only one object (Arp 102b) for which the accretion disc is really the *best buy* for explaining the observed profiles. In some other objects the evidence are either circumstantial or the assumption that a disc is present leads to inconsistencies.

2. Central dips of the profiles are uncommon.

3. Line profile asymmetries are difficult to understand unless non–uniform obscuration or illumination is invoked.

4. Line centroid blueshifts are a difficulty unless a second component is invoked;

5. High state–low state difference spectra show double peaked profiles that however do not exhibit simultaneous time variation.

6. Radial motions seems to be necessary for explaining the *Gaskell effect*

7. profile shapes are often logarithmic.

For:

1. the symmetric Lyα profile;

2. profiles are often stable over long times (*e.g.* tens of years);

3. the gas velocity increases toward the center;

4. the correlation between the Hβ width and the R parameter of Orr and Browne (1982);

5. the profile of Arp 102b; moreover there are some objects, mainly BLRG, with profiles that may be fittable by a relativistic accretion disc. The work on these objects is still in progress.

6. generally speaking, profiles computed for relativistic discs may account for some observed asymmetries. However the value of this suggestion is limited, since this work is still in progress (Calvani, Marziani and Sulentic, 1989b).

We believe that a *two–component* (*e.g.* a system of clouds in radial motion plus a rotating disc) model is encouraging, and it is sustained by some indirect confirmations. At the present time this scenario is however somewhat hypothetical.

4.6.3 Further work

Much further work remains therefore to be done in order to test the possibility that the accretion disc contributes to the BLR and, generally speaking, to clarify the kinematics of the emitting regions.

For the immediate future, from the theoretical point of view it is important to analyze thoroughly the relativistic effects on the line profiles. Most important, the line profile should be computed coupling the emission condition of the disc gas via a photoionization code.

From the observational point of view, it is necessary first to state with confidence whether there are difference in the kinematics of low and high luminosity objects. Many assumptions are extrapolated to different classes of objects, for which they may be no longer valid. This is not an easy task, since it would involve high resolution and high quality spectroscopy of a large sample of objects.

An accurate analysis of high dispersion, high signal–to–noise profiles can give a great deal of information on the BLR kinematics. This work is currently being done by myself, and a preliminary analysis of a few interesting examples has been made in the previous section. I believe that the quality of the data allows more quantitative considerations on the profile shapes, in particular on the profile skewness and on the curthosis. An analysis of the shapes based on the *statistical momenta*, *e.g.* considering the line profile as a statistical distribution, can give considerable information, provided that a large sample of AGN profiles is at disposal. Another important datum on the BLR dynamics, and more precisely on the presence of two kinematical components, is related to the velocity shifts of the HIL and LIL. As we have already stated, it is not an easy task to gain accurate data for the HIL in low redshift objects. The availability of these data is unfortunately bound to substantial instrumental advances.

Our hope to have definite arguments for testing our kinematical ideas relies also on variability studies. Low luminosity objects are the most suitable for this investigation. Systematic variability studies are only at the beginning, but, as widely stressed earlier, they provide the most powerful tool for analyzing both the geometry and the kinematics of the emitting regions. Simultaneous monitoring of the optical and UV range, as Space Telescope can at best provide on a large temporal basis, could give us a great insight on the BLR structure, and thus ultimately test whether the accretion disc emits part of the Broad Lines.

Appendix A

Accretion discs in AGN

In Chapter 1 the indication supporting the presence of an accreting supermassive black hole as the power source for AGN have been briefly analyzed. In this Appendix, a short and schematic review of the accretion modes expected in the various classes of AGN will be given, and physical parameters of the accretion flow relevant to the observations will be introduced.

The mode of accretion is primarily controlled by the specific angular momentum h (angular momentum per unit mass) of the infalling matter:

- if h$\leq \sqrt{12} r_g c$, the accretion flow can be considered radial;
- if h$> \sqrt{12} r_g c$ the accreting matter must reduce its angular momentum via viscous torques, before it can cross the event horizon,

where $r_g = 2GM/c^2$ is the gravitational radius of the black hole. If the second condition is satisfied, the accretion flow may build an accretion disc. The structure of the accretion disc is mainly governed by the ratio of the accretion rate $\dot{M}$ ($M_\odot$ yr^{-1}) to the Eddington accretion rate, $\dot{m} = \dot{M}/\dot{M}_E$, where $\dot{M}_E = L_E/c^2$, and

$$L_E = \frac{4\pi G M m_p c}{\sigma_T} \approx 1.3 \cdot 10^{46} (\frac{M}{10^8 M_\odot}) \; ergs^{-1} \tag{A.1}$$

is the Eddington luminosity, the luminosity at which radiation pressure forces balance gravity. G is the gravitational constant, M the mass of the compact object, m_p the proton mass, c the speed of light and σ_T the electron scattering cross section.

The Eddington ratio determines the vertical thickness and rules the radiative efficiency of the flow.

- A *thin accretion disc* forms if the accretion flow is able to radiate most of its binding energy, and $\dot{m} < 1$.
- Since the dynamical timescale depends on the black hole mass $t_{dyn} \propto M$ and the cooling timescale for thermal Bremsstrahlung processes is:

$$t_{cool} \propto 1/\rho \propto l^3/\dot{M}t \propto M/\dot{m}, \tag{A.2}$$

their ratio is $t_{cool}/t_{dyn} \propto 1/\dot{m}$. Hence, in the case $\dot{m} \ll 1$, the accretion flow may not be able to radiate its binding energy, and may inflate to form an *ion torus* (Rees *et al.*,1982).

- if the Eddington ratio is $\dot{m} > 1$, the accretion flow is also in this case unable to cool, due to the proportionality of the electron scattering opacity to the Eddington ratio itself $\tau_{es} \propto l\rho \propto \dot{m}$. The disc inflate to form a *radiation pressure supported torus.*

In the following section the most basic facts about each type of accretion disc are recalled.

A.1 Thin discs

In the framework of the Shakura and Sunyaev (1973, hereafter SS) model, it can be shown that the circular velocity v_Φ of the disc gas would be very close to its Keplerian value (Frank, King and Raine, 1985), $v_\Phi \approx (GM/R)^{1/2}$. In the following, the terms *thin disc* and *keplerian disc* will be therefore used as synonyms.

The dynamical t_{Kepl} timescale is given by the orbital period $t_{Kepl} = t_{orb} \approx 2\pi/\omega$. Keplerian motion implies differential rotation, which reflects the presence of shear viscosity, i.e. transport of momentum in the radial direction. SS introduced the phenomenological parameter α:

$$\nu = \alpha c_s H \tag{A.3}$$

where $\nu = \lambda_{turb} v_{turb}$, ($\lambda_{turb}$ is the scale size of the turbolent motion and v_{turb} is the turbolent velocity) is the coefficient of the shear viscosity, c_s is the sound speed of the gas and H is the height of the disc. Equation (1.3) becomes:

$$\alpha = \frac{\lambda_{turb} v_{turb}}{c_S H} \tag{A.4}$$

Since it is reasonable that $\lambda_{turb} \approx H$ and $v_{turb} < c_S$, α is ≤ 1 (Frank, King and Raine, 1985): *the thin disc assumption is consistent with the condition* $\alpha \leq 1$. The radial drift time scale can be estimated recalling that:

$$t_{vis} \sim \frac{R^2}{\nu} \sim \frac{R^2}{\alpha c_s H} \sim \frac{1}{\alpha} \frac{R^2}{H\sqrt{T} M^{-1/2} R^{1/2} H} \sim \frac{1}{\alpha}\left(\frac{H}{R}\right)^{-2} t_{Kepl} \tag{A.5}$$

The equation of the disc structure (conservation of mass, momentum, and energy) can be integrated for a steady, axisymmetric, non self–gravitating accretion disc (SS, 1973; reviews are given also by Rees (1984), Pringle (1981), Frank, King and Raine (1985)) to find an analytical solution for the temperature, the surface density, the disc height, the opacity as a function of the distance R from the

central object, M, $\dot{M}$ and α. The equation for the numerical density n (cm^{-3}) as a function of the disc radius is reported below, scaled as for the opportune values of the physical parameters for the AGN. n has been computed for the case c) of the SS model, that is when gas pressure overcomes radiation pressure ($P_r \ll P_g$) and when the free–free opacity dominates over the electron scattering, as is the case in the outer region of the disc.

$$n = 1.51 \cdot 10^9 (\frac{\dot{M}}{1 M_\odot yr^{-1}})^{11/20} (\frac{M}{10^8 M_\odot})^{5/8} (\frac{R}{10^{16} cm})^{-15/8} f^{11/5} \alpha^{-7/10} cm^{-3} \quad \text{(A.6)}$$

with $f = 1 - 6R_g/R)^{1/2}$.

The basic output radiation is thermal in origin, in the optically thick case. The shape of the spectrum is a *stretched* black body, since each disc annulus radiates as a black body, but at a different temperature, and can be found integrating the temperature distribution over the radius. Electron scattering and Compton processes in an *atmosphere* above the disc can *harden* the spectrum. Their role is discussed in Chapter 3 in connection with the observations.

A.2 Thick accretion discs

The shape of a thick disc can be computed once the surface angular momentum distribution, the inner edge r_{in} and the height at r_{in} are specified. It results that the shape of a thick disc is almost spherical.

The internal structure of a thick disc is schematically shown in Figure 1. In the innermost part of the disc, inside the radius where the pressure maximum is reached, the inward directed pressure gradient determines a velocity value larger than that of the local Keplerian velocity. Material is allowed to remain in stable circular orbits between the last marginally stable orbit $R_{ms} = 3R_g$ and the last marginally bound orbit $R_{mb} = 2R_g$, but its binding energy is reduced from its maximum value at r_{ms} to near 0 at r_{mb}. As a consequence tori will be less efficient energy converter than thin disc. At the inner radius r_{in} a cusp forms. The cusp acts like a Lagrangian point in a mass transferring binary, and marks the transition from a slow inward drift ($t_{vis} \sim 1/\alpha t_{Kepl}$, setting $H \sim R$) to nearly radial free fall.

Close to the rotation axis hydrostatic equilibrium is not possible, and a hollow axial region or *funnel* forms. It allows radiation and matter from the inner walls of the torus to escape. It is a suitable site for jet formation and collimation.

A.2.1 Ion tori

The onset of an ion torus is expected when:

- $\dot{m} \ll 1$;

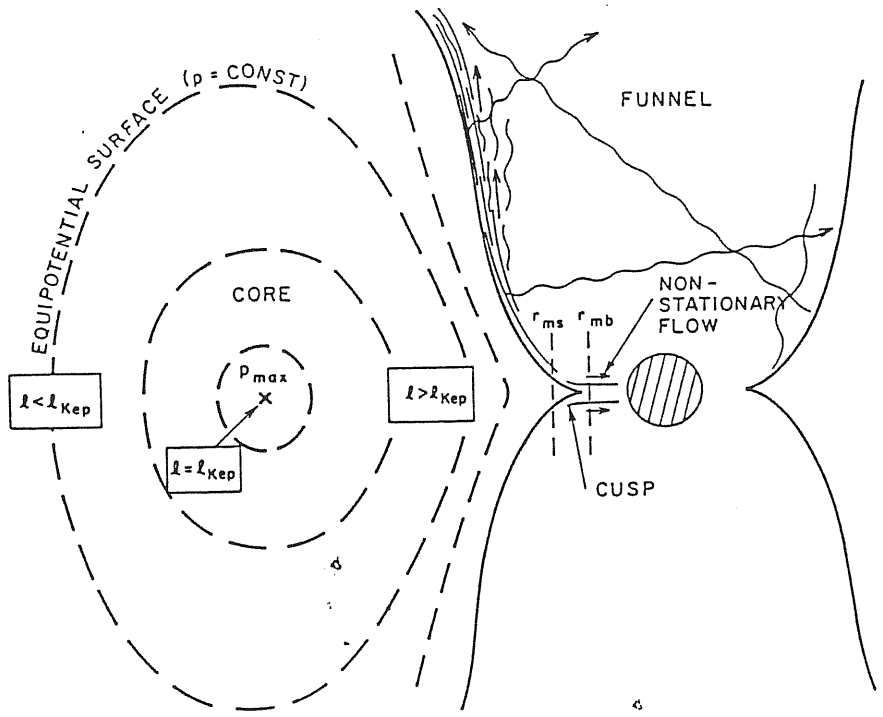

Figure A.1: The inner structure of a *thick accretion disc.* From: Begelmann (1985)

- electron and ions in the inner regions ($R < 2000R_g$) are thermally decoupled.

If these conditions are satisfied, the thermal pressure of the ions heated at their virial temperature, may be able to support the torus.

Thermal decoupling between ions and electrons means that thermal Bremsstrahlung is a non efficient coolant, thus providing the condition:

$$\dot{m} < 50\alpha^2 \tag{A.7}$$

Ion tori are very inefficient radiators; and they have been proposed by Rees *et al.* (1982) as the accretion flow for the Broad Line Radio Galaxies, in order to explain the low optical luminosity compared to the radio power in this class of objects.

The emitted radiation is mostly non thermal in origin, and is emitted predominantly in the infrared.

A.2.2 Radiation Tori

Radiation tori may occur when radiation pressure forces become comparable to gravity.

Self shadowing effects would affect both the observed spectrum and the apparent luminosity:

- the observed spectrum will be strongly dependent on the inclination angle, since radiation coming from the *funnel* is emitted by the internal parts of the disc, which are hotter than the surface. The harder radiation is detected only be the observer which sees the disc pole–on, while occultation of the innermost hottest parts of the torus at large angles between the rotation axis and the line of sight will occur.

- a radiation torus appears to radiate a factor ~ 20 super–Eddington at small viewing angles, whether the same thick disc seen edge on would seem to radiate nearly at the Eddington limit (Madau, 1987)

Appendix B

Computation of line profiles

In this Appendix the explicit integral expressions for the computation of the line profiles are introduced for various geometrical and kinematical configurations. Their physical significance and the results of the various models are discussed in Chapters 2 and 4.

B.1 Radially moving clouds

In Fig.(B.1) the choice of the frame of reference is represented. In a polar coordinate system, R is the distance of a cloud from the central objects that radiate the ionizing continuum, Φ is its azimuthal angle, θ its altitude angle the plane X–Y.

The component of the cloud velocity toward a distant observer is therefore: $v_r = v \cos\theta \cos\Phi$. Thus, the cloud contributes to the line profile at wavelength:

$$\lambda_{obs} = \delta[\lambda - \lambda_0(1 + \frac{v \cos\theta \cos\Phi}{c})] \tag{B.1}$$

where λ_0 is emission wavelength in the rest frame of the cloud. The use of a δ function is valid under the assumption that the broadening in the single cloud is negligible in comparison with the line broadening due to the bulk motion of the cloud ensamble.

We can now consider the emission of the cloud ensamble as a whole, assuming that the dimensions of the clouds are much less the thickness of the shell: let n_c be the numerical density of emitting clouds, each of emissivity j_c, in a shell constrained between radii R_1 and R_2. Here j_c (and generally speaking, also n_c) can be considered function of R mainly through the dependence on R of the electron density $n_{e,cl}$ of each cloud.

In this case, the total emission at a fixed wavelength λ is given integrating the contribution of each cloud over the volume of the shell. In spherical coordinates,

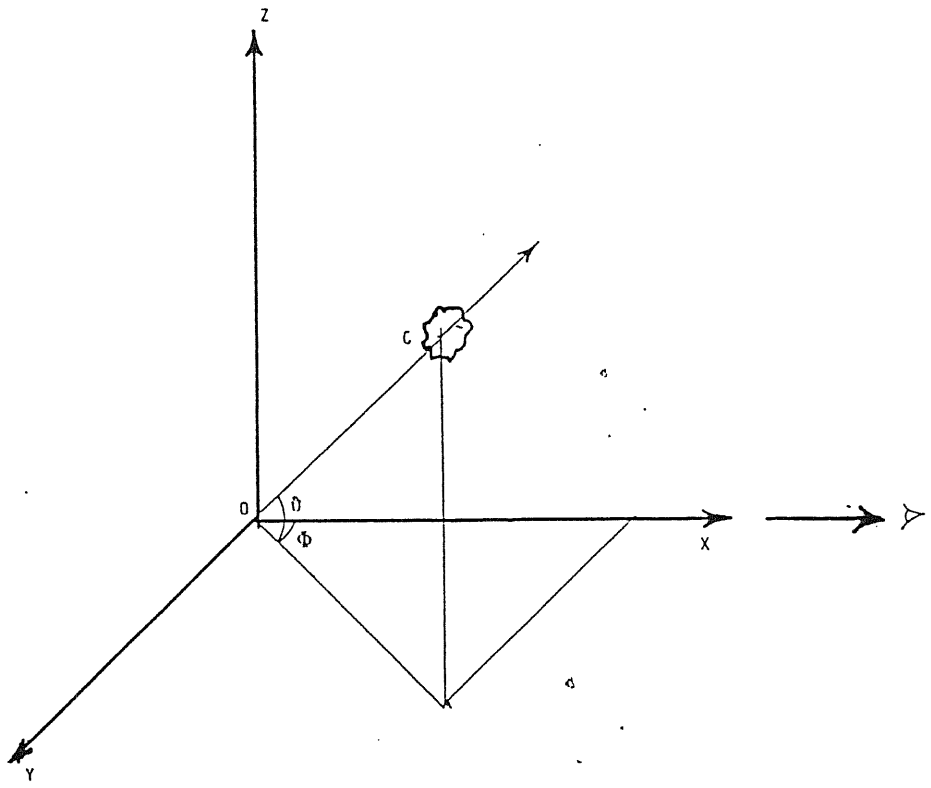

Figure B.1: Choice of the geometrical parameters for a radially moving cloud

the volume element is $dV = r^2 \sin\theta d\Phi dr d\theta$ and the integral may be written as:

$$L_{\lambda-\lambda_0} = \int_{R_1}^{R_2} \int_0^{2\pi} \int_{-1}^{+1} n_c j_c \cdot \delta[\lambda - \lambda_0(1 + \frac{v\cos\theta\cos\Phi}{c})] R^2 d\mu d\Phi dR \qquad \text{(B.2)}$$

where $\mu = \cos\theta$.

This expression gives the luminosity expected in the line as a function of $\lambda - \lambda_0$, and thus describes completely the line profile, once the functions $v(R)$, $j_c(R, \lambda, \mu)$ and $n_c(R)$ are specified.

B.2 Bipolar outflow

We consider a system of cloud constrained in a jet–like configuration. Each cloud moves with a velocity which is a function only of the distance to the center r, as in the precedent case. The meaning of the various geometrical parameters is shown in Figure 2. Here Φ_0 is the opening angle of the jet, θ is the angle between the centroid of the jet and the line of sight, and Θ the angle between of the velocity vector of a cloud and the line of sight. Its cosine μ may be found by solving the spherical triangle (see Fig.(B.2)) ABC, where C marks the cloud position:

$$\cos\Theta = \mu = \cos\Phi_0 \cos i + \sin\Phi_0 \sin i \cos\phi' \qquad \text{(B.3)}$$

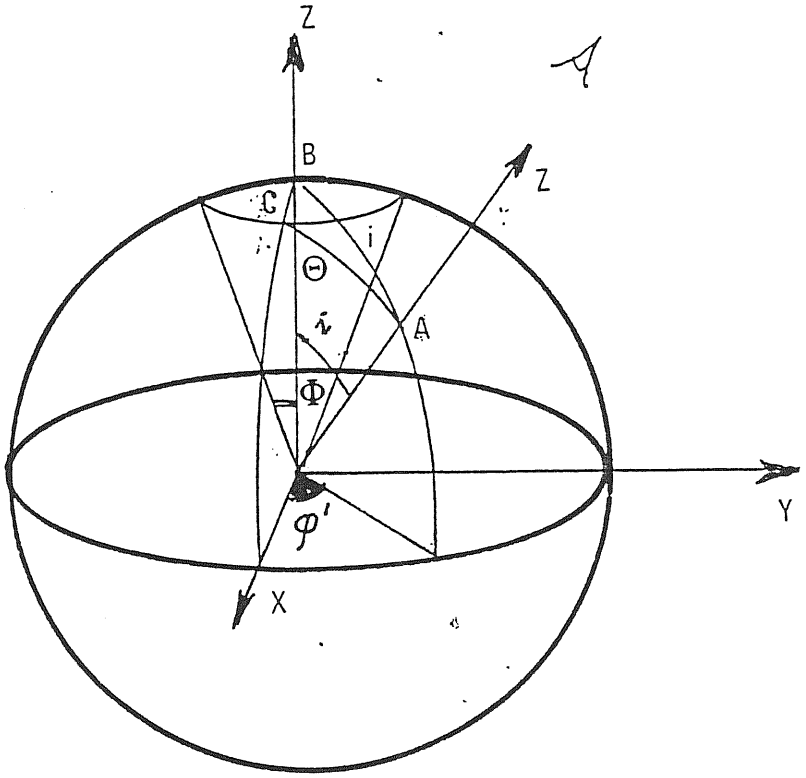

Figure B.2: The bipolar outflow geometry

where θ is the altitude angle, and ϕ' is an azimuthal angle, whose vertex lies on the jet axis, as shown in Figure (B.2), and varies between 0 and 2π. Each volume element in the solid angle of the jet contributes as:

$$dL_{\lambda-\lambda_0} = d\theta d\phi' dR R^2 \sin\theta n_c(r) j_c(r,\lambda,\mu)\delta[\lambda - \lambda_0(1+\frac{v\mu}{c})] \qquad \text{(B.4)}$$

Integrating over the whole solid angle:

$$L_{\lambda-\lambda_0} = -2\int_{-\Phi_0}^{\Phi_0} d\theta \int_0^{2\pi} \phi' \int_{R_{in}}^{R_{out}} j_c(R,\lambda,\mu)\sigma(R)\cdot\delta[\lambda-\lambda_0(1-\frac{v\mu}{c})]r^2 dr \qquad \text{(B.5)}$$

In this case, a double peaked profile may result. An interesting relation is given by van Groningen (1983) in case of small aperture angles. He found that the ratio of the red peak intensity I_{red} to the blue I_{blue} is given by:

$$\frac{I_{red}}{I_{blue}} \approx \frac{1+\cos\theta}{1-\cos\theta}\cos\Phi_0 \qquad \text{(B.6)}$$

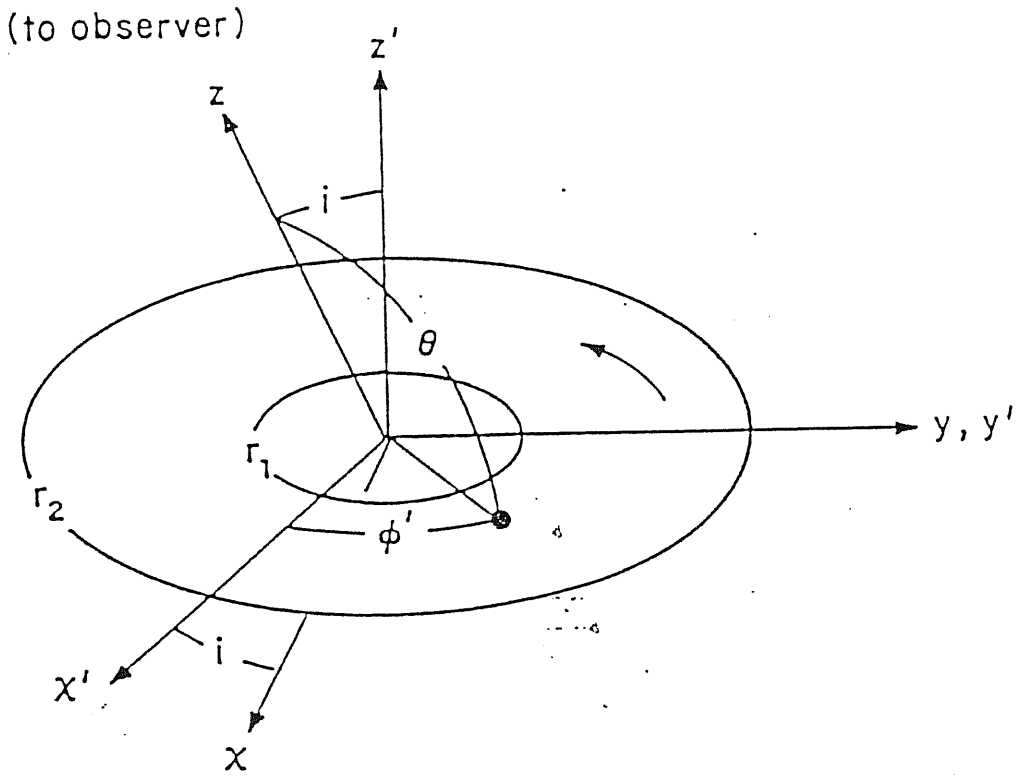

Figure B.3: The disc geometry

B.3 Disc geometry

B.3.1 Non relativistic disc

The geometry of the problem is shown in Figure 3. The normal to the disc forms an angle i with the tangent plane to the celestial sphere (*i.e.*, $i = 0°$ the disc is seen face–on). ϕ' is the azimuthal angle in the plane of the disc, while θ is the angle between the emitting surface element on the disc and the line of sight.

Let the disc have local surface emissivity j_σ $[erg\ g^{-1}\ s^{-1} cm^2]$ and surface density σ $([gcm^{-2}])$.

Each disc surface element will move with respect to a distant observer with radial velocity $v_r = v(R)\cos\phi'\cos i$. The observed radiation will be at wavelength λ_{obs}:

$$\lambda_{obs} = \delta[\lambda - \lambda_0(1 + \frac{v\cos i\cos\phi'}{c})] \tag{B.7}$$

Each disc element will give a flux at fixed λ:

$$dL_{\lambda-\lambda_0} = \sigma(R) j_\sigma(R,\lambda) d\Sigma \tag{B.8}$$

where $d\Sigma = R^2 d\phi' dR$ is the element of disc surface. Setting $\mu = \cos\phi'$, the integral over the whole disc surface may be written as:

$$L_{\lambda-\lambda_0} = -2\int_{R_{in}}^{R_{out}}\int_{-1}^{+1} j_\sigma(r)\sigma(r)\cdot\delta[\lambda-\lambda_0(1-\frac{v\mu\cos i}{c})]R(1-\mu^2)^{-1/2}d\mu dR \quad \text{(B.9)}$$

The numerical integration of this equation yields the dimensionless line profile of an optically thick disc since the emissivity is assumed independent on the angle relative to the normal of the disc.

B.3.2 Relativistic disc

The profiles of lines emitted by a relativistic accretion disc have been firstly analyzed by Mathews (1982), by Chen, Halpern, and Filippenko (1989) and Chen and Halpern (1989). Here a concise description of the procedure followed in the last two works is reported.

The geometrical configuration and the frames of reference are chosen as in Fig. 3. Azimuthal angles ϕ and ϕ' are measured with respect to the x and x' axis. In the case the Schwarzschild metric is assumed, it is possible to calculate the frequency in the rest frame of the emitting disc element ν_{em} of a photon originating at radius r from the knowledge of four velocity of the emitting element at r and of the four momentum of the emitted photon (Luminet, 1979; Chen, Halpern and Filippenko, 1989):

$$\nu_{em} = \frac{p^\alpha u_\alpha}{h} = \nu(1-\frac{3GM}{R})^{-1/2}(1+\frac{bG^{1/2}M^{1/2}}{c^2R^{3/2}}\sin i\sin\phi) \quad \text{(B.10)}$$

Let $\epsilon(\xi)$ be the emissivity as a function of $\xi = R/M$ is the adimensional radius. The emissivity in the emitting frame can be expressed by a delta function at the rest frequency of emission:

$$I_{\nu_e} = \epsilon(\xi)\delta(\nu_e-\nu)\ ergcm^{-2}\ s^{-1}sterad^{-1} \quad \text{(B.11)}$$

Taking into account that the ratio $I_\nu/v^3 = I_\nu/\nu$ is a Lorentz invariant, expressing the solid angle $d\Omega$ as $d\Omega = \frac{bdbd\phi}{d^2}$, where d is the distance to the AGN, and substituting $1+X = \lambda_0/\lambda$ the dimensionless profile is given by:

$$F_X = 1/d^2\int\epsilon(\xi)(1+X)^4\frac{bdbd\phi}{dX} \quad \text{(B.12)}$$

The parameter b can be written in term of r and θ in the weak field approximation. This allows to write:

$$L_{\lambda-\lambda_0} = \frac{2GM^2\lambda_0\cos i}{\lambda^2c^4d^2}\int_{\xi_a}^{xi_b} d\xi\frac{\alpha(1+X)^3\xi^{3/2}\epsilon(\xi)}{[(1+X)^2\sin^2 i-\beta]^{1/2}}\cdot[1+\frac{1}{\xi}\cdot(\frac{2(1+X)^2}{(1+X)^2\cos^2 i}+\beta)-1] \quad \text{(B.13)}$$

where $\alpha = (1-3/\xi)^{1/2}$ and $\beta = \xi(1+X-\alpha)^2$. The results of the integrations of this expression are reported in Chapter 4, for a choice of the emissivity:

$$\epsilon = \frac{\epsilon_0}{4\pi}\xi^{-q} \tag{B.14}$$

A more realistic treatment of the problem includes a local broadening source (*e.g.* a gaussian function; Chen and Halpern, 1989). This greatly complicates the computations, that are therefore not reported here. Results are discussed in Chapter 4 in connection with the observations.

References

Acosta–Pulido J., Perez–Fournon I., Calvani M., Wilson A.S.: 1989, *Astrophys. J. submitted*

Aller L.H.: 1984, *Physics of thermal gaseous Nebulae.* Dordrecht: Reidel

Alloin D., Baribaud T., Boisson C., Pelat D.: 1989, in: *Active Galactic Nuclei*, IAU Symposium No. 134. D.E. Osterbrock and J.S. Miller (Eds.) , p.259

Alloin D., Pelat D., Boisson C.: 1988, *Astron. Astrophys.* **200**, 17

Angel J.R.P., Stockman H.S.: 1980, *Ann. Rev. Astron. Astroph.* **18**, 321

Antonucci R.R.J.: 1983, *Nature* **303**, 358

Antonucci R.R.J., Cohen R.D.: 1983, *Astrophys. J.* **271**, 564

Antonucci R.R.J., Kinney A.L., Ford H.C.: 1988, *STSci Preprint No. 328.*

Antonucci R.R.J., Miller J.S.: 1985, *Astrophys. J.* 297, 621

Auer L.H., van Blerkom D.: 1972, *Astrophys. J.* **178**, 175

Baldwin J.A.: 1975, *Astrophys. J.* **201**, 26

Baldwin J.A.: 1977, *Astrophys. J.* **214**, 679

Baldwin J.A., Burke W.L., Gaskell C.M., Wampler E.J.: 1978, *Nature* **273**, 431

Baldwin J.A., Smith M.G.: 1983, *M. N. R. astr. Soc.* **204**, 331

Baldwin J.A., Wilson A.S., Whittle M.: 1987, *Astrophys. J.* **319**, 84

Band D.L., Malkan M.A.: 1988, in: *Active Galactic Nuclei*, Proceedings of the Conference held at Atlanta, Georgia, on October 28–30, 1987. H.R. Miller, P.J. Wiita (Eds.) , p. 230

Bassani L., Dean A.J., Di Cocco G., Perotti F.: 1985, in: *Active Galactic Nuclei.* Manchester: Manchester Univ. Press. J.E. Dyson (Ed.)

Baum S.A., Heckman T.M.: 1988, *preprint.*

Baum S.A., Heckman T., Bridle A., van Breugel W., Miley G.: 1988, *Astrophys. J. Supp.***68**, 463

Bechtold J., Czerny B., Elvis M., Fabbiano G., Green R.F.: 1987, *Astrophys. J.* **314**, 699

Begelman M.C.: 1985, in: *Astrophysics of Active Galaxies and Quasi-Stellar Objects* Mill Valley: University Science Books. J.S. Miller (Ed.), p. 411

Binette L., Robinson A., Courvoisier T. J.-L.: 1988, *Astron. Astrophys.* **194**, 65

Binney J., Tremaine S.D.: 1987, *Galactic Dynamics.* Princeton: Princeton University Press

Blandford R.D., McKee Chr. F.: 1982, *Astrophys. J.* **255**, 419

Blumenthal G.R., Mathews W.G.: 1975, *Astrophys. J.* **198**, 517

Blumenthal G.R., Mathews W.G.: 1979, *Astrophys. J.* **233**, 479

Boroson T.A.: 1989, *Astrophys. J. Letters* **343**, L9

Boroson T.A., Oke J.B.: 1984, *Astrophys. J.* **281**, 535

Browne I.W.A., Clark R.R., Moore P.K., Muxlow T.W.B., Wilkinson P.N., Cohen M.B., Porcas R.W.: 1982, *Nature* **299**, 788

Calvani M., Marziani P., Padovani P.: 1989, *SISSA preprint*
Calvani M., Marziani P., Sulentic J.W.: 1989a, *in preparation*
Calvani M., Marziani P., Sulentic J.W.: 1989b, *in preparation*
Capriotti E., Foltz C., Byard P.: 1980, *Astrophys. J.* **241**, 903
Carroll T.J., Kwan J.: 1985, *Astrophys. J.* **288**, 73
Capriotti E., Foltz C., Byard P.: 1979, *Astrophys. J.* **230**, 681
Chen K., Halpern J.P.: 1989, *preprint*
Chen K., Halpern J.P., Filippenko A.V.: 1989, *preprint*
Cheng F.H., Fang L.Z.: 1987, *M. N. R. astr. Soc.* **226**, 485
Clavel J., Altamore A., Boksenberg A., Bromage G.E., Elvius A., Pelat D., Penston M.V., Perola G., Snijders M.A.J., Ulrich M.–H.: 1987, *Astrophys. J.* **321**, 251
Cohen R.D.: 1983, *Astrophys. J.* **273**, 489
Cohen R.D., Rudy R.J., Puetter R.C., Ake T.B., Foltz C.B.: 1989, *Astrophys. J.* **311**, 135
Cohen R.D., Osterbrock D.E.: 1981, *Astrophys. J.* **234**, 81
Collin–Souffrin S.: 1986, *Astron. Astrophys.* **166**, 115
Collin–Souffrin S.: 1987, *Astron. Astrophys.* **179**, 60
Collin–Souffrin S., Dumont S., Tully J.: 1982, *Astron. Astrophys.* **106**, 362
Collin–Souffrin S., Joly M., Pequignot D., Dumont S.: 1986, *Astron. Astrophys.* **166**, 27
Collin–Souffrin S., Dumont A.M.: 1989, *preprint*
Collin–Souffrin S., Dyson J.E., Mc Dowell J.C., Perry J.J.: 1988, *M. N. R. astr. Soc.* **322**, 539
Collin–Souffrin S., Lasota J.-P.: 1988, *Publ. Astron. Soc. of Pacific* **100**, 1041
Corbin M.R., Baldwin J.A., Wilson A.S.: 1988, *Astrophys. J.* **334**, 584
Czerny B, Elvis M. : 1987, *Astrophys. J.* **321**, 305
Davidson K., Netzer H.: 1979, *Review of Modern Physics***51**, 715
de Bruyn A.G.: 1980, *Highlights of Astronomy* **5**, 631
De Robertis M.: 1985, *Astrophys. J.* **289**, 67
De Robertis M.: 1987, *Astrophys. J.* **316**, 597
Dressler, A: 1989, in: *Active Galactic Nuclei*, IAU Symposium No. 134. D.E. Osterbrock and J.S. Miller (Eds.) , p.217
Dumont A.M., Collin Souffrin S.: 1989a, *Preprint*
Dumont A.M., Collin Souffrin S.: 1989b, *Preprint*
Edelson R.A., Krolik J.H.: 1988, *Astrophys. J.* **333**, 646
Elitzur M., Netzer H.: 1985, *Astrophys. J.* **291**, 464
Elvis M.: 1989a, *Harvard–Smithsonian Center for Astrophysics Preprint No. 2585*
Elvis M.: 1989b, *Harvard–Smithsonian Center for Astrophysics Preprint No. 2846*
Fabian A.C., Guilbert P.W., Arnaud K.A., Shafer R.A., Tennant A.F., Ward M.J.: 1986 *M. N. R. astr. Soc.* **218**, 457

Ferland G.J., Shields G.A.: 1985, in: *Astrophysics of Active Galaxies and Quasi-Stellar Objects* Mill Valley: University Science Books. J.S. Miller (Ed.), p. 157

Filippenko A.V.: 1988a, in in: *Supermassive Black Holes*, Proceedings of the Workshop held at G.Mason University, Fairfax, Virginia, 14–16 Oct. 1986 M.Kafatos (Ed.) , p. 104

Filippenko A.V.: 1988b, *Adv. Space Res.* **8**, 5

Filippenko A.V., Sargent W.L.W.: 1988, *Astrophys. J.* **324**, 134

Frank J., King A.R., Raine D.J.: 1985, *Accretion Power in Astrophysics.* Cambridge University Press.

Fried J.W., SChulz H.: 1983, *Astron. Astrophys.* **118**, 166

Gaskell C.M.: 1982, *Astrophys. J.* **263**, 79

Gaskell C.M.: 1983, *Astrophys. J. Letters* **267**, L1

Gaskell C.M.: 1988, in: *Active Galactic Nuclei*, Proceedings of the Conference held at Atlanta, Georgia, on October 28–30, 1987. H.R. Miller, P.J. Wiita (Eds.) , p. 61

Gaskell C.M., Sparke L.S.: 1986, *Astrophys. J.* **305**, 175

Grandi S.A.: 1983, *Astrophys. J.* **268**, 591

Grandi S.A., Osterbrock D.E.: 1978, *Astrophys. J.* **220**, 783

Gregory S., Ptak R., Stoner R.: 1982, *Astrophys. J.* **261**, 30

Guilbert P.W., Rees M.J.: 1988, *M. N. R. astr. Soc.* **233**, 475

Haniff C.A., Wilson A.S., Ward M.J.: 1988, *Astrophys. J.* **334**, 104

Halpern J.P., Grindlay J.E.: 1980, *Astrophys. J.* **242**, 1041

Halpern J.P., Filippenko A.V.: 1988, *Nature* **331**, 46

Heckman T.M.: 1987 in *Starburst and Galaxy evolution.* Editions Frontieres. T.X. Thuan, T. Montmerle, J. Tran Thanh Van (Eds.).

Heckman T.M., Lebofky M.J., Rieke G.H., van Breugel W.: 1983, *Astrophys. J.* **272**, 400

Holt S.S.: 1987, *Astroph. Lett. and Communications* **26**,61

Holt S.S., Mushotzsky R.F., Becker R.M., Boldt E.A., Serlemitsos, P.J., Szymkowiak A.E., White N.E.: 1980, *Astrophys. J.* **241**, L13

Hutchings J.B.: 1989, *preprint*

Hutchings J.B., Cramton D., Campbell B.: 1983, *Astrophys. J.* **280**, 41

Joly M., Collin–Souffrin S., Masnou J.L., Nottale L.: 1985, *Astron. Astrophys.* **152**, 281

Junkkarinnen V.: 1989, in: *Active Galactic Nuclei*, IAU Symposium No. 134. D.E. Osterbrock and J.S. Miller (Eds.) , *in press*

Khachikian E. Y., Weedman D.W.: 1974, *Astrophys. J.* **192**, 581

Kinney A.L., Huggins P.J., Bregman J.N., Glassgold A.E.: 1985, *Astrophys. J.* **291**, 128

Kormendy J.: 1988, in: *Supermassive Black Holes*, Proceedings of the Workshop held at G.Mason University, Fairfax, Virginia, 14–16 Oct. 1986 M.Kafatos (Ed.) p.2191

Kormendy J.: 1989, in: *Dynamics and Interaction of Galaxies.* Proceedings of the Conference held in Heidelberg, 29 May – 2 June, 1989. A.Toomre and R Wielen (Ed.). *in press, in press*
Koski A.T.: 1978, *Astrophys. J.* **223**, 56
Krolik J.H.: 1988a, in: *Active Galactic Nuclei*, Proceedings of the Conference held at Atlanta, Georgia, on October 28–30, 1987. H.R. Miller, P.J. Wiita (Eds.) , p.19
Krolik J.H.: 1988b, *Astrophys. J.* **325**, 148
Krolik J.H.: 1989, in: *Active Galactic Nuclei*, IAU Symposium No. 134. D.E. Osterbrock and J.S. Miller (Eds.) , p.285
Krolik J.H., Kallman T.R.: 1988, *Astrophys. J.* **324**, 714
Krolik J.H., McKee Chr. F., Tarter C.B.: 1981, *Astrophys. J.* **249**, 422
Kruper J.S., Urry C.M., Canizares C.R.: 1989, *preprint*
Kwan J.: 1984, *Astrophys. J.* **283**, 70
Kwan J., Carroll T.J.: 1982, *Astrophys. J.* **261, 25**
Kwan J., Krolik J.H.: 1979, *Astrophys. J. Letters* **233**, L91
Kwan J., Krolik J.H.: 1981, *Astrophys. J.* **250**, 478
Laor A., Netzer H.: 1989, *preprint*
Lawrence A.: 1987, *Publ. Astron. Soc. of Pacific* **99**, 309
Lightman A.P., White T.R.: 1988, *Astrophys. J.* **335**, 57
Luminet J.-P.: 1979, *Astron. Astrophys.* **75**, 228
Malkan M.A.: 1983, *Astrophys. J.* **268**, 582
Malkan M.A., Sargent W.L.W.: 1982, *Astrophys. J.* **254**, 22
Maoz D., Netzer H.: 1989, *M. N. R. astr. Soc.* **236**, 21
Mardaljevic J., Raine D.J., Walsh D.: 1988, *Astroph. Lett. Communications* **26**, 357
Marziani P.: 1986, *Dissertation, University of Padova*
Mathews W.G.: 1982, *Astrophys. J.* **258**, 425
Mathews W.G.: 1986, *Astrophys. J.* **305**, 187
Mathews W.G., Blumenthal G.R.: 1977, *Astrophys. J.* **214**, 10
Mathews W.G., Capriotti E.R.: 1985, in: *Astrophysics of Active Galaxies and Quasi-Stellar Objects* Mill Valley: University Science Books. J.S. Miller (Ed.), p.185
Mathews W.G., Doane J.S.: 1989, *preprint*
Mathews W.G., Ferland G.J.: 1987, *Astrophys. J.* **323**, 456
Mathews W.G., Vielleux S.: 1989, in: *Active Galactic Nuclei*, IAU Symposium No. 134. D.E. Osterbrock and J.S. Miller (Eds.) , *in press.*
Mathews W.C., Wrampler J.: 1985, *Publ. Astron. Soc. of Pacific* **97**, 966
Mc Dowell J.C., Elvis M., Wilkes B.J., Polomsky E.W., Dey M.S.: 1989, *Bull. Am. Astron. Soc.*, p. 967
Miley G.K., Miller J.S.: 1979, *Astrophys. J.* **228**, L55

Miller J.S.: 1988, in: *Active Galactic Nuclei*, Proceedings of the Conference held at Atlanta, Georgia, on October 28–30, 1987. H.R. Miller, P.J. Wiita (Eds.) , p.112
Miller J.S., Antonucci R.R.J.: 1983, *Astrophys. J. Letters* **271**, L7
Morris S.L., Ward M.J.: 1989, in: *Active Galactic Nuclei*, IAU Symposium No. 134. D.E. Osterbrock and J.S. Miller (Eds.) , p. 135
Mushotzky R.F.: 1982, *Astrophys. J.* **256**, 92
Mushotzky R.F.: 1988, in: *Active Galactic Nuclei*, Proceedings of the Conference held at Atlanta, Georgia, on October 28–30, 1987. H.R. Miller, P.J. Wiita (Eds.) , p.239
Mushotzky R., Ferland G.J.: 1984, *Astrophys. J.* **278**, 558
Netzer H.: 1982, *M. N. R. astr. Soc.* **198**, 589
Netzer H.: 1985a, *M. N. R. astr. Soc.* **216**, 63
Netzer H.: 1985b, *Astrophys. J.* **289**, 451
Netzer H.: !987, *M. N. R. astr. Soc.* **225**, 55
Netzer H., Elitzur M., Ferland G.J.: 1985, *Astrophys. J.* **299**, 752
Netzer H., Kollatschny W., Fricke K.J.: 1987, *Astron. Astrophys.* **171**, 48
O'Brien P.T., Gondhalekar J., Wilson R.: 1986, *ESA SP-263-601*
O'Dell S.L.: 1986, *Publ. Astron. Soc. of Pacific* **98**, 140
Oke J.B.: 1987, in: *Superluminal Radio Sources.* Cambridge: Cambridge University Press. J.A. Zensus, T.J. Pearson (Eds.), p. 267
Orr M.J.L., Browne I.W.A.: 1982, *M. N. R. astr. Soc.* **200**, 1067
Osmer P.S.: 1980, *Astrophys. J. Supp.***42**, 523
; Osterbrock D.E.: 1974, *Astrophysics of Gaseous Nebulae.* S. Francisco: Freeman
Osterbrock D.E.: 1977, *Astrophys. J.* **215**, 733
Osterbrock D.E.: 1978, *Physica Scripta* **17**, 137
Osterbrock D.E.: 1979, *Astron. J.* **84**, 901
Osterbrock D.E.: 1981, *Astrophys. J.* **246**, 696
Osterbrock D.E.: 1985, in: *Astrophysics of Active Galaxies and Quasi-Stellar Objects* Mill Valley: University Science Books. J.S. Miller (Ed.), p.111
Osterbrock D.E., Koski A.T., Phillips M.M.: 1976, *Astrophys. J.* **206**, 898
Osterbrock D.E., Pogge R.W.: 1985, *Astrophys. J. Supp.***97**, 25
Osterbrock D.E., Shuder J.M.: 1982, *Astrophys. J. Supp.***49**, 149
Padovani P.: 1989, *preprint*
Padovani P., Rafanelli P.: 1988, *Astron. Astrophys.* **205**, 53
Pelat D., Alloin D.: 1982, *Astron. Astrophys.* **105**, 335
Penston M.V., Perez E.: 1984, *M. N. R. astr. Soc.* **211**, 33P
Perez E.: 1987, *Ph. D. Thesis.* Istituto de Astrofisica de Canarias
Perez E., Penston M.V., Tadhunter C., Mediavilla E., Moles M.: 1987 *M. N. R. astr. Soc.* , 353

Perola G.C., Piro L., Altamore A., Fiore F., Boksenberg A., Penston M.V., Snijders M.A.J., Bromage G.E., Clavel J., Elvius A., Ulrich M.-H.: 1986, *Astrophys. J.* **306**, 508
Peterson B.M.: 1987, *Astrophys. J.* **312**, 79
Peterson B.M.: 1988, in: *Active Galactic Nuclei*, Proceedings of the Conference held at Atlanta, Georgia, on October 28–30, 1987. H.R. Miller, P.J. Wiita (Eds.) , p. 38
Peterson B.M., Foltz C.B., Byard P.L., Wagner R.M.: 1982, *Astrophys. J. Supp.***49**, 469 Peterson B.M., Foltz C.B., Miller H.R., Wagner R.M., Crenshaw D.M., Meyers K.A., Byard P.L.: 1983, *Astron. J.* **88**, 926
Peterson B.M., Foltz C.B., Crenshaw D.M., Meyers K.A., Byard P.L.: 1984, *Astrophys. J.* **279**, 529
Peterson B.M., Meyers K.A., Capriotti E.R., Foltz C.B., Wilkes B.J., Miller H.R.: 1985, *Astrophys. J.* 292, 164
Phillips M.M.: 1978, *Astrophys. J. Supp.***38**, 187
Phillips M.M., Charles P.A., Baldwin J.A.: 1983, *Astrophys. J.* **266**, 465
Phinney E.S.: 1985, in: *Astrophysics of Active Galaxies and Quasi-Stellar Objects* Mill Valley: University Science Books. J.S. Miller (Ed.), p. 453
Pogge R.W.: 1988, *Astrophys. J.* **328**, 519
Pringle J.E.: 1981, *Ann. Rev. Astron. Astroph.* **19**, 137
Pringle J.E., Rees M.J., Pacholczyk A.G.: 1973, *Astron. Astrophys.* **29**, 179
Pronik I.: 1987, in: *IAU Symp. No. 121.* E. Ye. Khachikian, K.J. Fricke and J. Melnick (Eds.)., p. 169
Rafanelli P.: 1989, in: *Active Galactic Nuclei*, IAU Symposium No. 134. D.E. Osterbrock and J.S. Miller (Eds.) , *in press*
Rafanelli P., Marziani P., Birkle H., Thiele U.: 1989, *unpublished*
Raine D.J., Smith A.: 1981, *M. N. R. astr. Soc.* **197**, 339
Rees M.J.: 1984, *Ann. Review Astron. Astroph.* **22**, 471
Rees M.J.: 1987, *M. N. R. astr. Soc.* **228**, 47p
Reichert G.A., Mushotzky R.F., Petre R., Holt S.S.: 1985, *Astrophys. J.* **296**, 69
Richstone D.D., Ratnatunga K., Schaffer J.: 1980, *Astrophys. J.* **240**,1
Robinson A., Binette L., Fosbury R.A.E., Tadhunter C.N.: 1987, *M. N. R. astr. Soc.* **227**, 97
Schulz H., Rafanelli P.: 1981, *Astron. Astrophys.* **103**,216
Shakura N.I., Sunyaev R.A.: 1973, *Astron. Astrophys.* **24**, 337
Shields G.A.: 1978, in:*The Pittsburgh Conference on BL Lac Objects.* A.M. Wolfe (Ed.), p. 257
Shuder J.M.: 1981, *Astrophys. J.* **244**, 12
Shuder J.M.: 1982, *Astrophys. J.* **259**, 48
Shuder J.M.: 1984 *Astrophys. J.* **280**, 491
Shuder J.M., Osterbrock D.E.: 1982, *Astrophys. J.*
Siemiginowska A., Czerny B.: 1989, *preprint*
Smith M.D., Raine D.J.: 1985, *M. N. R. astr. Soc.* **212**, 425

Stauffer J.R.: 1982, *Astrophys. J.* **262**, 66
Stein W.A.: 1988, in: *Active Galactic Nuclei*, Proceedings of the Conference held at Atlanta, Georgia, on October 28–30, 1987. H.R. Miller, P.J. Wiita (Eds.) , p.188
Stirpe G.M., de Bruyn A.G., Van Gröningen E.: 1988, *Astron. Astrophys.* **200**, 9
Stockton A., McKenty J.W.: 1987, *Astrophys. J.* **316**, 584
Sulentic J.W.: 1989, *preprint*
Sulentic J.W., Calvani M, Marziani P.: 1989, *in preparation*
Sun W.–H., Malkan M.A.: 1988, in: *Active Galactic Nuclei*, Proceedings of the Conference held at Atlanta, Georgia, on October 28–30, 1987. H.R. Miller, P.J. Wiita (Eds.) p. 220
Sun W.–H., Malkan M.A.: 1989, in: *Active Galactic Nuclei*, IAU Symposium No. 134. D.E. Osterbrock and J.S. Miller (Eds.) p. 262
Tadhunter C.N., Fosbury R.A.E., di Serego Alighieri S.: 1988, *ESO Sc. Preprint No. 625*
Tarter C.B., Tucker W.H., and Salpeter E.E.: 1969, *Astrophys. J.* **156**, 943
Tohline J.E., Osterbrock D.E.: 1982, *Astrophys. J. Letters* 252Z, L49
Tsvetanov Z., Tadhunter C., Perez E., Perez R., Vilchez P.: 1989, in *Extranuclear activity in Galaxies*, ESO Workshop Proceedings, *in press.*
Turner T.J., Pounds K.A.: 1989, *preprint*
Turnshek D.A.: 1984, *Astrophys. J. Letters* —bf 278, L87
Ulrich M.-H.: 1989, *ESO Sc. Preprint No. 662*
Ulrich M.-H., Boksenberg A., Bromage G., Clavel J., Elvius A., Penston M.V., Perola G., Pettini M., Snijders M.A.J., Tanzi E.G., Tarenghi M.: 1984, *M. N. R. astr. Soc.* **206**, 221
Ulrich M.-H., Altamore A., Boksenberg A., Bromage G., Clavel J., Elvius A., Penston M.V.: 1985, *Nature* **313**, 747
Unger S.W., Pedlar A., Axon D.J., Whittle M., Meurs E.J.A., Ward M.J.: 1987, *M. N. R. astr. Soc.* **228**, 671
van den Berg S.: 1989, in: *Dynamics and Interaction of Galaxies.* Proceedings of the Conference held in Heidelberg, 29 May – 2 June, 1989. A.Toomre and R Wielen (Ed.). *in press, in press*
van Gröningen E.: 1983, *Astron. Astrophys.* **126, 363**
van Gröningen E.: 1984, *Ph. D. Thesis*, Sterrewacht Leiden
Veron–Cetty M.-P., Veron P., Tarenghi M.: 1983, *Astron. Astrophys.* **119**, 69
Voit G.M., Shull M., Begelman M.C.: 1987, *Astrophys. J.* bf 316, 573
Wampler E.J., Gaskell C.M., Burke W.L., Baldwin J.A.: 1984, *Astrophys. J.* **276**, 403
Wandel A., Yahil A.: 1985, *Astrophys. J. Letters* **295**, L1
Watcher K.W., Strauss M.A., Filippenko A.V.: 1988, *Astrophys. J.* **330**, 91
Warwick R.S., Yaqoob T., Pounds K.A.: 1989, in: *Active Galactic Nuclei*, IAU Symposium No. 134. D.E. Osterbrock and J.S. Miller (Eds.) , p. 182

Weedman D.W.: 1985, in in: *Astrophysics of Active Galaxies and Quasi-Stellar Objects* Mill Valley: University Science Books. J.S. Miller (Ed.), p. 497
Weedman D.W.: 1986, *Quasars Astronomy.* Cambridge: Cambridge University Press
Whittle M.: 1985, *M. N. R. astr. Soc.* **213**, 33
Whittle M., Haniff C.A., Ward M.J., Meurs E.J.A., Pedlar A., Unger S.W., Axon D.J., Harrison B.: 1986, *M. N. R. astr. Soc.* **213**, 33
Whittle M., Pedlar A., Meurs E.J.A., Unger S.W., Axon D.J., Ward M.J.: 1988, *Astrophys. J.* 326, 125
Wilkes B.J.: 1984, *M. N. R. astr. Soc.* **207**, 73
Wilkes B.J.: 1989, *preprint*
Wilkes B.J., Elvis M.: 1987, *Astrophys. J.* **323**, 243
Wills B.J., Browne I.W.A.: 1986, *Astrophys. J.* **302**, 56
Wills B.J., Netzer H., Wills D.: 1985 *Astrophys. J.* **288**, 94
Wills B.J., Wills D.: 1986, *IAU Symposium No. 119*, p.215. G.Swarup, V.K. Kapahi (Eds.)
Wilson A.S., Heckman T.M.: 1985, in: *Astrophysics of Active Galaxies and Quasi-Stellar Objects* Mill Valley: University Science Books. J.S. Miller (Ed.), p. 39
Wilson A.S., Ward M.J., Haniff Chr. A.: 1988, *Astrophys. J.* **334**, 121
Woltjer L.: 1959, *Astrophys. J.* **130**, 38
Wu C.-C., Grady C.A., Boggess A.: 1984, *Astrophys. J.* **280**, 491
Yee H.K.C.: 1980, *Astrophys. J. Letters* **241**, L133
Zamorani, G., Henry J.P., Maccacaro T., Tananbaum H., Soltan A., Avni Y., Liebert J., Socke P., Strittmatter P.A., Weymann R.J., Smith M.G., and Condon J.J.: 1981, *Astrophys. J.* **245**, 357
Zheng W.: 1988, *Astrophys. J.* **333**, 188
Zheng W., Burbridge E.M., Smith H.E., Cohen R.D., Bradley S.E.: 1987, *Astrophys. J.* **322**, 164 Zwitter T., Calvani M., Bodo G., Massaglia S.: 1989, *SISSA preprint.*